



FRIEDRICH-SCHILLER-UNIVERSITÄT JENA

PHYSIKALISCH-ASTRONOMISCHE FAKULTÄT

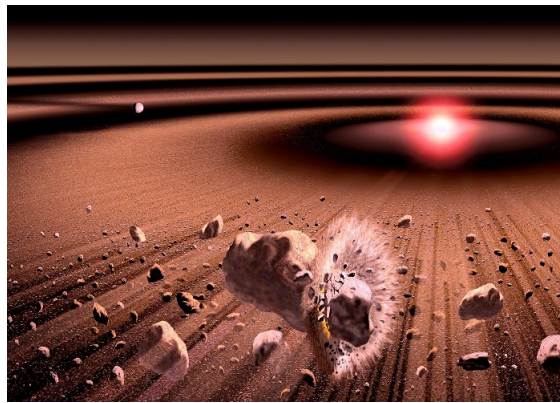
ASTROPHYSIKALISCHES INSTITUT UND
UNIVERSITÄTS-STERNWARTE



Finding Structural Analogues to the Solar System Debris Disc

—DISSERTATION—

zur Erlangung des akademischen Grades
Doctor rerum naturalium (Dr. rer. nat.)



vorgelegt dem Rat der Physikalisch-Astronomischen Fakultät
der Friedrich-Schiller-Universität Jena

von M. Sc. FABIAN GEILER
geboren am 15. August 1991 in Erlangen

12. April 2021

1. Gutachter:

Prof. Dr. ALEXANDER V. KRIVOV

Friedrich-Schiller-Universität Jena

2. Gutachter:

Dr. AMAYA MORO-MARTÍN

Space Telescope Science Institute

3. Gutachter:

Prof. Dr. SEBASTIAN WOLF

Christian-Albrechts-Universität zu Kiel

Tag der Disputation: 03.08.2021

Image on the title page:
Artist impression of a planetesimal collision in a circumstellar disc
(Illustration by Kouji Kanba, ISAS/JAXA)

Contents

Kurzfassung	vii
Abstract	ix
1. Introduction	1
1.1. The solar system debris disc	2
1.1.1. Zodiacal Cloud and short period comets	2
1.1.2. Asteroid belt	3
1.1.3. Edgeworth–Kuiper Belt and a bit beyond	5
1.2. Extrasolar debris discs	7
1.2.1. Cold components	7
1.2.2. Warm components	9
1.2.3. Hot components	10
1.3. Aims of this work	11
2. Fundamentals of debris discs	12
2.1. Growth of planetesimals and planets	12
2.2. Size distribution	13
2.3. Mechanical and optical properties	14
2.4. Dust dynamics	16
2.4.1. Photogravity	16
2.4.2. Drag forces	19
2.5. Migration	19
2.6. Collisions	21
2.6.1. Igniting the cascade	21
2.6.2. Result of collision	22
2.6.3. Complete collisional evolution	24
2.7. Links to observations	26
3. Asteroid belt analogues	29
3.1. Sample	29

Contents

3.2. Model	33
3.3. Results	37
3.4. Discussion	39
3.4.1. Good fits	39
3.4.2. Poor fits	43
4. Kuiper Belt analogues	46
4.1. HR 8799	48
4.1.1. Wide cold disc	49
4.1.2. Disc with halo	51
4.2. Collisional models	51
4.2.1. The ACE code	51
4.2.2. Age of the system	53
4.2.3. Excited disc	53
4.2.4. Wide cold disc	54
4.2.5. Synthesis model	56
4.3. Discussion	58
4.3.1. Comparison to the Kuiper Belt	58
4.3.2. New SMA data	59
4.3.3. Origin of the scattered disc	59
4.3.4. Other systems	62
5. Conclusion	64
5.1. Summary	64
5.2. Parting thoughts	66
A. SED-Data for HR 8799	69
Bibliography	70
List of Figures	95
List of Tables	99
Acknowledgements	100
Ehrenwörtliche Erklärung	101

Kurzfassung

Viele Trümmerscheiben zeigen eine Zwei-Komponenten-Struktur mit einer kalten äußeren und einer warmen inneren Komponente. Während die äußere häufig dem gut verstandenen Kuiper-Gürtel ähnelt, ist die Quelle der inneren häufig noch umstritten. Im ersten Teil dieser Arbeit untersuchen wir, ob der warme Staub ein Anzeichen für Asteroidengürtel-Analoga ist. Wir testen dies mit einer protoplanetaren Scheibe, in der, wohl durch Planeten, eine Lücke entstanden ist. Die dadurch gebildeten Teilscheiben entwickeln sich nach dem Beseitigen des Gases durch stationären Kollisionszerfall weiter. Dieser Ansatz wird mit einem analytischen Kollisionsmodell anhand eines Spitzer/IRS Katalogs mit 225 zwei-komponentigen Trümmerscheiben getestet. Wir stellen fest, dass eine überwältigende Mehrheit der Scheiben (220 von 224, 98%) mit dem Szenario übereinstimmen. Für die Vorgänger, die ursprünglichen protoplanetaren Scheiben, finden wir einen Exponenten der Dichteverteilung von -0.93 ± 0.06 und eine durchschnittliche Anfangsmasse von $(3.3_{-0.3}^{+0.4}) \times 10^{-3}$. Beide Werte stimmen mit Beobachtungen im Submillimeter Bereich von protoplanetaren Scheiben überein. Staubproduktion durch kurzperiodische Kometen und seltener auch Staubtransport aus dem äußeren Gürtel können realistische, nicht einander ausschließende Alternativen zu einem Asteroidengürtel-Analoga darstellen. Die übrigen vier Scheiben (2% des Samples) zeigen eine innere Komponente, die anscheinend inkonsistent ist mit Staubproduktion in einem Asteroidengürtel. Staub in diesen Systemen muss entweder durch Kometen wieder aufgefüllt werden, oder ist der Überrest eines sich unlängst zugetragenem, seltenen Ereignisses, wie einer Kollision großer Körper oder einer Instabilität im Planetensystems.

KURZFASSUNG

Im zweiten Teil der Arbeit betrachten wir ein Kuiper-Gürtel Analogon und versuchen seine Architektur nachzuvollziehen. HR 8799 ist ein junger Stern des Typs F0 mit vier Riesenplaneten und einer Zwei-Komponenten-Trümmerscheibe mit allen vier Planeten in der Lücke zwischen der warmen und der kalten Scheibe. Da die Architektur der unseres Sonnensystems ähnelt, aber auch Unterschiede aufweist wie die massereichen Planeten, die großen Ausmaße des Systems und der großen, kalten Staubmenge, gilt HR 8799 als das Referenzsystem, um Formations- und Evolutionsmodelle von Planetensystemen zu testen. Wir zeigen, dass die Modelle des äußeren Gürtels, die aus den Herschelbeobachtungen gewonnen wurden, nicht mit den ALMA-Daten übereinstimmen und umgekehrt. Um ein physikalisch motiviertes Modell zu finden, das mit beiden Beobachtungen übereinstimmt, führen wir Kollisionssimulationen durch. Wir zeigen, dass weder ein dünner Planetesimalgürtel mit einem Strahlungsdruck bedingtem Halo noch ein einzelner, breiter Planetesimalgürtel die radialen Helligkeitsprofile erklären kann. Stattdessen schlagen wir ein gekoppeltes Modell vor: eine Population mit Orbits geringer Exzentrizität (“klassischer Kuiper-Gürtel”) und eine mit Orbits hoher Exzentrizität (“zerstreute Scheibe”). Wir erörtern, wie diese Struktur mit einer Migration der Planeten erklärt werden kann, so wie es beim Kuiper-Gürtel der Fall ist.

Abstract

Many debris discs reveal a two-component structure, with a cold outer and a warm inner component. While the former is often similar to the well understood Kuiper Belt, the origin of the latter is still a matter of debate. In the first part of this work, we investigate whether the warm dust may be a signature of asteroid belt analogues. In the scenario tested the current two-belt architecture stems from an originally extended protoplanetary disc, in which planets have opened a gap separating it into the outer and inner discs which, after the gas dispersal, experience a steady-state collisional decay. This idea is explored with an analytic collisional evolution model for a sample of 225 debris discs from a Spitzer/IRS catalogue that are likely to possess a two-component structure. We find that the vast majority of systems (220 out of 225, or 98%) are compatible with this scenario. For their progenitors, the original protoplanetary discs, we find an average surface density slope of -0.93 ± 0.06 and an average initial mass of $(3.3^{+0.4}_{-0.3}) \times 10^{-3}$ solar masses, both of which are in agreement with the values inferred from submillimetre surveys. However, dust production by short-period comets and — more rarely — inward transport from the outer belts may be viable, and not mutually exclusive, alternatives to the asteroid belt scenario. The remaining five discs (2% of the sample) harbour inner components that appear inconsistent with dust production in an “asteroid belt.” Warm dust in these systems must either be replenished from cometary sources or represent an aftermath of a recent rare event, such as a major collision or planetary system instability.

In the second part of the work, we perform an in depth analysis of a Kuiper Belt analogue and try to reconstruct its architecture. HR 8799 is a young F0-type star with four directly imaged giant planets and a two-component debris disc, one located exterior and another one interior to the region occupied by the planetary orbits. Having an architecture similar to that of our solar system, but also revealing dissimilarities such as high masses of planets and a huge radial extent and a high mass of the outer debris belt, HR 8799 is considered to be a benchmark to test formation and evolution models of planetary systems. We demonstrate that the models of the outer disc, proposed previously to reproduce Herschel observations, are inconsistent with the ALMA data, and vice versa. In an attempt to find a physically motivated model that would agree

ABSTRACT

with both observational sets, we perform collisional simulations. We show that a narrow planetesimal belt and a radiation pressure induced dust halo cannot account for the observed radial brightness profiles. A single, wide planetesimal disc does not reproduce the data either. Instead, we propose a two-population model, comprising a Kuiper-Belt-like structure of a low-eccentricity planetesimal population (“the classical Kuiper Belt”) and a high-eccentricity population of comets (“scattered disc”). We argue that such a structure of the exo-Kuiper belt of HR 8799 could be explained with planet migration scenarios analogous to those proposed for the Kuiper Belt of the solar system.

1. Introduction

Our own solar system houses many different structures and phenomena, that serve as a point of comparison in studies of other systems. The solar system for example features multiple dust populations, two discs, the asteroid belt and the Kuiper Belt, with four giant planets in between and a prominent dust population in the inner solar system among the terrestrial planets called the Zodiacal Cloud. The Oort Cloud, a third population, surrounds the solar system as a shell. Within these discs we find planetesimals of the size of a few hundred kms down to dust with a size of a few μms . While the origins of the largest objects can be traced back almost uninterrupted to the early stages of the solar system, the dust has to have been newly created, since it either quickly migrates onto the star because of drag forces or is swiftly expelled from the system via wind and radiation pressure (e.g. Krivov et al., 2005; Wyatt et al., 2007a; Nesvorný et al., 2010). Dust production stems from collisions between larger objects or simply their fragmentation via sublimation and tidal disruption. The material produced is also often referred to as debris, due to the often violent nature of its origin, hence the name debris disc. Planets also play a part in the structure of debris discs, as they can gravitationally stir the planetesimals within the disc. This effect can still be seen through the amount of dust we find in the system today. Since we can observe dust much more easily than individual planets or planetesimals, modelling the production of dust can give us insight into the structure of the entire system. Debris discs also play an integral role in understanding planet formation, because they indicate a region where planet formation failed or was interrupted (e.g. Safronov, 1969; Lissauer, 1987; Kenyon & Bromley, 2008).

Continuing from the precedent set by the solar system, we expect extrasolar systems to adhere to a similar structure: planets influencing planetesimals and planetesimals generating dust. Models, initially developed by observing the solar system, can then be extended to other systems and help us not only decipher their evolutionary history but also predict aspects of the disc not yet visible by any other means. Thus the study of debris discs starts right at our doorstep.

1.1. The solar system debris disc

1.1.1. Zodiacal Cloud and short period comets

Looking at the sky shortly before dawn or after dusk is enough to see some of the dust in our solar system first hand. The glow just above the horizon seen at these conditions is called the zodiacal light and it was discovered late in the 17th century by Cassini. He also correctly interpreted the phenomenon as light being scattered by a dust population, which by now became known as the Zodiacal Cloud. It encompasses all the dust in the inner solar system and its total dust mass is estimated to be $\sim 10^{-8} M_{\oplus}$ (Nesvorný et al., 2010). Within the inner solar system, there are regions of enhanced dust density, e.g. there is dust trapped around some of the terrestrial planets (Dermott et al., 1994; Jones et al., 2013) and dust just outside the sublimation range near the Sun (Peterson, 1967; MacQueen, 1968), the nature of the latter still being a matter of debate.

The radial dust distribution as a whole follows a power law, which is a bit steeper than the one expected for dust produced in a narrow ring and then gradually moving inward (e.g. Briggs, 1962; Leinert et al., 1983). The explanation is that dust experiences collisions on its way inward, steepening the profile (e.g. Wyatt, 2005). Regarding the size distribution, most measurements are of the dust grains in the vicinity of the Earth, simply because of the ease of access, but some data of dust farther out allowed for modelling of the entire population (Grün et al., 1985; Love & Brownlee, 1993; Staubach et al., 1997; Kelsall et al., 1998; Dikarev et al., 2004; McNamara et al., 2004). These models show that grains of $\sim 1 \mu\text{m}$ are blown out of the system, while the larger grains of $\sim 30 \mu\text{m}$ are dominating the cross section and are drifting towards the star without experiencing collisions. Grains of $\sim 100 \mu\text{m}$ and above are dominant for the mass density.

Where the dust of the Zodiacal Cloud originates from is still a matter of debate. For it to be continuously visible we need a process that continuously feeds new dust, and luckily there are two such sources. Dust can originate from the asteroid belt and via drag forces drift inward, or it can stem from disintegrating comets on their way through the inner solar system. These comets either sublimate or tidally disrupt in the inner solar system. The emerging cloud of fragments continues to orbit the sun as a population of colliding material. To determine which method is correct a look at the observations at hand is necessary. They are carried out through scattered light (with e.g. SPHERE instrument at the ALMA observatory) and thermal emission (with e.g. the AKARI satellite), micro crater counts on the lunar surface, sediments within polar

ice and direct capture of dust entering the stratosphere or capturing with a spacecraft (as done with probes like e.g. Ulysses, Pioneers and Cassini). All of these methods reveal different aspects of dust (e.g. material properties, size and spatial distribution etc.), but also come with complications. Capturing dust entering the stratosphere for example shows two distinct groups of material attributed with different origins: lower density grains of cometary origin and higher density grains of asteroidal origin (Joswiak et al., 2007). Judging by the amount of dust found in these groups, the zodiacal dust seems to be of asteroidal origin, but these measurements are biased, since cometary dust has higher speeds which not only leads to less of it being captured by the earth, but also to higher thermal alteration when entering the stratosphere, making it harder to identify them (Kral et al., 2017). It is therefore important to obtain measurement of dust farther away than our immediate vicinity. Scattered light, thermal observations and direct capture with a spacecraft fulfil these requirements. These observations showed that the vertical height of the Zodiacal Cloud is consistent with a cometary origin and that at the millimetre size range the ratio of cometary to asteroidal dust is 9 to 1 (Ueda et al., 2017). So the evidence is mounting that zodiacal dust mostly stems from comets and not asteroids (Nesvorný et al., 2010). Speaking of the latter, they inhabit their own region with interesting qualities.

1.1.2. Asteroid belt

When calculating the planets' orbits, Johannes Kepler found too large a gap between Mars at 1.5 AU and Jupiter at 5 AU and predicted a planet in between, which was supposed to be found with the discovery of Ceres in 1801 by Guiseppe Piazzi. Since the telescopes at the time could not resolve Ceres, it remained a point source – like a star – and gained the classification of "asteroid", star-like. In the following years more of these asteroids were found in the region in between Mars and Jupiter. The frequency of these objects and their close proximity, indicated that these were not planets, but that they were part of the structure which is now called the asteroid belt. Studying it more closely unveiled some features, the explanations to which seem to be linked to planetary formation.

One of the most striking is the overall mass, which is very low compared to the surrounding planetary regions, with a mass of $\sim 5 \times 10^{-4} M_{\oplus}$, representing a loss of over 99% compared to what is expected from the surroundings. Such a strong depletion cannot have been accomplished by collisional evolution over the age of the solar system (e.g. Bottke et al., 2005).

Another feature is the material composition of the objects. It varies with their po-

CHAPTER 1. INTRODUCTION

sition within the belt with silicate rich S-type asteroids found in the inner regions of the disc and carbonaceous C-type asteroids mainly orbiting further out. This radial distribution of planetesimals can be seen as an intuitive consequence of their distance to the sun at their formation and their varying evolution, were it not for the huge overlap between these two populations. Consequently a mixing of the belt has to have occurred. A third feature to discuss is the high excitation levels of the belt. Most of the primordial (i.e. big) asteroids have a high excitation (up to 0.3 and a median of 0.15) and a similarly high inclination (up to 30 deg and a median of around 10 deg). These values are much larger than for any other planet in the solar system and conflict with the supposedly circular initial orbits expected from formation. Mutual gravitational interaction between the planetesimals and planetary embryos would create some amount of excitation, but they are not the only possible source of excitation. Planets can also perturb the asteroids. The Kirkwood gaps in the asteroid belt are a clear sign that the influence of Jupiter in particular is enough to shape the appearance of the disc, but while this may be the case it is also not sufficient to explain the excitation observed (Petit et al., 2002).

So despite not actually being planets, the asteroids show multiple features that help understand planetary formation. One simple solution to all this is that the asteroid belt just never had that much mass to begin with (Izidoro et al., 2015; Raymond & Izidoro, 2017). This can be achieved by inward drifting planetesimals in the gas disc, which leads to a material pile-up consistent with planet formation via pebble accretion (e.g. Levison et al., 2015). While models were able to recreate the low mass of both Mars and the asteroid belt, the steep slopes required for the initial distribution are hard to justify.

Another solution points to the evolution of the giant planets in the solar system. Of particular interest is the orbital evolution of Jupiter, which is believed to have moved in and out of the inner solar system due to interactions with the primordial gas disc and with Saturn. On this migration it supposedly not only scattered a significant amount of material out of the region of the asteroid belt but also limited the formation region of the terrestrial planets to 0.7 ...1.0 AU thus limiting the mass available to the terrestrial planets severely (“Grand Tack” hypothesis; Hansen, 2009; Walsh et al., 2011). The inwards migration is stopped and eventually reversed by the formation of the other gas giant Saturn. By the end of its wanderings Jupiter will have crossed the region of the current asteroid belt twice, and while a small portion will have been scattered back into the belt, most will not be and the overall depletion is enough to explain our observations. The models following this hypothesis, although successful in reproducing the mix of asteroid types, create populations with higher inclinations than observed

(Deienno et al., 2016).

A third hypothesis is an early instability in the planetary system. It differs from the migrating Jupiter model in that it occurs specifically after the gas dispersed from the primordial disc. From cratering on the moon we know of a spike in collisions, assumed to have occurred within some few hundred million years after the gas dispersal, also called the Late Heavy Bombardment (Gomes et al., 2005; Morbidelli et al., 2005). The exact time of this instability has lately come into question (Boehnke & Harrison, 2016; Zellner, 2017; Morbidelli et al., 2018; Nesvorný et al., 2018) and it may have happened much earlier, within 10 Myr of the gas dispersing, leading to Heavy Bombardment being a more apt name. The main problem arising with these models is that they are heavily dependent on the exact instability considered (Clement et al., 2019). This shows how much of the planetary evolution can be gleaned from the structure and the orbital elements of the planetesimals in the asteroid belt. Although a definitive answer has not been reached, it is rather certain that some form of migration or instability has to be taken into account.

1.1.3. Edgeworth–Kuiper Belt and a bit beyond

The asteroid belt together with Zodiacal Cloud is also not the only debris disc in our solar system. Only at the end of the 20th century did we observe the second debris disc in the solar system, the Edgeworth–Kuiper Belt. It serves as the reservoir of most of the comets, is located at roughly ~ 45 AU and encompasses a mass of roughly $0.01 M_{\oplus}$ (e.g. Fraser et al., 2014). Its fractional luminosity, the ratio of dust luminosity to stellar luminosity, is estimated to be only 10^{-7} with its emission peak at ~ 60 K (Vitense et al., 2012). Direct observations are challenging, due to the large distance and small size of its objects. Therefore obtaining a complete picture of the radial and/or size distribution of the Kuiper Belt is difficult to achieve (e.g. Bannister et al., 2016). Similarly to the asteroid belt, we can identify different populations of objects within the Kuiper Belt. Common classifications of the outer population distinguish between resonant objects, the classical belt and the scattered disc (Jewitt et al., 1998). Resonant objects are defined, as the name suggests, by their resonances with the nearby Neptune, leading to them inhabiting only specific semimajor axis ranges. The most famous example of this population is probably Pluto with its satellites, orbiting in a 3:2 resonance. Some of the objects in this group cross Neptune’s orbit regularly, but since they are phase shifted, they do not encounter Neptune. Classical Kuiper Belt objects are not in resonance and predominantly inhabit semi-major axes ranging from 40 AU to 48 AU. They themselves can be separated into two populations: the Cold Classical Kuiper Belt and the Hot

CHAPTER 1. INTRODUCTION

Classical Kuiper Belt. The distinguishing factor is their level of excitation, with the inclination value of $i = 5$ deg as separating threshold (Brown, 2001; Gulbis et al., 2010), but also in their material composition, as the Cold Classical population appears reddened in reflective spectra (Tegler & Romanishin, 2000). The threshold between the two populations is somewhat arbitrary, since the population is continuous in that region, suggesting that mixing must have occurred (Volk & Malhotra, 2011). These characteristics imply a different dynamical origin.

Even farther out is the “scattered” population. Its members orbit at perihelia of 35 – 40 AU with high eccentricities. Beyond that there are the detached objects (Gladman et al., 2002), found on orbits with perihelia > 48 AU, outside of Neptune’s sphere of influence. These characteristics together with the rather small sizes of the planetesimals leads to difficulties when it comes to observing these populations accurately and the risk of biases has to be considered carefully (e.g. Shankman et al., 2017; Brown & Batygin, 2019). Interest into their origin and their current orbital parameters has been intensified with the emerging idea of a ninth planet (Trujillo & Sheppard, 2014; Batygin & Brown, 2016).

The overall large fraction of planetesimals in the Kuiper Belt with high eccentricities suggest an origin somewhat analogous to the asteroid belt, but with the main cause of excitation being Neptune instead of Jupiter. The commonly adopted model is a stepwise migration of Neptune (Nesvorný & Vokrouhlický, 2016; Lawler et al., 2019), driven by its encounters with Pluto-sized planetesimals. As a result the Hot Classical Kuiper Belt and the scattered and detached population formed at $\lesssim 30$ AU, while the Cold Classical Kuiper Belt was formed more or less at its current position and was only minimally impacted by the migrating Neptune (e.g. Levison et al., 2008; Morbidelli et al., 2008; Kavelaars et al., 2009; Wolff et al., 2012), explaining the differences in composition.

Farther out still at $\gtrsim 1000$ AU another population, the Oort Cloud, is expected but not yet directly observed (Oort, 1950). We know of its existence because of the long period comets with an isotropic inclination distribution (e.g. Meech et al., 2016), suggesting they originate from a shell like population of planetesimals at the outermost edge of the solar system. The planetesimals were placed at these large distances most likely through scattering by giant planets (Weissman & Levison, 1997; Shannon et al., 2019). Since then their dynamical evolution could have been affected by not only the giant planets, but also by more exotic gravitational influences like stellar fly-bys, passing giant molecular clouds or galactic tidal forces (Heisler & Tremaine, 1986; Duncan et al., 1987; Torres et al., 2019). Accounting for these, we can glimpse through the distribution of these long period comets into the early history of the solar system (Bannister et al., 2017; Vokrouhlický et al., 2019; Shannon et al., 2019).

In summary, we are aware of a variety of different populations within the solar system and each of them can be mined for information on the evolution of the giant planets and the system as a whole. This detailed structure and the wealth of information it contains, beg the question if we can see similar structures around other stars and with what level of detail.

1.2. Extrasolar debris discs

Extrasolar debris discs were discovered in the mid 80s when Aumann et al. (1984) found a far-infrared excess in the spectral energy distribution (SED) of Vega as seen on the left in Fig. 1.1. They concluded that the excess had to be emitted by dust in thermal equilibrium around the star. The number of identified debris discs quickly grew (Smith & Terrile, 1984; Aumann, 1985). One of them, β Pic, conclusively revealed that the dust is confined to a disc of the excess in visible light observations (Smith & Terrile, 1984), as seen on the right in Fig. 1.1. Already needed for modelling the SED of Vega was also a two component structure of the infrared excess, which has since been found to be a frequent occurrence (e.g. Morales et al., 2011; Su et al., 2013; Ballering et al., 2013; Chen et al., 2014; Pawellek et al., 2014; Kennedy & Wyatt, 2014). For some, the detection of a warm component is uncertain due to sensitivity of the instruments (Kennedy & Wyatt, 2014), while for others a resolved image might have been accomplished (Greaves et al., 2014; Ricci et al., 2015). Discussing this we start with the type of component first observed, the cold ones.

1.2.1. Cold components

They are found in the far-infrared to millimetre, on average exhibit temperatures between 80 – 100 K and fractional luminosities ranging from 10^{-6} to 10^{-3} (cf. Kuiper Belt fractional luminosity estimate of 10^{-7}). Combining the surveys of resolved and unresolved discs shows that around 20% of stars host cold components (e.g. Su et al., 2006; Hillenbrand et al., 2008; Carpenter et al., 2009; Eiroa et al., 2013; Chen et al., 2014; Thureau et al., 2014; Montesinos et al., 2016; Sibthorpe. et al., 2018). In addition there seems to be a trend of higher detection rates for earlier spectral types independent of age of the system (Moór et al., 2016). Curiously it drops drastically to around 2% around M-class stars (Lestrade et al., 2012; Kennedy et al., 2014). The reason behind this discrepancy is still debated and the possibilities range from debris discs just being less common due to formation processes inherent to M stars (Gaidos, 2017) or the discs around M-stars just being much fainter (Morey & Lestrade, 2014; Luppe et al., 2020).

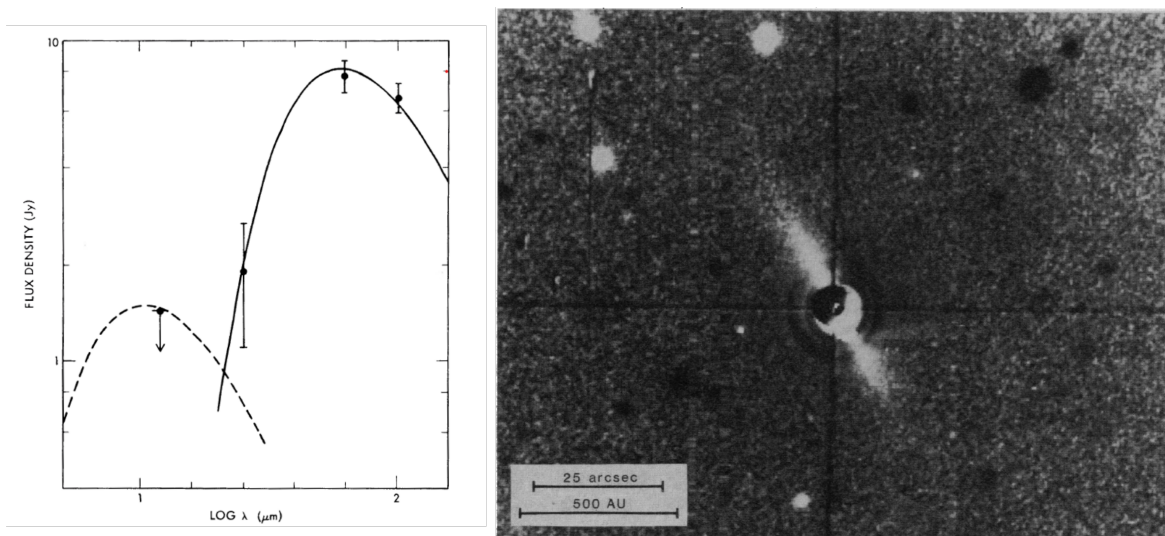


Figure 1.1.: Left: A spectral energy distribution (SED) of the infrared excess of Vega taken from Aumann et al. (1984). The black body spectra used in the model are a 85 K model (thick line) and a 350 K model (dashed line). The latter is only based on the $17 \mu\text{m}$ upper limit data and therefore arbitrary. Right: First resolved image of β Pic (Smith & Terrile, 1984). The disc can clearly be seen extending from the star to the top left and bottom right of the image.

Through resolving these discs analysis of planet induced structures, such as clumps and gaps has already been attempted (e.g. Wyatt, 2003, 2006).

In general the cold components we do see are wide and far away from the star, but fundamentally they are comparable to the Kuiper Belt, as dust production is dominated by collisions. It can be demonstrated by showing that the decline of the fractional luminosity of discs follows what we expect from a collisional evolution (Wyatt et al., 2007b; Löhne et al., 2008). So while the overarching model is clear, there are still many nebulous details, which often need to be discussed for each system individually. The influence of planets on the evolution of the debris disc (Wyatt et al., 2017; Marino et al., 2018; Sende & Löhne, 2019) for example or when and how the collisional evolution started. Using the latter as an example, one can resort to different mechanisms, each with their own caveats. Perturbation by planets for example requires them to be at specific regions (Wyatt et al., 2005; Mustill & Wyatt, 2009), while self stirring by the disc's planetesimals can only take place where planetesimals have grown large enough (Kenyon & Bromley, 2010; Krivov & Booth, 2018). Transient events can also be responsible, such as planet-planet-scattering (Raymond et al., 2009) or stellar flybys (Kenyon & Bromley, 2002).

Unfortunately the problems encountered while studying cold components do not all

translate to the warm component.

1.2.2. Warm components

The next population to discuss is warm dust with temperatures of about ~ 300 K and is usually found in the mid- to near-infrared, corresponding to radii of a few AU down to ~ 1 AU. It is usually just as bright as the cold components with fractional luminosities of 10^{-5} to 10^{-3} . Transient events are a possible explanation (e.g. Meng et al., 2012; Jackson & Wyatt, 2012), but usually a steady-state population is favoured.

Resorting to the solar system as reference, we can suspect that dust at these distances stems from either comets (Nesvorný et al., 2010; Wyatt et al., 2018) or dust transport via drag forces (Burns et al., 1979; Gustafson, 1994; Plavchan et al., 2005) or from a collisionally evolving disc similar to the asteroid belt (Su et al., 2013; Schüppler et al., 2016). For comets to be a reliable source an outer cold component is required. Transport between the components is possible via planet chains scattering material closer to the star, but that heavily depends on the, mostly unknown, system architecture and modelling these planet chains is therefore often inconclusive (Bonsor et al., 2012). Via observations of red-shifted absorption lines around β Pic evidence for “falling evaporating bodies” had been discovered (e.g. Ferlet et al., 1987; Beust et al., 1990). Their common interpretation as comets would be undeniable evidence for some form of transport and can be used to constrain possible cometary orbits and the planetary architecture (Marino et al., 2017; Kennedy, 2018). Drag forces are sufficient to create observable warm components (e.g. Kennedy & Piette, 2015), modelling of which has been done for individual systems in multiple studies (e.g. Reidemeister et al., 2011; Löhne et al., 2012a; Schüppler et al., 2014, 2015). This influx again is limited by planets as they scatter or accrete material on their orbit and a lack of a warm component could be interpreted as the influence of unseen planets (Bonsor et al., 2018). The luminosity achieved via drag forces is largely independent of the overall mass of the outer component, so even cold components too faint to be observed can be the source of warm dust in supposedly single-component systems. Thus both comets and drag forces are a valid explanation for the tentative correlation found between the existence of warm and cold components (Ertel et al., 2018, 2020).

An alternative solution is that the warm component is more akin to the asteroid belt, i.e. it is a collisionally evolving population. The validity of this solution is strongly dependent on the position of the disc in the system. Smaller orbits correspond to shorter collisional timescales and thus a shorter lifetime for these populations (Wyatt et al., 2007b; Löhne et al., 2008). So resolving these populations and finding accurate orbit

radii is tantamount to determining the source of the warm population.

1.2.3. Hot components

The closest population to a star is the hot population. It can have temperatures of up to ~ 2000 K and emits in the near-infrared ($1\ \mu\text{m} - 7\ \mu\text{m}$), where its emission usually makes up only about 1% of the total flux (Mennesson et al., 2014; Ertel et al., 2018). This corresponds to dust being at distances of less than 1 AU. To expose this small emission, the stellar flux is modelled and subtracted from the SED, but neither the observations nor the model have small enough uncertainties to always reliably identify an excess, so upper limits are often the best obtainable results. Infrared interferometry, however, has been able to reliably resolve emissions at these wavelengths. Such observations have been carried out in different surveys (e.g. Mennesson et al., 2014; Defrère et al., 2015; Ertel et al., 2020) and found an incidence rate similar to the one found in infrared detections.

Studies of known hot dust populations have shown that these dust grains besides being very hot also have to be very small (Kirchschlager et al., 2018). This is challenging for two reasons: grains of these sizes are usually expelled from the system on very short timescales and these temperatures are high enough to sublime most material. Since these components are found in many systems (Ertel et al., 2020) transient events are less likely to be their origin. So either massive replenishing processes or trapping mechanisms have to be invoked.

One suggestion is that for such small dust grains at very short distances from the star the Lorentz forces become much more important. Binding the grains to the stellar magnetic field would increase their lifetime in the system and models of this appear to be promising (Rieke et al., 2016). The validity of this approach, however, is still debated, because contributing factors like the magnetic field of the star are not well known and depending on the assumptions the models fail (Kimura et al., 2018). Another mechanism is the so called differential Doppler effect, that appears, because the extent of the star increases in importance the closer the dust grain is to it (Kimura et al. 2017¹, Sezestre et al. 2019). It results in an additional push for the grains, prolonging their lifetime on very close orbits. Initial studies of this process however seem to indicate that its influence is not strong enough to have an effect (Sezestre et al., 2019). (Pearce et al., 2020).

Another peculiar aspect of this population is where it came from. One would assume that dust close to the star was brought there by drag forces and originally was generated

¹https://www.cps-jp.org/~dust/Program_X_files/dust10-d2-04.pdf

in another population further out, but thus far a hot dust population does not seem to necessitate a warm component (Mennesson et al., 2014; Ertel et al., 2018), but there seems to be a connection to cold components (Ertel et al., 2020). A major bias to consider is that the small number of actual examples of hot dust is statistically challenging. So while a final verdict is pending, the character of these hot components is still open for debate.

1.3. Aims of this work

The aim of this work is to analyse debris discs in other systems and compare them to the discs found in the solar system. For the inner components our focus is on whether these can be called asteroid belt analogues, i.e. on whether they are collisionally dominated. Using a semi-analytical collisional model (Löhne et al., 2008) we will check the sample of two-component systems of Chen et al. (2014). Consequently we will have to distinguish between the different dust production mechanisms and test the plausibility of a collisional evolution as the source of the warm components.

For the outer component we focus on the structure of Kuiper Belt analogues and the implication derived thereof. The evolution of the Kuiper Belt is deeply entwined with the evolution of the planets in the outer solar system. It stands to reason that Kuiper Belt analogues are similarly involved with planet evolution. In this work we chose the system of HR 8799 to model and to study the implications resulting from our models. A detailed collisional model using the *ACE-Code* was created to explain multiple observations at different wavelengths (Matthews et al., 2014a; Booth et al., 2016) and compare the results to the Kuiper Belt. The *ACE-Code* is a numerical model successfully applied in a multitude of studies (e.g. Krivov et al., 2000; Krivov et al., 2005; Löhne et al., 2012a; Vitense et al., 2012; Reidemeister et al., 2011; Schüppler et al., 2016; Sende & Löhne, 2019).

In Chapter 2 we go into the physics involved in the formation, evolution and modelling of debris discs. In Chapter 3 we show the analysis of warm components in a large debris disc sample (Geiler & Krivov, 2017). In Chapter 4 we present the modelling of the cold component of HR 8799 (Geiler et al., 2019), ending this work with a final summary and outlook in Chapter 5.

2. Fundamentals of debris discs

2.1. Growth of planetesimals and planets

To understand debris discs we first have to consider their formation. At the start of their growth grains are ranging from μm to mm . These particles are strongly bound to the gas and their relative velocities are caused mainly by Brownian Motion (Weidenschilling, 1977; Weidenschilling & Cuzzi, 1993). The resulting relative speed of $\ll 1 \text{ m s}^{-1}$ (Weidenschilling, 1977) is ideal for such small grains to stick together upon collision, leading to very loosely bound dust aggregates. Growth via mutual collisions continues, with the dust aggregates being compressed in the process, until sizes in the range of mm to cm are reached. At these sizes collisions no longer grow particles but they bounce off of each other, this is also known as the bouncing barrier (e.g. Zsom et al., 2010). These larger grains are decoupled from the gas and move at keplerian speed. The gas on the other hand is moving at sub-keplerian velocities, decelerating the grains and resulting in a quick inward drift ($\sim 100 \text{ yr}$ at 1 m at 1 AU , Weidenschilling & Cuzzi (1993)). This is setting a time frame for the grains in which we need to grow the grains.

Different ideas have been proposed to achieve faster growth. Assuming, for example, a more sticky and less compressible material, i.e. small icy monomer grains, allows for a shift of the bouncing barrier (Okuzumi et al., 2012; Kataoka et al., 2013, 2014). This growth mechanism fails, however, when relaxing either the stickiness or the compressibility assumption. There exists little empirical data of the collisional behaviour of these grains and additional studies are needed to judge the feasibility of this mechanism (Blum, 2018). Another proposed method of growth is the accumulation of smaller grains (Windmark et al., 2012a,b; Garaud et al., 2013; Booth et al., 2018), created by cratering and erosion collisions between larger grains. These small grains can be swept up by faster moving bodies, growing them beyond the bouncing barrier. This mechanism slows down with increasing distance to the star and at 30 AU resulting planetesimals are not larger than a few metres. Considering that erosion also affects the growing planetesimals, it is unlikely that their final sizes are much larger than 0.1 m

(Schr apler et al., 2018). The most promising growth mechanism is a “soft” gravitational collapse of a high particle density region. Similar to the stellar cloud, pebble clouds can also collapse because of their own gravity. Streaming instability (Youdin & Goodman, 2005), vortex trapping (Klahr & Bodenheimer, 2003) or pressure bumps (Johansen et al., 2012), are all mechanisms that can increase the local density, while turbulence would be a hindrance. The details regarding these mechanisms are still a matter of debate.

Continuing from planetesimals of 1 km in size, gravity is an easy way to grow them even further, as the gravitational pull of these objects is strong enough to accrete smaller objects, leading to a process called runaway growth (Safronov, 1969). A gas envelope grows simultaneously to the core. Over time the core growth slows down due to the planetary embryo scattering material on its orbit and accreting most of the solids in its gravitational reach. The envelope growth meanwhile is mostly unaffected by this, so that eventually the envelope mass exceeds the core mass. Following this process Jupiter mass planets are built within a few Myrs depending on the properties of the disc. This process as a whole is known as the core accretion model (Pollack et al., 1996; Kenyon & Bromley, 2009) and is one of the two main models for explaining giant planet formation. The other process is growth by gravitational instability (Boss, 1997). Similarly to the soft gravitational collapse it begins by fragmentation within the protoplanetary disc, i.e. regions of enhanced material density where self gravity leads to clumps. These clumps grow further and can create planets of a variety of compositions, but can also be destroyed by tidal forces. In contrast to core accretion, gravitational instability is better at creating giant planets at large radii (Pollack et al., 1996; Ida & Lin, 2004) The exact circumstances, however, for these clumps to evolve and survive are still strongly debated. After gas is dispersed from the disc, collisional growth between left-over embryos leads to the formation of terrestrial planets. Failing to grow these rocky planets, we are left with a population reaching from planetesimals down to dust, commonly referred to as a debris disc.

2.2. Size distribution

After finishing the growth of material around the star, we need the size distribution of the final population before we can quantify any further evolution. In its simplest form it follows a power law and can be written as

$$n(s) = n_0 \left(\frac{s}{s_0} \right)^{-q} \quad (2.1)$$

CHAPTER 2. FUNDAMENTALS OF DEBRIS DISCS

where $n(s) ds$ is the number of particles of a specific size range $[s, s + ds]$, n_0 and s_0 denoting reference values and q being the slope of the size distribution. This distribution can be expanded with a radial dependency to

$$n(r, s) = n_0 \left(\frac{s}{s_0} \right)^{-q} \left(\frac{r}{r_0} \right)^{-p} \quad (2.2)$$

where r_0 denotes a reference distance and $n(r, s) ds dr$ now denoting the number of objects of the size range $[s, s + ds]$ at the distance range $[r, r + dr]$ from the star. It can be rewritten from a size to a mass distribution by

$$n(m, r) dm = 4\pi s^2 \rho n(r, s) ds \quad (2.3)$$

where ρ is the density of the material. Important parameters can thus be calculated via integration over the spherical coordinates

$$N(r, s) = 2 \int_0^\varepsilon n(r, s) r \cos \theta d\theta \quad (2.4)$$

$$\Sigma(r) = \int_{s_{\min}}^{s_{\max}} 4\pi \rho s^2 N(r, s) ds \quad (2.5)$$

$$M_{\text{tot}} = \int_0^{2\pi} \int_{r_{\min}}^{r_{\max}} \Sigma(r) r dr d\phi \quad (2.6)$$

with $N(r, s)$ being the number of objects of size s in a surface area element, ε being half of the opening angle of the disc, Σ being the mass surface density and M_{tot} being the total mass of the population. The hidden assumption in these steps being that the disc is azimuthally symmetric and that grains are spherical in shape. Such a simplification is of course not always applicable and asymmetries can occur as soon as planets are considered (e.g. Lee & Chiang, 2016; Löhne et al., 2017; Sende & Löhne, 2019). Being able to describe the distribution, we still need a model to describe the objects comprising the distribution.

2.3. Mechanical and optical properties

There are two interactions to be considered: Collisions and radiation forces. We assume the particles to be a compact monolith as predicted by classical slow growth models. The material and the object size dictate the critical energy Q_D^* , which is commonly described with the sum of two power laws and a factor accounting for the impact

2.3. MECHANICAL AND OPTICAL PROPERTIES

velocity (Benz & Asphaug, 1999; Stewart & Leinhardt, 2009)

$$Q_D^* = \left[A_s \left(\frac{s}{1 \text{ m}} \right)^{3b_s} + A_g \left(\frac{s}{1 \text{ km}} \right)^{3b_g} \right] \left(\frac{v_{\text{imp}}}{3 \text{ km s}^{-1}} \right)^\kappa. \quad (2.7)$$

Here b_s , A_s , and b_g , A_g are material dependent pairs of constants. We chose $b_s = -0.12$, $b_g = 0.45$, and $A_g = A_s = 5 \times 10^6 \text{ erg g}^{-1}$, close to the commonly used reference values for basalt (Benz & Asphaug, 1999). The velocity exponent κ was set for this work to 0.5 following Stewart & Leinhardt (2009).

The first term of Eq. 2.7 describes the material strength of the object decreasing with size. The second describes the cohesion of the object gained through self-gravity and increases with size. This creates a population separated in two parts, each dominated by one of the terms, with the dividing line, where both forces contribute equally, denoted by the breaking size s_b .

Relaxing the assumption that our objects are monolithic, we can describe the objects as grown by near indestructible dust pebbles, which form for larger more "fluffy" grains, i.e. the growth by agglomerates model (see Section 2.1). This forms highly porous planetesimals, which are much easier to destroy than the monolithic objects assumed in the formulae by Benz & Asphaug (1999). The grains on the other hand are harder to destroy the less pebbles they consist of, as these pebbles are almost indestructible (Blum, 2018). Incorporating this into the calculation of the critical energy leads to a large dip in mid-sized grains (Krivov et al., 2018). Although the observations in our solar system favour pebble-pile models (Blum et al., 2017), we assume compact in our studies, since both models reproduce the observations in other systems.

Besides the mechanical behaviour we also need to consider the grains' interactions with radiation. One important value for this is the factor Q_{rp} , which describes the efficiency of radiation pressure. For perfect blackbody objects it is $Q_{\text{rp}} = 1$. This can also be used for non-blackbody objects, as long as their size is much larger than the wavelengths considered. We calculated this factor for the different materials considered via Mie theory (Bohren & Huffman, 1983). Q_{rp} depends on two terms: Q_{abs} , the absorption efficiency, and Q_{sca} , the scattering efficiency. To calculate the optical parameters of mixed materials we used the rule of Bruggeman (1935). Having described methods to characterize both the population as a whole and an individual object, we now explore their orbits.

2.4. Dust dynamics

2.4.1. Photogravity

Movement in the vast expanse of space is generally dictated by gravity. In its classical incarnation it is written as:

$$\mathbf{F}_G = -\frac{\mathcal{G}m_1m_2}{r^3}\mathbf{r} \quad (2.8)$$

with $m_{1/2}$ being two masses attracting each other, \mathcal{G} being the gravitational constant and r being the distance between the two objects. This distance throughout its orbit can then be described by

$$r = \frac{\ell}{1 + e \cos \theta} \quad (2.9)$$

with ℓ being the semilatus rectum, e being the eccentricity of the orbit and the true anomaly θ being the angle between the minimum distance between two objects on their orbit and their current position. Eccentricity denotes the type of orbit the object inhabits and the value of ℓ changes accordingly:

$$\begin{aligned} \text{circle:} & \quad e = 0, \quad \ell = a, \\ \text{ellipse:} & \quad 0 < e < 1, \quad \ell = a(1 - e^2), \\ \text{parabola:} & \quad e = 1, \quad \ell = 2q, \\ \text{hyperbola:} & \quad e > 1, \quad \ell = a(e^2 - 1), \end{aligned} \quad (2.10)$$

where a denotes the semimajor axis and q the closest distance between the central object and its orbiting companion, the periapsis.

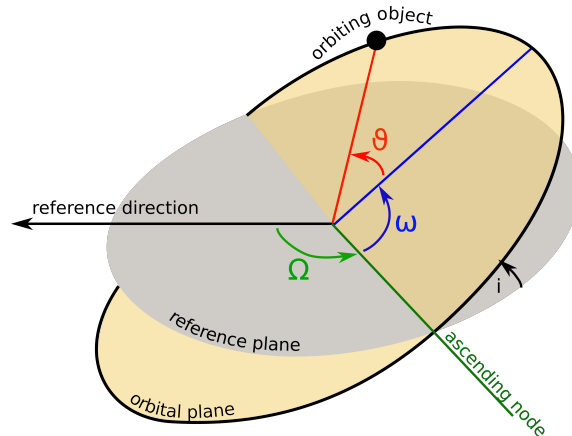


Figure 2.1.: Sketch of an orbit with some of the elements needed to describe it. In addition to the reference lines and planes the following parameters are shown: Ω being the longitude of the ascending node, ω being the argument of the pericenter, i being the inclination and the true anomaly being θ .

Using the semimajor axis, the eccentricity and the true anomaly one can describe an orbit in a plane, but we need additional parameters to describe its orientation in three dimensional space. A set of parameters capable of this is shown in Fig. 2.1. In addition to the established parameters the inclination i (shown in black) is required, denoting the angle between the orbital plane and a given reference plane. Defining the line of ascending nodes as the line created by the orbital plane crossing the reference plane, we introduce the longitude of the ascending node Ω as the angle between a reference line and the line of nodes (both angle and line shown in green). Finally we define the argument of pericenter ω , denoting the angle between the pericenter of the orbit and the line of nodes (shown in blue). The longitude of ascending node and the argument of pericentre are often combined into a single parameter, the longitude of pericentre $\varpi = \Omega + \omega$. All in all, these six parameters (a/q , e , θ , i , Ω , ω) are well suited to describe any orbit in three dimensional space.

Applying these parameters and the description of gravity in Eq. 2.8 we can already calculate the orbits of planets and planetesimals. Shrinking the size of an orbiting object down to a few μm , however, requires the consideration of additional forces. Most relevant is the radiation pressure \mathbf{F}_{rad} exerted by the star and the pressure exerted by the stellar wind \mathbf{F}_{sw} . They are described in relation to gravity with

$$\beta_{\text{rp}} = \frac{|\mathbf{F}_{\text{rad}}|}{|\mathbf{F}_{\mathcal{G}}|}, \quad \beta_{\text{sw}} = \frac{|\mathbf{F}_{\text{sw}}|}{|\mathbf{F}_{\mathcal{G}}|}. \quad (2.11)$$

Since both pressures counteract gravity and scale with r^{-2} their effect can simply be added into Eq. (2.8) with β_{rp} and β_{sw} as

$$\mathbf{F}_{\mathcal{P}\mathcal{G}} = -\frac{\mathcal{G}M_{\star}m(1 - \beta_{\text{rp}} - \beta_{\text{sw}})}{r^3}\mathbf{r} \quad (2.12)$$

with m being the particle mass and M_{\star} being the stellar mass. We can calculate both β_{rp} and β_{sw} for a dust grain of the size s via the formulae of Burns et al. (1979) and Gustafson (1994):

$$\beta_{\text{rp}} = \frac{\sigma L_{\star} Q_{\text{rp}}}{4\pi m c \mathcal{G} M_{\star}} \quad \beta_{\text{sw}} = \frac{\sigma \dot{M}_{\star} v_{\text{sw}} (C_{\text{D}}/2)}{4\pi m \mathcal{G} M_{\star}} \quad (2.13)$$

with L_{\star} being the stellar luminosity, ρ being the grain density and σ being the cross section of the dust particle. We assume $C_{\text{D}} = 2$ according to the case of reflecting stellar wind particles on the dust grain surfaces (Mukai & Yamamoto, 1982). Finally, v_{sw} and \dot{M}_{\star} are the stellar wind speed and the mass loss rate of the star. The former typically assumes values of a few hundred km s^{-1} , while the latter reaches $10^{-14} M_{\odot} \text{yr}^{-1}$ (e.g.,

Parker 1958). Stellar wind for typical values is three orders of magnitude lower than radiation pressure, rendering it virtually unimportant although drag effects from this force can be important.

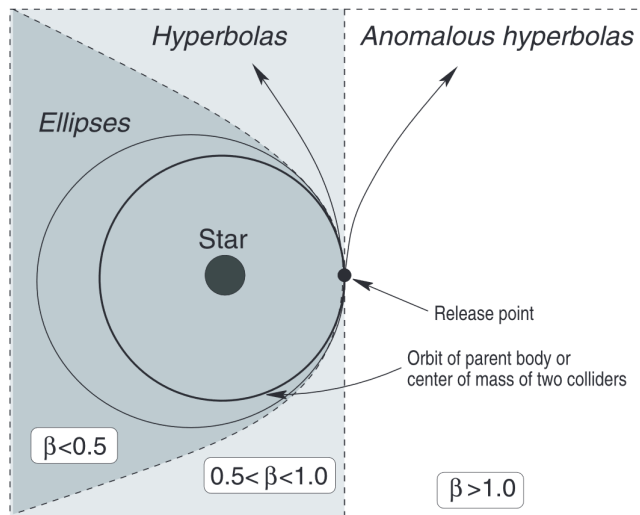


Figure 2.2.: Different β -values and their corresponding orbits assuming initially circular orbits and only gravity and radiation pressure as acting forces from Krivov et al. (2006).

Examining the equations (2.13) and (2.12) shows that the influence of β on planetesimals of a few km is negligible and that decreasing the grain size increases its effect. Assuming grains are released on a circular orbit, one can distinguish between three cases (Fig. 2.2). First, if $\beta = \beta_{\text{rp}} + \beta_{\text{sw}}$ of a grain is < 0.5 , then it enters into an eccentric orbit but is still bound to the system. If $0.5 \leq \beta < 1.0$ grains enter unbound hyperbolic orbits, making $\beta = 0.5$ a limit for bound orbits. Finally if $1.0 < \beta$, the grains leave the system on anomalous hyperbolae. Relaxing the condition of initially circular orbits imposes a dependency of the critical β on the position within the orbit of their parent object. If they are created when the parent object is in its pericenter, then the critical β can be lower than 0.5, and it can rise above 0.5 when the parent body is at its apocenter. So all grains with $\beta \gtrsim 0.5$ are blown out of the system, leading to a minimum grain size, called the blowout size s_{blow} , of typically a few μm (Burns et al., 1979). For late type stars these β s are not necessarily reached and therefore other removal mechanisms have to be considered, e.g. erosion via stellar radiation (e.g. Grigorieva et al., 2007; Czechowski & Mann, 2010). Both of these sources of outward pressure, have accompanying drag forces counteracting them.

2.4.2. Drag forces

The most prominent drag force is the Poynting-Robertson drag. It occurs when an object orbits a source of radiation. For radiation pressure we assumed the wind to act perpendicular to the grain radius vector, but according to special relativity the grains themselves “see” a wind of photons. The photons hitting from the front, decelerating the particle, seem squashed and therefore blue-shifted, while the ones approaching from the rear, accelerating the particle, are stretched and thus seem red-shifted. The classical Poynting-Robertson drag only takes blue-shifted photons into account, since the red-shifted photons become relevant only when stellar rotation is considered (Sezestre et al., 2019). The total radiation force can then be written as (Burns et al., 1979)

$$\mathbf{F}_{\text{rad}} = |\mathbf{F}_{\text{rp}}| \left[\left(1 - \frac{\dot{r}}{c} \right) \hat{\mathbf{r}} - \frac{\mathbf{v}}{c} \right]. \quad (2.14)$$

The difference between Poynting-Robertson drag and stellar wind drag is that stellar wind does not move with light speed. This leads to a total force exerted by stellar wind with

$$\mathbf{F}_{\text{wind}} = |\mathbf{F}_{\text{wp}}| \left[\left(1 - \frac{\dot{r}}{v_{\text{wind}}} \right) \hat{\mathbf{r}} - \frac{\mathbf{v}}{v_{\text{wind}}} \right]. \quad (2.15)$$

Here stellar wind regains a lot of its importance since v_{wind} is much lower than c and stellar wind drag values for the solar system are 30% of PR-drag values (Gustafson, 1994). Depending on the values for mass loss and wind speed this force can even become stronger than radiation pressure. Stellar wind drag might be essential to understand the orbital evolution around more active stars such as young or late-type stars, e.g. AUMic (Augereau & Beust, 2006; Schüppler et al., 2016) or ε Eridani (Wood et al., 2002; Reidemeister et al., 2011).

There are other forces possibly influencing the orbit of dust particles. The magnetic field of the star (e.g. Rieke et al., 2016) or the differential Doppler effect (Kimura et al., 2018) for example. Both are likely only important for very small grains very close to the star (Czechowski & Mann, 2010; Sezestre et al., 2019) and the discussion on their effectiveness is still ongoing. Thus they were not considered in this work.

2.5. Migration

The movement of the individual planetesimals is in the preceding sections only considered in combination with the host star. The interactions between the planetesimals and their surroundings had so far been neglected, but these are the driving factor

CHAPTER 2. FUNDAMENTALS OF DEBRIS DISCS

behind migration. Migration and its prevalence in planetary formation has long been evident from observed extrasolar planetary systems and even our own (Goldreich & Tremaine, 1979, 1980). Especially the close orbits of Hot Jupiters suggest that they migrated since their formation (e.g. Lin et al., 1996; Murray et al., 1998).

The underlying principle of any migration is the gravitational interaction between planets and their surroundings (e.g. Ward & Hourigan, 1989; Artymowicz, 1993; Tanaka et al., 2002; Lubow & Ida, 2010; Baruteau & Papaloizou, 2013; Baruteau et al., 2014). To discuss migration we need to take a few steps back from the fully formed planets back to planetesimals or planet embryos within a gas disc. While they will not open a gap in the disc they can still migrate either inward or outward depending on the disc surroundings in what is called type I migration. The migration timescales in this process are around $\sim 10^5$ yr, which is not long enough for the embryos to grow to giant planets before falling into their star or for the protoplanetary disc to dissipate ($10^6 - 10^7$ yr). Growing during migration the embryo can become large enough to open up the gap and enter type II (Lin & Papaloizou, 1986a,b; Ward, 1997). The planet is then suspended between two, presumably, much larger gas masses on either side and will migrate with the viscous accretion timescale of the disc. If the planet is more massive than the surrounding disc, its migration is slowed. Should the planet be small enough and density of the adjacent disc on one side of the planet's orbit large enough, then the planet can experience migration type III, runaway migration (Masset & Papaloizou, 2003; Artymowicz, 2004). In general it can move the planet either inward or outward until a change of disc density in the migration direction occurs. It can happen on very short timescales ($10^2 - 10^3$ orbits). These three types of migration all take place in the protoplanetary disc; planets, however, can still migrate even after gas dispersal through the so called planetesimal-driven migration.

An example for this can be found in the solar system, as Neptune, Uranus and Saturn are believed to have migrated in that way (e.g. Fernandez & Ip, 1984; Malhotra, 1993; Nesvorný & Vokrouhlický, 2016). Migration seems counterintuitive when considering the possible outcomes of close encounters of planetesimals and planets. One result, ejection of material out of the system, leads to a loss of momentum and an inward drift of the planet, while the next in line, accretion, is a net neutral effect, and the third result, scattering of material inward, leads to outward migration. So one would at most expect an inward migration as ejected material cannot interact again and reverse any momentum change. This picture changes when including the possibility of multiple planets in the system. For example, a planet A might scatter a planetesimal inward and another planet B further in ejects it without it interacting again with the outer planet A. As a result planet A moves outward and planet B inward. Using the solar system

as an example it was shown that the interplay of our four giant planets facilitated an inward migration of Jupiter and an outward migration of the rest (Fernandez & Ip, 1984; Gomes et al., 2004). This migration left deep marks within the Kuiper Belt showing how a migration can play an important role in the evolution a debris disc. Due to Jupiter’s size the actual distance it migrated is far less than the distance traversed by the other planets. A limit to the migration in either direction is given by the scatterable material and the efficiency of transporting this material from one planet to another. Larger distances between the planets and less material to interact with, will decrease the probability of this process working.

In contrast to migration, scattering can also change a planet’s orbits. Planet scattering, for example, can lead to planets on wide orbits, as can dynamical instabilities in multi-planetary systems (Raymond et al., 2009). Planetesimal discs can serve as a cushion, dampening the planet’s orbits and being partially scattered as a result (Thommes et al., 1999), or it can simply be in the way of a planet exiting the system and being scattered by it. To describe how this scattering and dampening ultimately effects the evolution of the disc, a look at collisions overall is required.

2.6. Collisions

Material around a star – as seen above – experiences a tug-of-war between a number of forces, all influencing the motion of the particle and leading it to its ultimate fate: either ejection from the system or falling onto the star, if it has not sublimated before reaching it. During this time other events influence the evolution of the material and the one we are most interested in are collisions. They grind down large bodies to medium sized bodies, which in turn are also destroyed in collisions and release dust onto their orbit, hence the process is also called the collisional cascade.

2.6.1. Igniting the cascade

This cascade, however, has to start somehow. The presence of gas within the primordial disc dampens relative velocities and circularises orbits facilitating planetesimal growth and preventing destructive collisions. For the disc to collisionally evolve after the gas has been dispersed, it needs to be stirred so that two colliding objects (target and projectile) of the masses m_t, m_p reach the relative velocity

$$v_{\text{cr}} = \sqrt{\frac{2(m_t + m_p)^2}{m_t m_p} Q_{\text{D}}^*}, \quad (2.16)$$

with Q_D^* being the specific critical energy (Eq. 2.7).

Proposed as stirring mechanisms are typically either internal or external processes. Internal means that the gravitational interactions of the already formed planetesimals are the exciting factor (Kenyon & Bromley, 2008, 2010; Kennedy & Wyatt, 2010; Krivov & Booth, 2018). Depending on the growth mechanism applied the maximum planetesimal size varies. Kenyon & Bromley (2008) assume growth via mutual collisions and afterwards Pluto-sized bodies stir the disc. As the excitation with these bodies is (astronomically speaking) instantaneous, the only limiting factor is the time required for the Pluto-sized bodies to form. Krivov & Booth (2018) on the other hand assumed “soft” gravitational collapse of pebble clouds, which grows planetesimals of a few hundred kms significantly faster. With this significant speed up of the formation the limiting factor is now the time needed for these smaller planetesimals to significantly stir the disc. In general Krivov & Booth (2018) find that their method widens the amount of possibly self stirred discs significantly, but not all discs can be stirred this way.

Another possibility are external processes. In no specific order, these can range from stellar flybys (Kenyon & Bromley, 2002) through planet-planet scattering events (Raymond et al., 2009) to massive companions on inclined, eccentric orbits (Nesvold et al., 2016). The most common form of exterior influence on the disc are planetary perturbations (Wyatt, 2005; Mustill & Wyatt, 2009). These can cause clumps from the resonant trapping of material (Wyatt, 2003, 2006; Krivov et al., 2007), warps within the disc (Golimowski et al., 2006; Lagrange et al., 2010) or a gap (Kenyon & Bromley, 2004; Marino et al., 2019).

Whichever mechanism incites collisions, we need a method to describe them.

2.6.2. Result of collision

Different collision outcomes are possible depending on the impact velocities. Starting at very low impact velocities planetesimals tend to stick together, but these velocities are not typical of debris discs and do not significantly contribute to the overall evolution (Blum & Wurm, 2008; Krivov et al., 2013). When impact energies are large enough as to prevent sticking but not high enough to destroy the target or the projectile, bouncing collisions can occur. They do not change the mass of either participant and while this might lead one to argue that this kind of collision is thus only important to collisional timescales, it was discovered that compaction of the participating objects permanently changes their behaviour (e.g. Weidling et al., 2009).

If the impact energy is too low to destroy the target and the projectile is large

enough, the projectile can still excavate mass from it. This process is called cratering and models (Wyatt & Dent, 2002; Thébault & Augereau, 2007) show that the excavated mass can be described as

$$m_{\text{crat}} = \frac{1}{4} \frac{m_t m_p}{m_t + m_p} \frac{v_{\text{imp}}^2}{Q_D^*}. \quad (2.17)$$

If the impact energy is larger than the fragmentation energy, the target is completely destroyed, meaning that by definition largest fragment of the collision is at most half of the target's mass (Paolicchi et al., 1996; Benz & Asphaug, 1999). The largest fragment $m_{\text{frag,max}}$ is then proportional to the specific critical energy (e.g. Paolicchi et al., 1996) and can be calculated via

$$m_{\text{frag,max}} = \frac{1}{2} (m_t + m_p) \left(2 \frac{(m_t + m_p)^2}{m_t m_p} \frac{Q_D^*}{v_{\text{imp}}^2} \right)^c \quad (2.18)$$

with $c = 1$ assumed due to uncertainties in the laboratory values (Fujiwara et al., 1977; Benz & Asphaug, 1999; Arakawa, 1999). The number of fragments in the mass range of $[m, m + dm]$ from a destructive collision can then be described by (Krivov et al., 2005)

$$g(m) dm = (2 - q_m) \left(\frac{m}{m_{\text{frag,max}}} \right)^{-q_m} \frac{m_t + m_p}{m_{\text{frag,max}}^2} dm \quad (2.19)$$

with impact experiment results giving values of q_m of 1.5...2.0 equivalent to a differential size distribution with an exponent q of 3.0...4.0. The ‘‘classical’’ value for q_m is 11/6 (Fujiwara et al., 1977). This form of $g(m)$ ensures that

$$\int_0^{m_{\text{frag,max}}} g(m) m dm = m_t + m_p. \quad (2.20)$$

To adapt Eq. 2.19 and Eq. 2.20 for cratering collisions, one only needs to replace $m_t + m_p$ with m_{crat} and set the number of largest fragments to 1 (Krivov et al., 2006). We can now describe two objects on their orbits and the result of their collision. Continuing from there we need to ramp up the number of collisions considered, to model the entire evolution of the disc.

2.6.3. Complete collisional evolution

Handling a larger number of collisions can be done with a size distribution of the form $dn_{dens}(m, \vec{p})/dt$. It characterises the evolution of the number of objects of a mass in the range $[m, m + dm]$ and on an orbit within $[\vec{p}, \vec{p} + d\vec{p}]$. \vec{p} is a vector consisting of orbital parameters and together describing an orbit. \vec{p} and m denote the phase space in which all motion and relevant physical processes can be calculated. Using the formula by (Smoluchowski, 1916), we can now write down the evolution of the disc as

$$\frac{d}{dt}n_{dens}(m, \vec{p}) = \left(\frac{\partial}{\partial t}n_{dens}(m, \vec{p}) \right)_{\text{gain}} - \left(\frac{\partial}{\partial t}n_{dens}(m, \vec{p}) \right)_{\text{loss}} - \text{div} \left(n_{dens}(m, \vec{p}) \frac{d}{dt}\vec{p} \right). \quad (2.21)$$

The last term shows changes in the orbital parameters due to non-collision effects, such as transport mechanisms or planetary perturbations. The first two terms, on the other hand, describe the gain and loss of material due to collisions. In more detail

$$\begin{aligned} \left(\frac{\partial}{\partial t}n_{dens}(m, \vec{p}) \right)_{\text{gain}} &= \int_{m_p} \int_{m_t} \int_{\vec{p}_p} \int_{\vec{p}_t} f(m_t, \vec{p}_t; m_p, \vec{p}_p; m, \vec{p}) n_{dens}(m_t, \vec{p}_t) \\ &\quad \times n_{dens}(m_p, \vec{p}_p) v_{\text{rel}}(m_t, \vec{p}_t; m_p, \vec{p}_p) \sigma(m_t, m_p) \\ &\quad \times \delta(\vec{r}(\vec{p}_p) - \vec{r}(\vec{p}_t)) dm_p dm_t d\vec{p}_p d\vec{p}_t \end{aligned} \quad (2.22)$$

and

$$\begin{aligned} \left(\frac{\partial}{\partial t}n_{dens}(m, \vec{p}) \right)_{\text{loss}} &= n_{dens}(m, \vec{p}) \int_{m_p} \int_{\vec{p}_p} n_{dens}(m_p, \vec{p}_p) v_{\text{rel}}(m_p, \vec{p}_p; m, \vec{p}) \\ &\quad \times \sigma(m_p, m) \delta(\vec{r}(\vec{p}_p) - \vec{r}(\vec{p})) dm_p d\vec{p}_p, \end{aligned} \quad (2.23)$$

with $f(m_t, \vec{p}_t; m_p, \vec{p}_p; m, \vec{p})$ being the fragmentation distribution, σ being the collisional cross section and the Dirac- δ assuring the evaluation of the integral only for collisions (Krivov et al., 2006). Here the fragmentation distribution has to entail more than just the fragments' size distribution discussed in Sec. 2.6.2 but also their orbital distribution h , giving

$$f(m_t, \vec{p}_t; m_p, \vec{p}_p; m, \vec{p}) = g(m_t, \vec{p}_t; m_p, \vec{p}_p; m) \times h(m_t, \vec{p}_t; m_p, \vec{p}_p; m, \vec{p}). \quad (2.24)$$

The collisional cross section σ is the size of the area both projectile and target have to “hit” to guarantee a collision. It is enhanced by gravitational lensing, which results

in the additional Safronov factor (Safronov, 1969):

$$\sigma(m_p, m) = \pi \left(\frac{3}{4\pi\rho} \right)^{2/3} (m_p^{1/3} + m_t^{1/3})^2 \left(1 + \frac{v_{\text{esc}}^2}{v_{\text{rel}}^2} \right), \quad (2.25)$$

with the escape velocity of the combined body of target and projectile given by

$$v_{\text{esc}}^2 = \frac{2\mathcal{G}(m_p + m_t)}{s_p + s_t}. \quad (2.26)$$

Evaluating this set of equations for each time step gives the evolution of the system. This process however is a complicated, time expensive undertaking and not necessarily suitable for every system. So we are in need of a simpler model which can be applied more easily.

In the following we describe the approach used by Löhne et al. (2008). Assuming a quasi-steady state disc, we can write the time dependency separately. The distribution is then given by

$$n_{\text{dens}}(m, \vec{p}) = n_{\text{dens},0}(m, \vec{p}) T(t), \quad (2.27)$$

where $T(t)$ is the temporal evolution of the distribution and $n_{\text{dens},0}$ being the initial number density. Neglecting transport and using this new description of $n_{\text{dens}}(m, \vec{p}, t)$ we can rewrite the gain and loss terms of Eq. 2.21 using Eq. 2.22 and Eq. 2.23 to

$$\left(\frac{d}{dt} n_{\text{dens}}(m, \vec{p}) \right) = T^2(t) \times \int_{m_p} \int_{m_t} \int_{\vec{p}_p} \int_{\vec{p}_t} \dots dm_p dm_t d\vec{p}_p d\vec{p}_t, \quad (2.28)$$

with the terms within the integral omitted for clarity. So comparing Eq. 2.27 and Eq. 2.28 we find that

$$\frac{d}{dt} n_{\text{dens}}(m, \vec{p}) \propto T^2(t) \propto \dot{T}(t), \quad (2.29)$$

The solution to this equation is

$$n_{\text{dens}}(m, \vec{p}) = \frac{n_{\text{dens},0}(m, \vec{p})}{1 + t/t_0}, \quad (2.30)$$

where t_0 is taken to be the collisional lifetime of the largest planetesimals. This relies on the collisional equilibrium, i.e. the idea that the material produced by the objects entering the cascade is equal to the amount lost at the lower end of the population. This means that the overall dust in disc stays constant as long as the largest objects have not participated in the collisional cascade (Wyatt et al., 2007a; Löhne et al., 2008). Staying true to keeping this model simple we only use the radial distance to the star

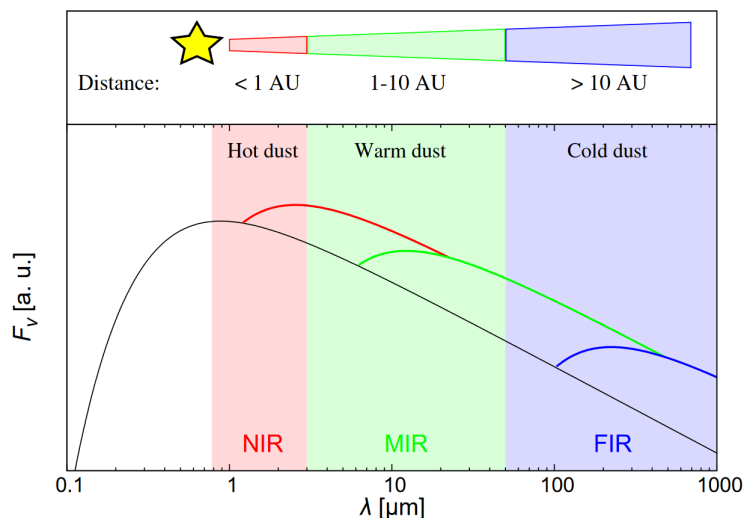


Figure 2.3.: Sketch of debris disc spectral energy distributions (SED) at different temperatures and their expected distance and wavelength regime (Kirchschlager et al., 2017).

for the orbital parameters and use a simple power-law size distribution. The resulting distribution

$$n_{dens}(r, s) = n_{dens,0} \left(\frac{r}{\text{AU}} \right)^{-p} \left(\frac{s}{\text{m}} \right)^{-q} \quad (2.31)$$

can now be combined with its temporal evolution to describe the disc's evolution with Eq. 2.4 to Eq. 2.6. We now have to connect these model descriptions to observations.

2.7. Links to observations

The dust produced in collisions is mainly observed in thermal emission as seen in Fig. 2.3. Since we already have a description of the size distribution we can derive the emission of the population by first looking at the emission of a single body.

This emission is given by

$$F_{\nu,em}(T, \lambda, r, s) = 4\pi s^2 Q_{abs}(\lambda, s) \pi B_{\nu}(T, \lambda) \quad (2.32)$$

with Q_{abs} denoting the absorption efficiency at a given wavelength λ and particle size s and $\pi B_{\nu}(T, \lambda)$ being the flux emitted by a body of the temperature T over a unit area. The absorbed radiation by such a grain can then be given by

2.7. LINKS TO OBSERVATIONS

$$F_{\nu,\text{abs}}(\lambda, r, s) = \pi s^2 Q_{\text{abs}}(\lambda, s) \pi B_{\nu,\star}(T_{\star}, \lambda) \left(\frac{R_{\star}}{r}\right)^2. \quad (2.33)$$

Here $\pi B_{\nu,\star}(T_{\star}, \lambda)$ gives the emission by the star per unit area and the factor $(R_{\star}/r)^2$ upscales the radiation from the stellar surface with radius R_{\star} to the position of the dust particle at distance r .

Using the assumption that the disc can be seen as optically thin, so that the dust grains are all equally illuminated by the star, Eq. 2.32 can be used to calculate the fractional luminosity, the ratio of disc to stellar luminosity, as

$$f_{\text{d}} = \frac{L_{\text{d}}}{L_{\star}} = \frac{2\pi \sin(\varepsilon)}{L_{\star}} \int \int \int r F_{\nu,\text{em}}(T, \lambda, r, s) n(r, s) d\lambda dr ds. \quad (2.34)$$

where ε is half the opening angle of the disc. Only two dust parameters are needed for the above formula to be applicable: the dust temperature, which can be read from the disc SED, and the position of the dust, which is a little bit harder to determine. Assuming the dust grains to be perfect blackbodies ($Q_{\text{abs}} = 1$), one can calculate the distance of the disc from its star using its temperature

$$\frac{r_{\text{BB}}}{1 \text{ AU}} = \left(\frac{278.3 \text{ K}}{T_{\text{BB}}}\right)^2 \left(\frac{L_{\star}}{L_{\odot}}\right)^{1/2} \quad (2.35)$$

where r_{BB} is called the blackbody radius. The assumption that the dust grains behave like perfect blackbodies, however, is not quite correct. Numerous works have shown that the grains diverge from the blackbody emission (Booth et al., 2013; Kennedy & Wyatt, 2014; Pawellek et al., 2014). One way to alleviate the discrepancy, is by using what is known as the modified blackbody model (Backman & Paresce, 1993). It takes into account that the absorption and emission is less efficient for longer wavelengths by setting

$$Q_{\text{abs}} = \begin{cases} 1, & \text{if } \lambda \leq \lambda_0 \\ (\lambda/\lambda_0)^{-\beta}, & \text{otherwise.} \end{cases} \quad (2.36)$$

there, β is the opacity index and is a free parameter for fitting purposes, while λ_0 is the wavelength corresponding to the grain size via $s = 2\pi \lambda_0$. Another way to infer a more accurate radius from the blackbody temperature is by applying the formula from Pawellek & Krivov (2015). They analyzed a set of resolved debris discs and found that the ratio of the resolved radius and the blackbody radius, Γ , can be described by a

CHAPTER 2. FUNDAMENTALS OF DEBRIS DISCS

formula dependent on the stellar luminosity:

$$\Gamma = A \left(\frac{L_{\star}}{L_{\odot}} \right)^B. \quad (2.37)$$

with the coefficients A and B being dependent on the material. Pawellek & Krivov (2015) gives a table of these parameters for a multitude of material compositions. This is an easy correction to a blackbody radius.

The true radius of the disc can be determined more reliably by resolving the disc. So far over 150 debris discs have been resolved at various wavelengths ¹. In such an image more detailed structures like clumps, asymmetries and gaps are evident, which are impossible to deduce from the SED. Radial profiles obtained from such images open up new avenues of comparing observations with modelling results. Debris discs are generally seen at an angle so that for accurate profile comparisons, transformations factoring in the inclination of the disc and point-spread function (short: PSF) of the instrument are needed. Another way to collect more information about debris discs is observing them in the scattered light. Because of the general structure of a disc a certain amount of the scattered light is expected to be polarized, which can give information on the size, material and porosity of the dust material (e.g. Schüppler et al., 2015). Scattered light observations were not considered in this work. With the basics out of the way, we can now delve into the main body of work.

¹<https://www.astro.uni-jena.de/index.php/theory/catalog-of-resolved-debris-disks.html>

3. Asteroid belt analogues

(The following chapter is based on the work done in Geiler & Krivov (2017). I did the implementation of the model from Löhne et al. (2008) and the interpretation of the results with guidance by Alexander V. Krivov.)

Trying to identify an asteroid belt analogue for one particular system has already been done in detail by Schüppler et al. (2016). They used **ACE** to model the q^1 Eridani two-component system in a way analogous to the solar system. This means a set of giant planets forms within a protoplanetary disc, they stir the remaining material on either side of the set and prevent other planets from growing. Simultaneously the planets remove material from their orbit, opening up a gap. On either side of this gap, the now stirred planetesimal populations evolve separately from one another. The analysis of Schüppler et al. (2016) is extensive and in-depth, but also very time consuming and work intensive and thus not suited for an application to a suite of DDs. With the analytical model from Löhne et al. (2008), we are able to systematically check the sample of unresolved discs from Chen et al. (2014) and perform a statistical analysis.

3.1. Sample

Chen et al. (2014) published the spectral data of a total of 571 main-sequence stars with ages up to a few Gyrs. They tested these with a zero-, one- or two-blackbody model and chose the most probable with Bayes theorem. In doing so they weighted the measurements of each star, giving a higher confidence to the Spitzer/MIPS $24\ \mu\text{m}$ and $70\ \mu\text{m}$ data than to the Spitzer/IRS spectra. In the end 333 systems showed a two-component-blackbody solution to be the most plausible, but 72 of these reached the higher bound (500 K) or lower bound 30 K of the temperature fit and were consequently excluded.

We took the 261 remaining debris discs. For all of them, we have a set of stellar parameters (mass, luminosity, age) and a set of derived debris disc parameters (fractional luminosity and dust temperature), both sets of which were derived in a uniform manner. The only change to the data from Chen et al. (2014), was done to the debris

CHAPTER 3. ASTEROID BELT ANALOGUES

disc radii. Chen et al. (2014) derived the blackbody temperature from the SED modeling and deriving the blackbody radius from this is not necessarily the real radius. We applied the correction formula Eq. 2.37 from Pawellek & Krivov (2015) as

$$\Gamma = 5.42 \left(\frac{L_{\star}}{L_{\odot}} \right)^{-0.35}, \quad (3.1)$$

with the coefficients as appropriate for compact dust grains composed of astrosilicate (Draine, 2003) and ice (Li & Greenberg, 1998) in equal parts. This choice is rather arbitrary, as there is no way to determine the composition in these systems, but the results would not change drastically when incorporating moderate porosity or carbonate inclusions. So we use the blackbody temperature from Chen et al. (2014) to calculate the blackbody radii of both warm and cold component and correct them with the Γ -factor.

After discarding some components for being too hot or too cold, we can refine our sample even further by investigating the relation between the two components. A component being too bright compared to the other or both having similar temperatures can call a two component solution into question. Kennedy & Wyatt (2014) investigated this problem and introduced two ratios to quantify the relation between the warm (“w”) and cold (“c”) components: $R_T \equiv T_w/T_c$, the ratio of temperatures, and $R_f \equiv f_w/f_c$, the ratio of fractional luminosities. Now assuming a central star and a typical cold component, one can test the various values of R_f and R_T for different warm components. For each case a SED is calculated and each data point is matched with the measurement uncertainties typical for the observation instruments most commonly used for this data. Finally one tries to model a one-component SED to the data set and the discrepancy between the best fit and the data can be used to infer how prominent the two component structure is. Typically the reduced χ^2 -value is chosen as a measure of this discrepancy and we choose $\chi^2 = 5$ as the limit, under which a second component is deemed too unreliable. In contrast a second component is deemed reliable when the χ^2 -value is higher than 5.

Visualisation of the results is shown in Figs. 3.1 and 3.2. Figs. 3.1 depicts the systems in the R_f – R_T plane, clearly showing when the ratios exceed our limits, whereas Fig. 3.2 shows them in the f – r plane, giving a comprehensive view of the spatial distribution of the discs. With this new round of testing we lose another 29 systems, leaving us with 232 systems.

Surely there are still systems in the sample that only contain a single component, as the test is not infallible. Most notably, Kennedy & Wyatt only consider the ratios of

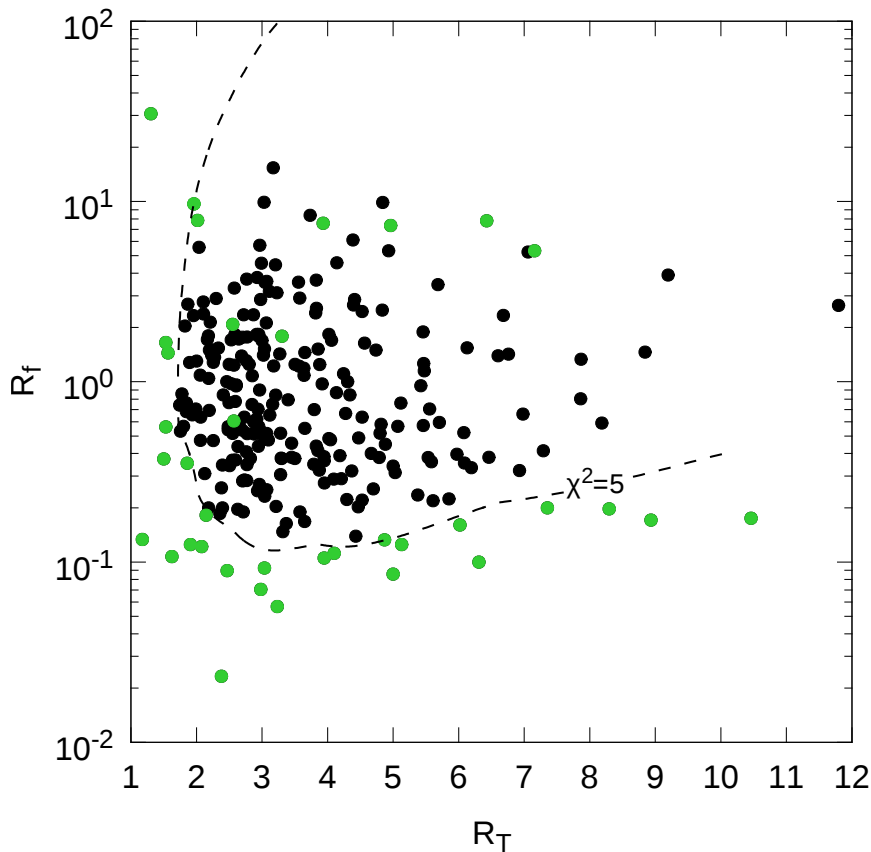


Figure 3.1.: $R_f = f_w/f_c$ plotted over $R_T = T_w/T_c$ for the sample. The line is calculated with the method described in Kennedy & Wyatt (2014) and in the text. Assumptions made: a star with $L = 9 L_\odot$ (the log-averaged value for the sample), a cold component at $r_c = 100$ AU with $f_c \approx 10^{-4}$, and warm components with various r_w and f_w . For each artificial system, we simulated measurements at 13 wavelengths from a few μm to sub-mm, each with a 5% error. The reduced χ^2 -values are gathered from the results of attempting to fit a single component to the fiducial measurements. Systems with $\chi^2 < 5$ imply a single component model to be plausible; $\chi^2 \geq 5$ solidifies the need for a second component. The two component solution for systems with $\chi^2 < 5$ and systems with $f_c < 4 \times 10^{-6}$ is deemed to be too uncertain. The affected systems are shown in green.

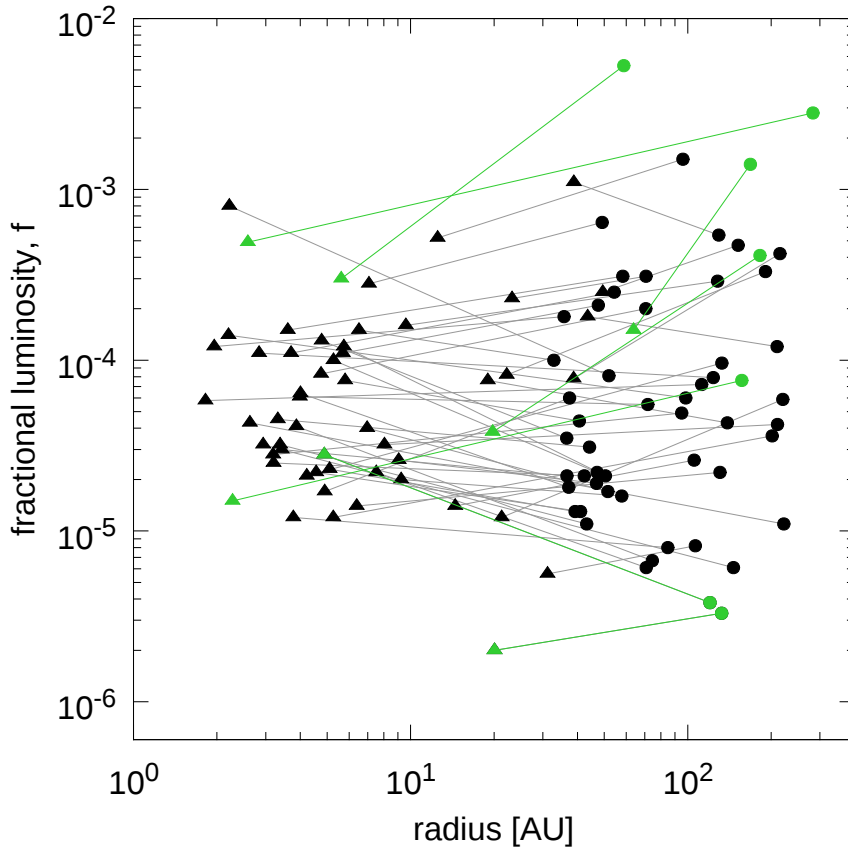


Figure 3.2.: Radius–fractional luminosity plane with the two component systems in our sample, cold (circles) and warm (triangles) components from a system are connected with a straight line. Black symbols denote systems that passed all additional tests we put them through ($\chi^2 \geq 5$ and $f_c > 4 \times 10^{-6}$), while green shows systems that failed in one or more cases ($\chi^2 < 5$ or $f_c < 4 \times 10^{-6}$). To keep the diagram readable, we chose to depict roughly a fifth of the entire sample.

observables and not their absolute values. To exclude systems with two very faint components, which should not be classified as reliable, to be considered, we decided to cut systems where the cold component was lower than the sensitivity limit of Spitzer/MIPS at $70\ \mu\text{m}$ ($f_c < 4 \times 10^{-6}$, Bryden et al. 2006). This affects another seven systems, leaving the sample with 225 systems that we consider to be reliable two-component discs. These are plotted in Figs. 3.1 and 3.2 in black, while green shows the systems cut from the sample.

3.2. Model

Fig. 3.3 shows the underlying ideas for this part of the work. We describe each component in a two component debris disc with set of parameters: both discs have a relative width dr/r , a radius $r_{w/c}$ and a fractional luminosity $f_{w/c}$. To have two collisionally evolving discs, both need to come from a protoplanetary disc. Since two different protoplanetary discs within one system are irreconcilable, we need a single protoplanetary disc to explain both components. In our model we consider a protoplanetary disc extending from r_w to r_c , in which an arbitrary mechanism opens up a gap. Obviously the most exciting choice is a planet clearing its orbit, but the actual mechanism does not need to be specified. After the clearing of the gap both components evolve separately, meaning gas dispersal, ignition of the cascade and depletion of both discs happen simultaneously. Now we search for a protoplanetary disc, out of which two debris discs can be cut, which in turn collisionally evolve to reach the observed fractional luminosities f_w and f_c by the time t . t is the (collisional) age of the system and we set it to be equivalent to the stellar age. We are interested in whether this scenario is viable for the systems in the sample and if so, for which parameters of the protoplanetary disc.

To check this hypothesis, we need a model that can be applied to 225 systems and give results within a reasonable time frame. ACE is not appropriate as it is a time intensive modelling procedure, the analytical model of Löhne et al. (2008), on the other hand, can be quickly applied to many systems. Before a more specific description of that model is given, we need to be clear on the parameters we have and the ones we want to vary. Since we have two observables, the fractional luminosities of both the warm and cold component, to which we can compare the results of the model, we cannot vary more than two parameters. Other free parameters will either need to be fixed to typical values or a few educated guesses have to be tested, depending on how much we actually know of these parameters. This leaves us with these two equations

$$f_c = f(t, r_c, c_1, c_2), \quad f_w = f(t, r_w, c_1, c_2), \quad (3.2)$$

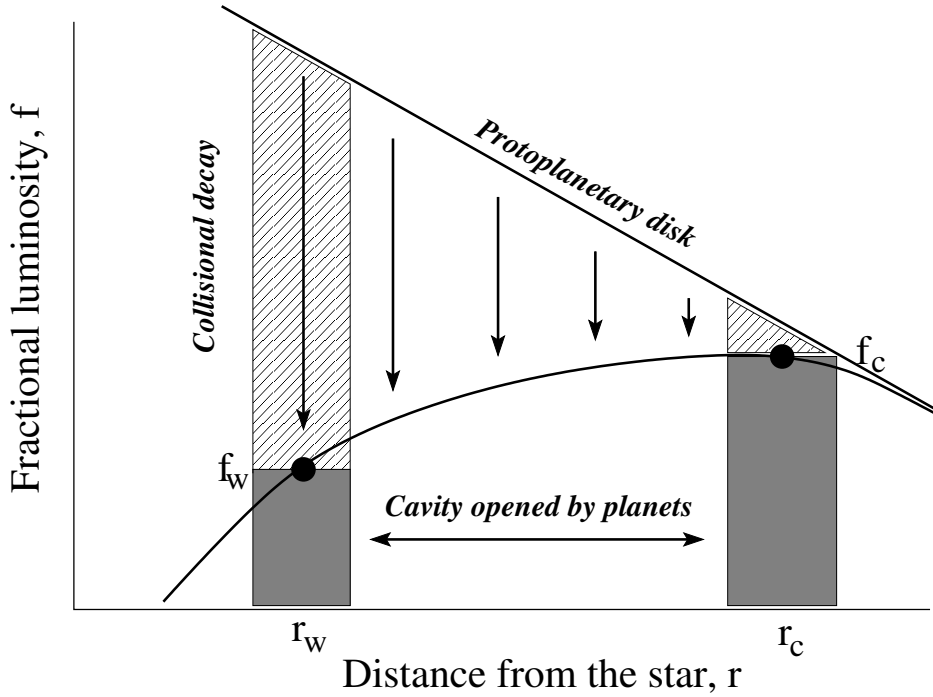


Figure 3.3.: Formation of a two-component debris disc.

to be solved for c_1 and c_2 , the two parameters we can afford to vary freely.

The reasoning behind the two parameters is as follows. As a standard model for describing a protoplanetary disc we use the “Minimum-Mass Extrasolar Nebula” (MMEN; Kuchner 2004) of the form:

$$\Sigma(r) = x_{\text{scal}} \Sigma_0 \left(\frac{r}{1 \text{ AU}} \right)^p \quad (3.3)$$

with $\Sigma_0 = 1 M_{\oplus} / \text{AU}^2$ being the surface density of solids in the Minimum-Mass Solar Nebula (MMSN; Weidenschilling 1977; Hayashi 1981). In this formula x_{scal} and p take on the role of the free parameters c_1 and c_2 . An alternative parameter to x_{scal} is the total mass of the protoplanetary disc M_{PPD} , that is defined by Eq. (3.3) integrated from the radii r_w to r_c :

$$M_{\text{PPD}} = 100 \times 2\pi \int_{r_w}^{r_c} \Sigma(r) r \, dr, \quad (3.4)$$

where the factor 100 is chosen as the canonical gas-to-dust ratio (Hildebrand, 1983). In summary, we seek a mass and slope for an extended protoplanetary disc, the edges of which reach the observed values of fractional luminosity after collisionally evolving over the systems age.

To describe the collisional evolution, we use the model of Löhne et al. (2008). It

generally follows the idea presented in the second half of Section 2.6.3, but with a crucial addition to assumed size distribution, by addressing the idea that the entire population is not part of the collisional cascade at all times. Different sized objects will have different collisional lifetimes (Wyatt et al., 1999; Wyatt & Dent, 2002). So at any given point during the lifetime of the system, there may be objects larger than a specific time dependent size s_t , that have not yet experienced collisions, i.e. their collisional lifetime is larger than the system's age. With time s_t will be larger than the largest objects s_{\max} , meaning the entire population is involved in the collisional cascade. Up until this point the distribution of material above the size s_t are still following the primordial distribution of $n(s) \propto s^{3q_p-2}$, with q_p being the primordial slope of the mass distribution. Following Löhne et al. (2008), we chose $q_p = 1.87$. Now introducing Eq. 2.7 we already discussed two different distributions described by this equation: the strength regime following $n(s) \propto s^{3q_s-2}$ and the gravity regime following $n(s) \propto s^{3q_g-2}$. The limit in between these two distributions is the break size s_b , resulting in the two regimes extending from s_{\min} to s_b (strength) and from s_b to s_{\max} (gravity). s_{\min} is smallest size present, usually set to the blowout limit discussed in section 2.4.1, and s_{\max} is the largest size within the population. The slopes for each regime are derived from the b 's in Q_D^* as (O'Brien & Greenberg, 2003)

$$q_{s,g} = \frac{11 + 3b_{s,g}}{6 + 3b_{s,g}}. \quad (3.5)$$

Up to now we are left with three distinct size distributions: the strength regime, gravity regime and the primordial regime. The transition size between the latter two is still not defined.

To remedy this we require a method to describe s_t . As a simplification we regard all objects of size s to enter the collision at the same time $t(s)$ as described in Wyatt et al. (2007a)

$$t(s) = \frac{4\pi}{\sigma_{\text{tot}}} \left(\frac{s}{s_{\min}} \right)^{3q_p-5} \frac{r^{5/2} dr}{(\mathcal{G}M_\star)^{1/2}} \frac{I}{f(e, I)G(q_p, s)}, \quad (3.6)$$

where σ_{tot} is the total initial cross section of the entire population, r the distance to the star, dr the disc width, e and I the orbital eccentricity and inclination of objects (we assume $e = I/2$), s_{\min} the smallest grain size, \mathcal{G} is the gravitational constant, and M_\star the stellar mass. The function $f(e, I)$ is given by $f(e, I) = (1.25e^2 + I^2)^{1/2}$ and $G(q, s)$ is taken from Löhne et al. (2008, Eq. (24)). The latter provides the number of particles able to disrupt the target particle of size s . It introduces the factor $X_c(s)$, the ratio of the size of the smallest projectile, that can disrupt a target, and the size of

CHAPTER 3. ASTEROID BELT ANALOGUES

that target s :

$$X_c(s) = \left(\frac{2rQ_D^*(s)}{f(e, I)^2 \mathcal{G}M_\star} \right)^{1/3}. \quad (3.7)$$

Combining these equations, we can now calculate the time t at which an object of size s will enter the collisional cascade and also the other way around we can find the size s_t separating primordial and evolved populations at a given time t .

Overall the following size distribution takes shape:

$$n(s, t) = n_{\max} \left(\frac{s_{\max}}{s} \right)^{3q_p-2} \quad (3.8)$$

for $s_t < s < s_{\max}$,

$$n(s, t) = n_{\max} \left(\frac{s_{\max}}{s_t} \right)^{3q_p-2} \left(\frac{s_t}{s} \right)^{3q_g-2} \quad (3.9)$$

for $s_b < s < s_t$,

$$n(s, t) = n_{\max} \left(\frac{s_{\max}}{s_t} \right)^{3q_p-2} \left(\frac{s_t}{s_b} \right)^{3q_g-2} \left(\frac{s_b}{s} \right)^{3q_s-2} \quad (3.10)$$

for $s_{\min} < s < s_b$,

assuming that $s_t > s_b$. For $s_t \leq s_b$, then collisions only occur in the strength regime, and s_b has to be replaced by s_t . If $s_t \geq s_{\max}$, then the entire population is involved in the collisional cascade and no part of the disc still follows the primordial distribution, and s_t has to be replaced by s_{\max} . With no new material entering the collisional cascade and the smallest grains leaving the system, the overall mass of the system decreases and with it the fractional luminosity of the disc. This is not directly captured in Eqs. (3.8)–(3.10), but stealthily hidden in n_{\max} .

One way to describe this, is with the time dependency of Eq. (2.30) creating:

$$n_{\max} = \frac{n_{\max}(0)}{1 + t/t_{\max}} \quad (3.11)$$

where $n_{\max}(0)$ is the number of objects of the largest size at the start of the evolution and t_{\max} , being the collisional lifetime of these largest objects, can be obtained from Eq. (3.6) by replacing q_p with q_g and s with s_{\max} .

Now we can calculate the evolution of the dust luminosity with

$$f_d(t) = \frac{1}{4\pi r^2} \sigma(t) = \frac{1}{4\pi r^2} \pi \int_{s_{\min}}^{s_D} n(s, t) s^2 ds, \quad (3.12)$$

where the integration limits only go up to $s_D \sim 1$ mm as the contribution of larger objects to the cross section is negligible. As a final hurdle we need to express $n_{\max}(0)$

Table 3.1.: Changes to Eq. (3.13) depending on the evolutionary stage.

Stage of evolution	Replace	With
$s_t \leq s_b$	s_b	s_t
$s_b < s_t < s_{\max}$	-	-
$s_{\max} \leq s_t$	s_t	s_{\max}

with known quantities, a convenient way is through the initial mass of the evolving disc $M_{\max}(0)$ (Löhne et al., 2008, Eq. (29)). Yielding the fractional luminosity as:

$$\begin{aligned}
f_d(t) = & \frac{6 - 3q_p}{16\pi\rho r^2 s_{\max}^4 (q_s - 5/3)} \left[1 - \left(\frac{s_{\max}}{s_{\min}} \right)^{3q_p - 6} \right]^{-1} \\
& \times \frac{M_0 s_b^3}{1 + t/t_{\max}} \left(\frac{s_{\max}}{s_t} \right)^{3q_p - 2} \left(\frac{s_t}{s_b} \right)^{3q_s - 2} \\
& \times \left[\left(\frac{s_b}{s_D} \right)^{3q_s - 5} - \left(\frac{s_b}{s_{\min}} \right)^{3q_s - 5} \right], \tag{3.13}
\end{aligned}$$

with ρ being the bulk density of the material. As with the size distribution equations (Eqs. 3.8)–(3.10), this equation is only valid in the range of $s_b < s_t < s_{\max}$. Tab. 3.1 shows the different stages of evolution and what changes are required for the equation to stay valid.

3.3. Results

We now used the model and searched for the set of parameters (p , x_{scal}) that produce the best solutions for a set of combinations of dr/r and e . Of the 225 systems examined we found good fits for 220 of them. A good fit is defined here as a fit where the quadratic sum of the relative deviations of modelled fractional luminosities and observed ones is smaller than 10%.

Fig. 3.4 shows the histogram of the exponents p of good fits in black and bad fits in red. The resulting distribution is a slightly slanted with a sharp cut-off at $p = 0.5$ and a mean value of -0.93 ± 0.06 . Compared to the MMSN slope of $r = -1.5$ and the MMEN slope of $r = -1.6$ as derived from systems with super-Earth-type planets (Chiang & Laughlin, 2013). It is, however, comparable with slopes of protoplanetary discs found with submillimetre observations (Williams & Cieza, 2011, and references therein). The range and slant of the distribution may on the one hand stem from uncertainties inherent to observations or from imperfections in our approach, but on

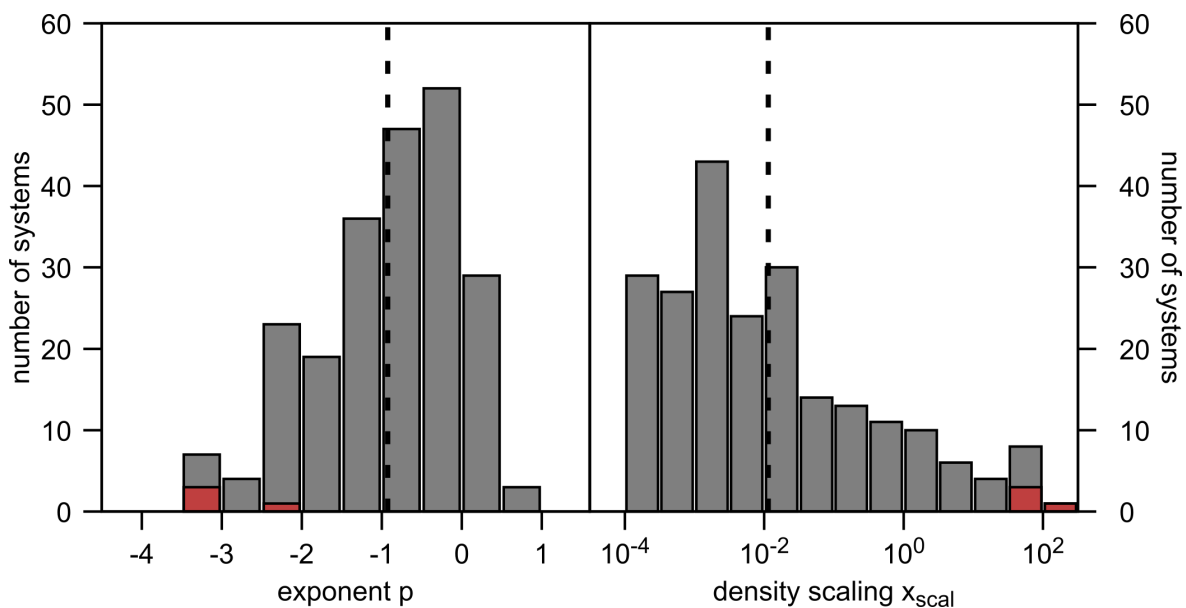


Figure 3.4.: Left: Histogramm of radial profile slopes p , right: Histogramm of scaling factors x_{scal} . Black: all systems with good fits, red: bad fits.

the other hand it may reflect that there is no singular slope to be expected. Raymond & Cossou (2014), for example, find a range of slopes in $-3.2\dots 0.5$ by creating MMENs from systems with multiple low-mass planets.

The same distribution histogramm is plotted for the density scaling parameter on the right side in Fig. 3.4. Its mean value is $x_{\text{scal}} = 10^{-1.94 \pm 0.10}$, although its significance is much lower here as the distribution is very broad and shows an almost monotone decrease with increasing x_{scal} . As x_{scal} was defined as the density at 1 AU it indicates the dust levels in the warm component. A larger amount of systems at the lower end of the distribution indicates that the warm components are too faint compared to the model. On the other hand, if a system requires a high x_{scal} , it indicates that the warm components are too bright compared to the model. All poor fits fail because of the warm component being too bright.

x_{scal} alone, however, is only an indicator of the mass in the innermost regions and not for the whole disc. Using a combination of a smaller density scaling x_{scal} and a larger (i.e. flatter) slope p , it is possible to create the same initial mass as when using a higher density and smaller (i.e. steeper) slope. This correlation between x_{scal} and p is shown in Figure 3.5. We can deal with this by analysing the initial mass of the protoplanetary disc M_{PPD} , thus incorporating the position of the two discs as shown in Eq. (3.4), instead of using x_{scal} . That this new parameter is nearly independent of the slope p can be seen in Figure 3.6.

The distribution of the protoplanetary disc mass to stellar mass, shown in Fig. 3.6,

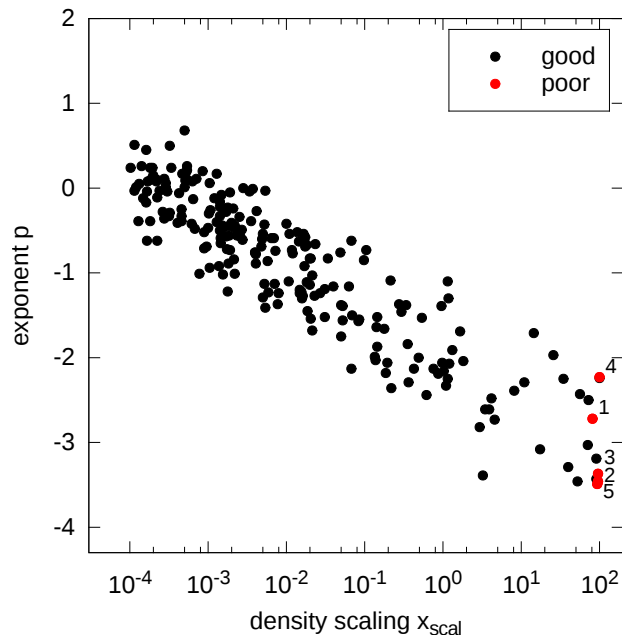


Figure 3.5.: Scatter plot of the scaling factor x_{scal} against the exponent p . Black symbols stand for the good fits and the red circles for the poor fits. The systems with poor fits are listed in Table 3.2.

is almost symmetric and centred at $M_{\text{PPD}}/M_{\star} = (2.0^{+0.3}_{-0.2}) \times 10^{-3}$. Changing the normalisation from the individual system’s stellar mass to the solar mass yields a similar distribution with a new mean mass of $M_{\text{PPD}}/M_{\odot} = (3.3^{+0.4}_{-0.3}) \times 10^{-3}$. Both values fall within the range of protoplanetary disc masses M_{PPD}/M_{\star} between 10^{-3} and 10^{-2} , obtained via sub-millimetre observations (Williams & Cieza, 2011). The obvious correlation to check is the one between M_{PPD} and M_{\star} . Due to the large scatter we could only suggest a subtle trend towards more massive discs around more massive stars, if any at all, thus not confirming the previously found correlation (see Williams & Cieza, 2011, and references therein). This discrepancy can also be attributed to the limited range of stellar masses in our sample.

3.4. Discussion

3.4.1. Good fits

A successful fit with our model does not rule out the possibility of other mechanisms. Instead of an asteroid belt the warm component could be created via transport of material from an outer belt. Kennedy & Piette (2015) describe the normal geometrical optical depth as created via dust transport, while also considering collisions during

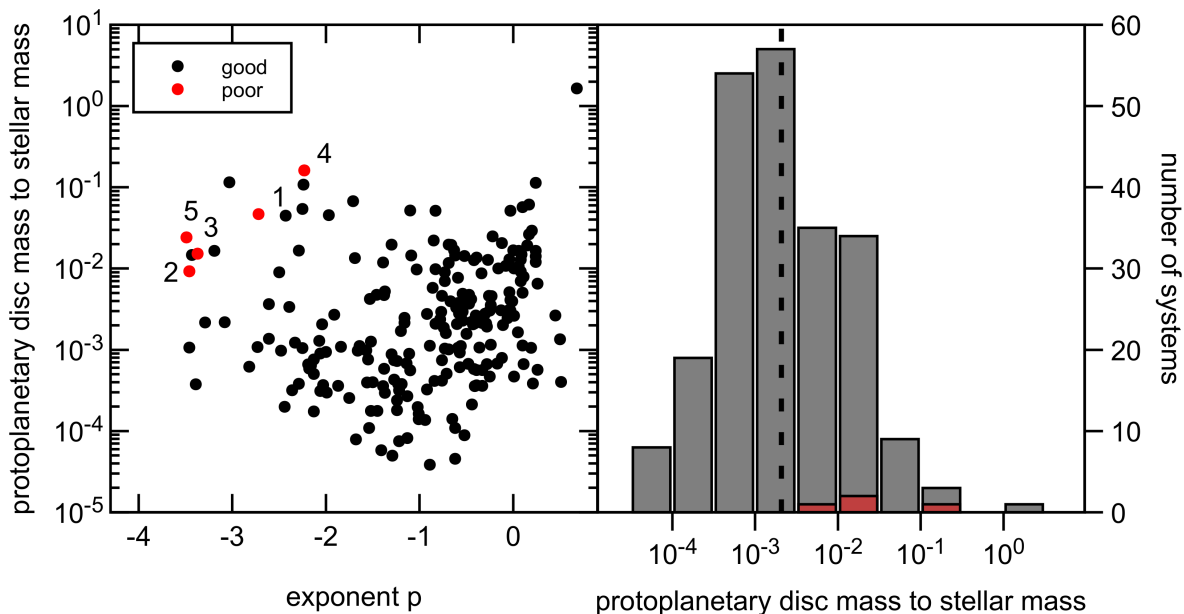


Figure 3.6.: Left: Total disc mass to stellar mass ratio M_{PPD}/M_{\star} and exponent p . The outlier in the top right is the ~ 5 Myr old system HD 36444 that may not be a debris disc, but rather a protoplanetary or transitional disc (Hernández et al., 2006). Poorly fit systems are listed in Table 3.2. Right: Distribution of the initial masses of the protoplanetary discs in units of stellar mass. For the gas to solids ratio in the protoplanetary disc 100 : 1 was chosen.

transport. They discussed different collisional rates of which we adopted the “low collisional rate” version to portray the highest dust levels for warm components in their study. Eqs. (1)–(2) from Kennedy & Piette (2015) were transformed into fractional luminosity via $f = (1/2)(dr/r)\tau$, where $dr/r = 0.1$ was assumed. Transcribing this in to the R_f – R_T plane reveals the warm components that can be the result of dust transport. We discuss a total of six different cases with a cold disc at either $r_c = 100$ AU or 30 AU and a fractional luminosity of $f_c = 10^{-4}$, 10^{-5} , or 10^{-6} in Fig. 3.7.

With this model we conclude that only a 4 out of 220 systems were compatible with the dust transport scenario and that these were all systems with two very faint components. So most systems are not plausibly created by transport alone. The Kennedy & Piette (2015) model, however assumes that P-R drag to be only force responsible for the inward drift of dust, which is only true for stars with a luminosity of at least equal to or higher than the sun. As such, stars with strong stellar winds, i.e. late-type stars, can have a stronger drag force and higher levels of transported dust (Plavchan et al., 2005) and indeed we have seen systems where this was successfully shown to create warm components (see, e.g. Reidemeister et al., 2011; Schüppler et al., 2014, 2015). Our sample however only has a small number of late type stars, so that transport can

only be used as the cause for some but not the majority of the warm components.

So far we have not considered the possibility of comets supplying the dust in warm components. Unfortunately, as both the asteroid scenario as well as the cometary dust production assume the dust to be produced where it is observed, it is hard for us to distinguish between the two with our modelling.

Take for example the asteroid belt in our solar system. It is so faint that it would not be observable with the current instruments (e.g. Booth et al., 2009; Greaves & Wyatt, 2010; Vitense et al., 2012), but if it were, it would exhibit a two-component structure (e.g. Nesvorný et al., 2010). Both components, the dust inside to Jupiter’s orbit and the dust outside of Neptune’s orbit, have fractional luminosities of $\sim 10^{-7}$ (Vitense et al., 2012; Roberge et al., 2012). At this low fractional luminosity level, collisions are negligible at dust sizes and applying our model will show a success of the asteroid belt scenario. As mentioned in Sec. 1.1 this is not necessarily true, as there is a significant amount of dust in the inner solar system produced by long period comets (Nesvorný et al., 2010). This confluence of different mechanisms contributing to the overall dust level is of course also a conceivable scenario for discs around other stars.

Having established that we cannot distinguish between the cometary and asteroidal sources of dust with our modelling, we seem to be left at an impasse, but re-examining the systems in our sample can alleviate some of our worries. The model of Marboeuf et al. (2016) describes a distance above which the dust production of comets via evaporation drastically decreases (s. their Eq. (19)). The value depends on the luminosity of the star. Roughly 37% from our warm components are located outside of their star’s respective critical distance. It is fair to assume collisions of comets at these distances are rare or at least not sufficient to support the warm components observed. For the other 63% we need to consider the scattering mechanisms for comets to reach that far into the inner system. Bonsor et al. (2012) showed that while transport of comets over large distances is possible, the architecture required has to be very specific. So this scenario very much hinges on the position of the warm component, but unfortunately the position of warm dust is not resolved for our sample. As a result we cannot definitively discard cometary origins for two thirds of our systems. Overall we can tentatively exclude the possibility of cometary origin for the other third.

To make more definitive statements we need additional information on the dust components. Interferometric and scattered light observations as well as thermal emission measurements over a range of wavelengths would improve our information on the size distribution and the material composition of both the warm and cold components. Another way is using spectra to find exocomets (e.g. Lagrange et al., 1987; Ferlet et al., 1987). With regular observations one can determine flux variations, individual

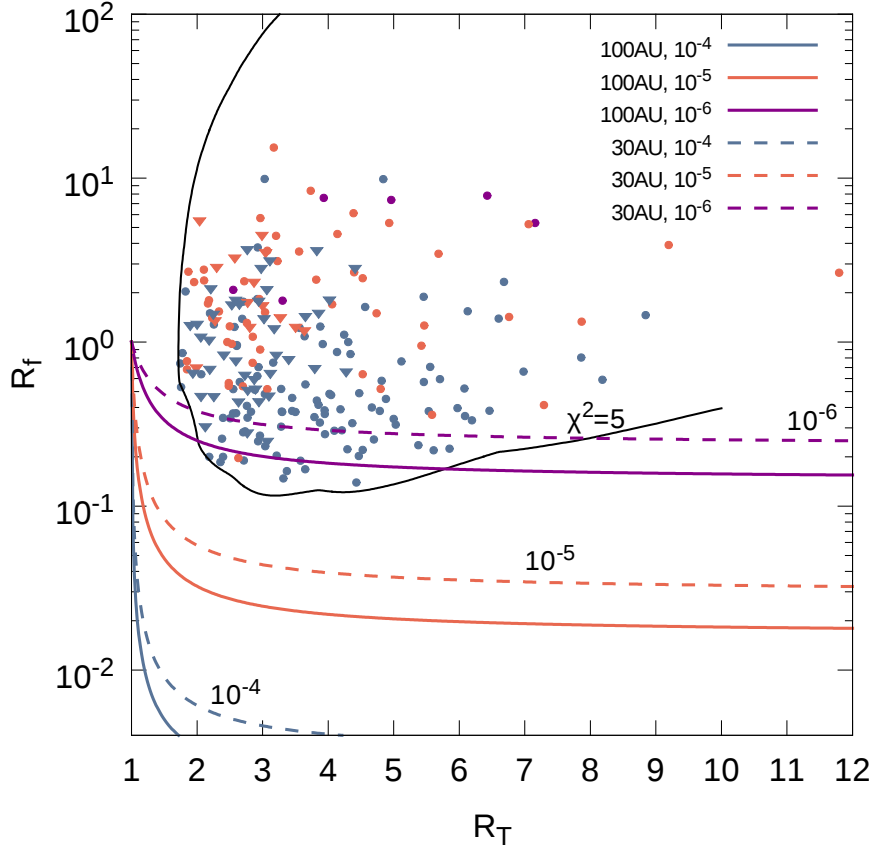


Figure 3.7.: Similar plot to Fig. 3.1, but only showing systems with good fits. Curves show the transported dust levels calculated by the Kennedy & Piette (2015) model for our assumed cold components. For all six cases the central star has a mass $1.8 M_{\odot}$ and each component has a relative width of $dr/r = 0.1$. Linestyles indicate the position of the outer component (solid: 100 AU, dashed: 30 AU), whereas the colours indicate the fractional luminosity of the outer component (magenta: 10^{-6} , orange: 10^{-5} , blue: 10^{-4}). Symbol shapes reference the disc radius (circles: $r_c > 50$ AU, triangles: $r_c < 50$ AU), while symbol colours again refer to their fractional luminosity (magenta: $\sim 10^{-6}$, orange: $\sim 10^{-5}$, blue: $\sim 10^{-4}$). Therefore a disc is compatible with the transport scenario if its triangle/circle symbol is below the solid/dashed line of the same colour.

Table 3.2.: Systems with poor fits.

No.	System	Radius [AU]		$f_{\text{obs}} \times 10^{-5}$	
		warm	cold	warm	cold
1	HIP 11486	3	89	4.6	4.0
2	HIP 23497	3	43	3.2	1.1
3	HIP 57971	3	42	4.6	1.8
4	HIP 85790	3	152	2.7	8.4
5	HIP 89770	2	20	7.9	14

dust releases (e.g. Wyatt et al., 2018) and even try to reverse engineer cometary orbits (Kennedy, 2018). This can give an overview of the dust production and whether it is enough to create the warm component observed, but it has to be done for each system individually. Increased knowledge of the planetary system can also impose a limit to how many comets reach the inner system, but this again has to be done case by case. Overall for a better differentiation more data and individual studies of each system are necessary.

3.4.2. Poor fits

The poor fits, five in total, all share one characteristic: they all inhabit the high x_{scal} and low exponent p (steep slope) range as seen in Fig. 3.5. Looking at the position of the warm component seen in Tab. 3.2 we can say that the warm components are atypically bright. The model cannot accommodate such bright discs at such small distances, as the collisional lifetime there is much too short. In an attempt to retain enough material more material is put into the warm components necessitating steeper slopes to keep the mass of the outer component the same. So while the outer components are reproduced, it is the warm components for which the model fails.

So we are left with two possibilities. Either we encounter a problem in the execution, some assumptions we made or the parameter ranges we probed are insufficient, or we deal with a fundamental problem in that the model truly cannot be reconciled with these systems. In other words we either have to reconsider the model or dust production via a steady-state collisional cascade like the asteroid belt is not the process supplying these warm components.

As a first step we critically reconsider the parameters. For example we could decouple the eccentricity of both components and allow for different eccentricities in each. A lower eccentricity in the inner component would slow down the collisions, lead to a

CHAPTER 3. ASTEROID BELT ANALOGUES

lower density and shallower slope overall. This would require a planet on an eccentric orbit stirring the outer component and planets on circular orbits carving the gap but having little to no influence on the inner component. Overall a strange architecture. In addition, we also checked what eccentricity would be needed for the warm component to maintain its dust and found values of the order of $e \sim 0.001$. At these values the collisional velocities are not high enough to cause destructive collisions (e.g. Krivov et al., 2013).

Besides the parameters of the disc, the material composition of the material in them can also influence the evolution. Harder materials have longer lifetimes. The ice line, the distance from the star at which temperature is low enough for water ice to form (~ 150 K), is commonly referenced when considering the growth of planetesimals and would allow for ice in the outer components, changing their composition. Warm components in our poor fits, however, are too close to their star to harbour any ice and thus this change would not affect their evolution. The maximum size of planetesimals was set arbitrarily, but decreasing it is on the one hand problematic as 100 km sized objects are needed for collisions to set in via self-stirring (Kenyon & Bromley, 2008) and larger objects have lifetimes of a few Gyrs and thus do not contribute significantly to the dust production in the systems discussed here. Dust production in our model is only due to destructive collisions, neglecting cratering collisions as a source completely. Although even with this restriction a vast majority of the systems are compatible with the model, lending credence to this approach as well as highlighting the distinctness of the systems where it fails. So because changing the parameters or the assumptions does not help or cannot be justified, the five systems seem to be special cases.

So locating these five systems in Fig. 3.8 and comparing their position to the Kennedy & Piette (2015) lines in Fig. 3.7 readily shows that transport is not sufficient for these discs. A number of alternatives have been proposed (see Section 7 in Matthews et al., 2014b, for a list of conceivable scenarios). Transient events like major collisions between large planetesimals (Song et al., 2005) or a sudden large influx of comets induced by planetary instabilities (Wyatt et al., 2007a; Booth et al., 2009).

There are other possibilities besides transient phenomena. As with the good fits, these poor fits can also be the result of cometary dust sources. In this case we need a planetary architecture that transports comets efficiently from the outer belt over long periods of time. How multiple planet scattering of comets works has been discussed, e.g. in Bonsor & Wyatt (2012), Bonsor et al. (2012), Faramaz et al. (2016). So the outer component provides the material for both the discs in the system. Comets do not necessarily need to be continuously scattered by planets, there can also be an extended population of comets on very eccentric orbits with periastra at the warm component

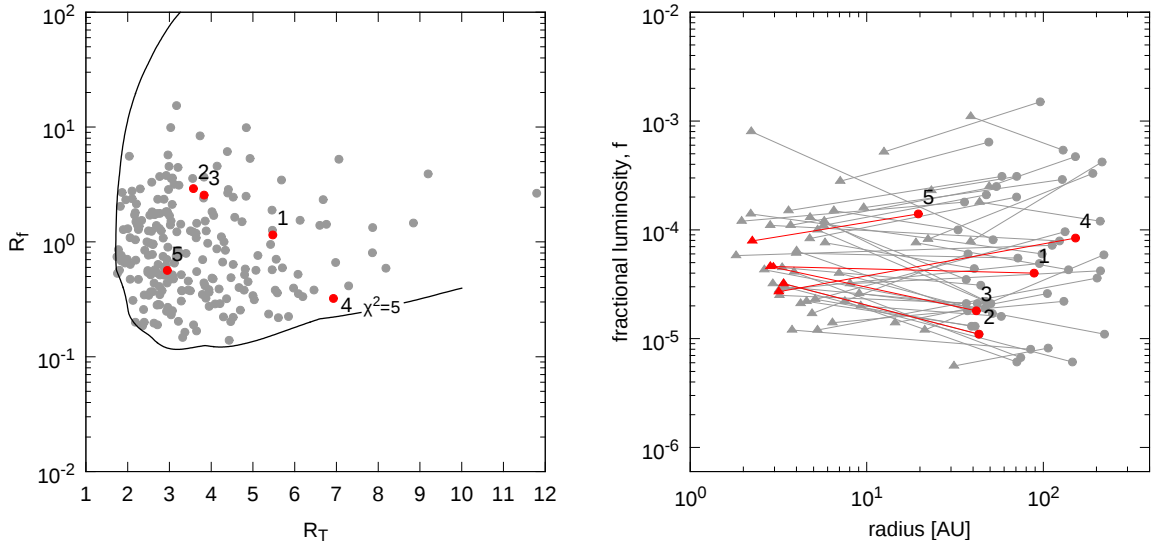


Figure 3.8.: Similar plot to Fig. 3.1 and Fig. 3.2, but only showing systems with good fits in grey and the five failed systems numbered as they are in Tab. 3.2 in red.

(Wyatt et al., 2010). There they would partially sublimate and disintegrate, releasing dust. Such a “mini-Oort cloud” would most likely arise from planet-planet scattering events (Raymond & Armitage, 2013).

All of these poorly fit systems are older than 1 Gyr with their inner component $\sim 2\text{--}3$ AU, and have a fractional luminosity of $(3\text{--}8) \times 10^{-4}$. With 5 out of 225 systems they make up roughly 2%, which is in agreement with other studies of atypically bright dust to be found in $\sim 2\%$ of systems (Bryden et al., 2006; Wyatt et al., 2007a; Ishihara et al., 2016). The only disc of these five previously identified as atypically bright is HIP 89770 (HD 169666, Moór et al. 2009). Discs that are considered as outliers by other studies except in our sample are ζ Lep (Moerchen et al., 2007) and q^1 Eri. The different categorization here can be attributed to different models used, as Schüppler et al. (2016) showed that q^1 Eri can be explained with a standard evolutionary scenario and the same may be true for ζ Lep. Additionally it was brought to our attention that HIP 11486 can also be explained with a single disc and that it slipped through our process to weed out such systems. This goes to show that different models lead to different interpretations of observations and how important detailed modelling and mindful use of data is.

4. Kuiper Belt analogues

(The following chapter is based on the work done in Geiler et al. (2019). The age estimate via the new Gaia-data was done by Mark Booth. I did the collisional modelling and lead the interpretation of the simulations in collaboration with Alexander V. Krivov, Mark Booth and Torsten Löhne.)

Beside the warm components with all their intriguing details as to their origin and underlying dust production mechanisms, the cold components mostly give rise to questions in different aspects. Since cold components, due to their large radii, are more easily resolved, we know that their dust is most likely produced by mutually colliding material. It is fair to call these discs Kuiper Belt analogues, both because of the dust production mechanism and the large radii. With more detailed knowledge, however, more detailed questions can be asked, e.g. how is the debris disc structured and what does this reveal about the system's history? Similarly to the Kuiper Belt where the scattered population and specific gaps in its structure reveal the violent history of the early solar system and the influence of Neptune, so too can we derive similar answers for extrasolar systems after doing extensive modelling for them. Since the modelling is time extensive we chose to only look at a single system.

That system is HR 8799, an F0V (Gray et al., 2003) star located 41.29 ± 0.15 pc (Gaia Collaboration et al., 2018) away from Earth with four directly imaged giant planets at projected distances of 27, 43, 68, and 15 AU (Marois et al., 2008, 2010). It also harbours a warm dust component (6 – 10 AU) and a Kuiper Belt analogue (> 100 AU, Sadakane & Nishida 1986; Su et al. 2009; Hughes et al. 2011; Matthews et al. 2014a; Booth et al. 2016).

Four giant planets at large radii confined by two dust components is a structure that brings up questions as to the stability of the planets' orbits as well as their formation history. The stability has been the topic of many dynamical studies (e.g. Reidemeister et al. 2009, Fabrycky & Murray-Clay 2010, Goździewski & Migaszewski 2009, Marois et al. 2010, Goździewski & Migaszewski 2014, Goździewski & Migaszewski 2018). The formation is puzzling in the sense that the two leading models of planet formation both have trouble accounting for all four of them. Neither core accretion nor gravitational instability can explain the planets of HR 8799 at the orbits they are observed (Marois

et al., 2010; Currie et al., 2011) without requiring additional mechanisms, like migration (Crida, 2009) and planet-planet scattering (Chatterjee et al., 2008). For both of these the debris discs are often mentioned as a way to facilitate the migration or dampen the orbits of scattered planets (Moore et al., 2013).

An in depth analysis might be able to give answers as to if the discs played either or both of these roles during planet formation. To answer this question and to better understand the structure of the discs, HR 8799 has been the target of many observations, sometimes with quite diverging results. Observations of the inner edge of the outer disc found it at both ~ 100 AU (Su et al., 2009; Matthews et al., 2014a) and at 145 AU (Booth et al., 2016). The large gap between the latter result and the outermost planet HR 8799b raises the question as to why this should be the case, as HR 8799b's chaotic zone is not wide enough to remove material at these distances, though an inner edge at ~ 100 AU is plausible (Matthews et al., 2014a). To clear up to the inner edge found by Booth et al. (2016) planet b would require an eccentricity of at least 0.3 (Moro-Martín et al., 2010). Alternatively a fifth planet as proposed by Booth et al. (2016) with a mass of $1.25 M_{\text{Jup}}$ and at 110 AU would sculpt the inner edge at that distance. The required mass decreases as the radius or the eccentricity of its orbit increases.

The outer edge of the cold component extends to roughly 300 AU in both the models of Su et al. (2009) and Matthews et al. (2014a) with a halo extending out to 2000 AU. They attribute the halo to the radiation pressure blowing out material. Booth et al. (2016) do not find this halo in the ALMA data and the outer edge is found to be at 450 AU. So both observations show the disc reaching over more than 200 AU, which poses a problem as to how the entirety of this disc became sufficiently stirred to lead to destructive collisions. Both the Kenyon & Bromley (2008) using Pluto-sized planets and the Krivov & Booth (2018) model using smaller planetesimals to stir the disc cannot account for stirring such a wide disc within the age of the system. So the disc is either a primordial disc (Heng & Tremaine, 2010; Krivov et al., 2013) or an additional stirring mechanism is required.

Previous models of this system's debris disc did not utilize a collisional model but empirical in nature. So we set out trying to model the disc while incorporating both the Herschel/PACS (Poglitsch et al., 2010) and the ALMA (Brown et al., 2004) observations, and interpreting the model in relation to the entire planetary system.

4.1. HR 8799

We already have a wealth of information on the system due to the many observations undertaken. First the infrared excess was discovered by IRAS (Sadakane & Nishida, 1986; Zuckerman & Song, 2004; Rhee et al., 2007), then a warm component by Spitzer/IRS (Jura et al., 2004; Chen et al., 2006; Su et al., 2009) and lastly the four giant planets by the Keck and Gemini telescopes (Marois et al., 2008, 2010). We specifically look at the data from Matthews et al. (2014a) and Booth et al. (2016), since they resolved discs at wavelengths dominated by the cold disc emission. From Matthews et al. (2014a) observations at 70, 100 and 160 μm are available and some additional SPIRE data. We chose to neglect the 160 μm and the SPIRE data as these were strongly affected by background emission and overall have poorer resolution. The ALMA observations were done at 1.34mm. These high resolution images at longer wavelengths are a good indicator of the position of larger grains, which are presumably closer to the planetesimals.

Both studies proposed models to explain the observations they were based on. To compare these models to each other we recreated them with the ACE code with the parameters given in the respective works. Unless stated otherwise we assumed populations of μm to km sized objects distributed between the inner and outer edge of the disc. For the material we used in this part of the work a mixture of astrosilicate (50%, Draine 2003), ice (Li & Greenberg, 1998), and vacuum (each 25%) with a bulk density of $\rho = 2.0 \text{ g cm}^{-3}$. Here vacuum serves as a substitute for porosity. With these “dummy models” we are able to create images not only for the observed wavelengths, but also for any other. It has to be noted that some divergence from the models is expected due to the different approaches to modelling the grains, with ACE being as close to the real grains as possible and the models using the streamlined modified blackbody approach.

One additional axis of comparison is the SED of the system. The photometry used for the HR 8799 system is presented with literature references in Tab. A.1. To transform the B , V , I magnitudes into flux values we used the standard calibration system of Johnson, while we used the calibrations of Cohen et al. (2003) to transform the J , H and K_S magnitudes from 2MASS. The stellar component was modelled with data from the PHOENIX model (Brott & Hauschildt, 2005) fitted by Matthews et al. (2014a).

To create the images we accounted for the dust and material properties to calculate the thermal emission, which was then convolved with a Gaussian Beam corresponding to the point spread function (PSF) of the respective instrument. We used normalised elliptical Gaussians with sizes of $5.8'' \times 5.5''$ for the 70 μm images, $6.9'' \times 6.7''$ for the 100 μm images and $1.3'' \times 1.7''$ for the 1340 μm images.

Next we compare these dummy models of Matthews et al. (2014a) and Booth et al. (2016) to their originals and how the extrapolated images fare with the observations.

4.1.1. Wide cold disc

In this model based on the PACS observations the disc extends from 100 AU up to 310 AU with a halo extending to 2000 AU (see Tab. 4.2). Planetesimals are unlikely to reach distances of up to 2000 AU and creating enough dust for it to be visible, which is why the halo has been attributed to radiation pressure blowing out small grains (Krivov et al., 2006). Peculiarly Matthews et al. (2014a) noted different temperatures for the main belt and the halo when comparing the $24\ \mu\text{m} + 70\ \mu\text{m}$ data to the $70\ \mu\text{m} + 100\ \mu\text{m}$ data. This could hint at two distinct populations of grains.

The brightness profiles in Matthews et al. (2014a) follow different slopes at different wavelengths, but since we utilize the optical depth distribution and not the surface brightness, we are allowed some leeway in adapting the radial slope of the dust. So we use the position of the disc, as given by Matthews et al. (2014a), but assume a single slope for the optical depth for all wavelengths. We chose this slope in such a way that the profiles best recreated the ones found in the observations (see Tab. 4.2). Since the halo is supposed to be consisting of small grains pushed out by radiation pressure, we set their minimum size to the blowout limit of $s_{\text{blow}} \approx 3\ \mu\text{m}$ (Burns et al., 1979) and the maximum size of the grains in the halo to three times that value. The halo in this dummy model however is not created by radiation (as in the Su et al. 2009 and the Matthews et al. 2014a models), but set to resemble a halo by distributing small grains in such a way. For each unknown parameter we assumed values that best reproduced the PACS data. We calculate the error bars as the root mean square of the azimuthally averaged flux within an annuli of a width of 1 pixel.

The resulting dummy model, as seen in red in Fig. 4.1, does well in recreating the Herschel data with only a small flux deviation in the $100\ \mu\text{m}$ profile. Shifting the gaze to the ALMA profile shows a somewhat different picture however. The peak flux is not only closer to the star but also much less pronounced than in the observations. While the peak position might be related to the position of the inner edge of the model, the lack of flux seems to be a fault inherent to the assumption of a small grain halo, as the SED is much too steep at longer wavelengths. This is contrast to the SED presented in Matthews et al. (2014a) as they fit the photometry data directly with a modified blackbody rather than following our approach of deriving the image and SED from one model. So larger grains might be able to remedy the problem, but then we require another mechanism to transport the grains to these distances, as radiation pressure is

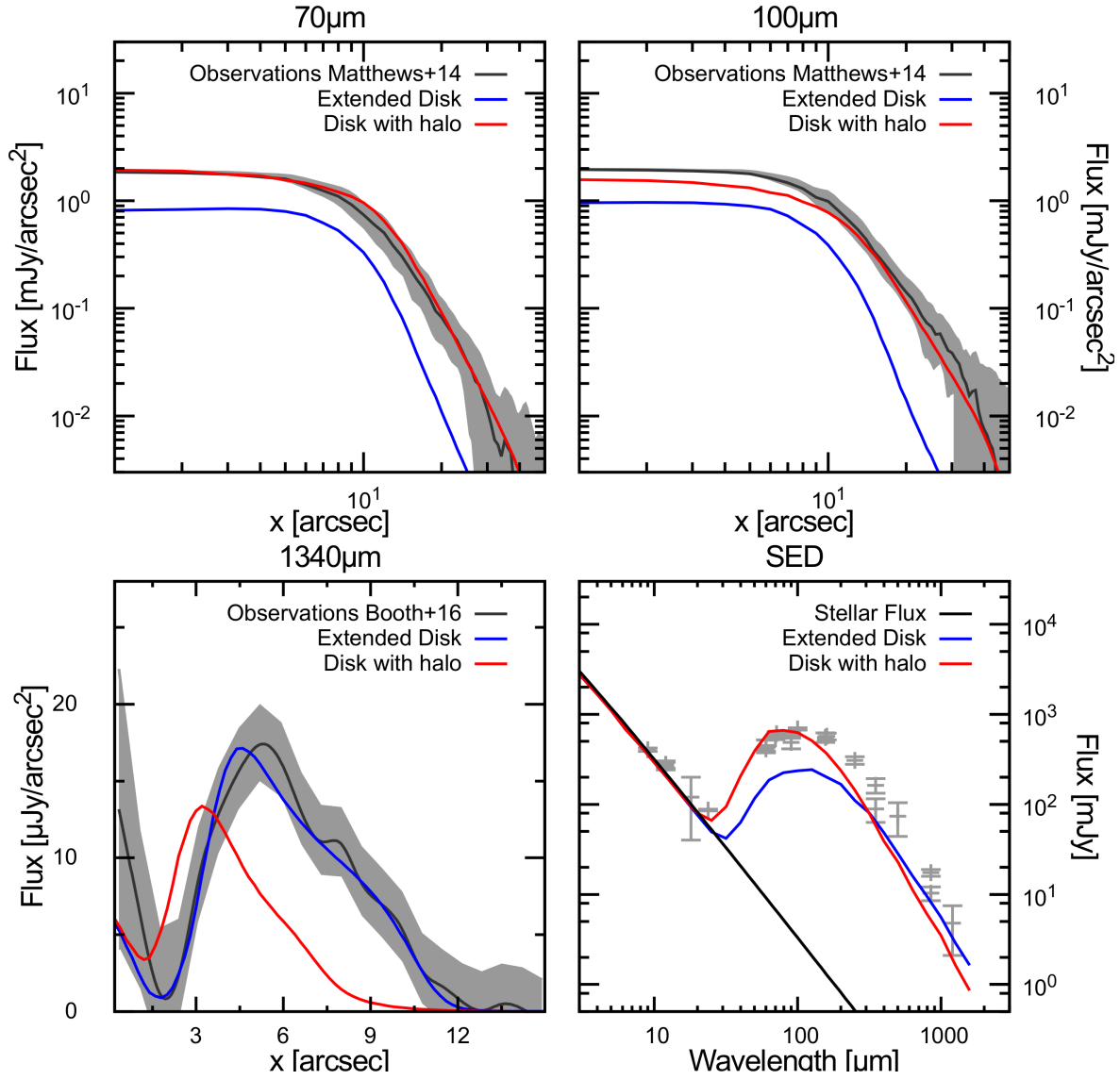


Figure 4.1.: Radial profiles at 70, 100, 1340 μm and the SED for the previously proposed system architectures. In black: observations and error bars (in grey). Red: a debris disc from 100 - 310 AU and a halo of small grains out to 2000 AU (Matthews et al., 2014a). Blue: a debris disc with planetesimals from 145 AU to 430 AU with eccentricities up to 0.1 (Booth et al., 2016).

not likely to be strong enough. In summary, we would need the inner edge further away from the star to shift the peak flux and we would need larger grains to increase the flux in the SED at higher wavelengths.

4.1.2. Disc with halo

The ALMA observations were done in Band 6 at $1340 \mu\text{m}$ by Booth et al. (2016). Their model set the inner edge of the disc at around 145 AU and the outer edge at 430 AU (see Tab. 4.2). In this data there is no sign of the halo, but this does not mean that the ALMA data contradicts the Herschel data in that regard. Observations at these wavelengths are more effective at probing larger grains, meaning that while we can be rather certain that planetesimals are at these ranges, we cannot rule out the existence of a small grain halo.

The radial profile of the model of Booth et al. (2016) was computed with the parameters given by them and can be seen in blue in Fig. 4.1. Again we chose any unknown parameters in a way to best represent the ALMA observations the model of Booth et al. (2016) was based on. The resulting images and SED are shown in Fig. 4.1. Our dummy model is in good agreement with the ALMA observations. Any small differences can be attributed to the different ways of generating the images. The PACS images show some discrepancies however as the profiles do not reach out far enough and have less flux than the observed radial profiles.

4.2. Collisional models

4.2.1. The ACE code

The `Analysis of Collisional Evolution`, `ACE` for short, is a C++-based code for the numerical analysis of the collisional evolution of a debris disc and has been in development for the better part of two decades (Krivov et al., 2005; Löhne et al., 2012b; Sende & Löhne, 2019). It solves Eq. 2.21 for each point in the phase space at each time step. This simple description hides the extensive calculations and the large number of parameters required. In addition to the orbit parameters and the overall mass of objects in a debris disc, the characteristics of the material themselves will have to be considered, as well as the star's attributes.

Disregarding the finer aspects, like the material and stellar parameters, we first focus on the calculation of the size distribution and the handling of collisions in the code. For our purposes we assume the disc to be uniformly distributed within a fixed

Table 4.1.: List of ACE parameters

Category	Parameter	Description	Standard Value
Star	M_\star	stellar mass	-
	L_\star	stellar luminosity	-
	\dot{M}_\star	mass loss rate	-
	v_{sw}	stellar wind speed	400 km s ⁻¹
Population	M_0	init. mass	-
	q_p	init. size distribution slope	1.87
	s_{max}	max planetesimal size	-
	p	init. radial surface slope	-
Orbit	$[a_{\text{min}} \dots a_{\text{max}}]$	range of semi-major axis	-
	$[e_{\text{min}} \dots e_{\text{max}}]$	range of eccentricity	-
	ε	max. orbital inclination	$e_{\text{max}}/2$
Planetesimal	ρ	bulk density	-
	$Q_{\text{D,s/g}}$	material strength	-
	$b_{\text{s/g}}$	material strength	-
	β	radiation pressure efficiency	-
	q_m	fragment size distribution slope	1.83

Notes: This table shows the essential physical parameters needed for the computation in ACE. Only the stellar mass and luminosity have a low uncertainty attached to them, as all other parameters are either unknown or hard to quantify. The standard values are all commonly used values. The stellar wind is based on the value from Ferreira et al. (2003). The initial size distribution q_p is derived from the modified value of Dohnanyi (1969) as seen in e.g. Durda & Dermott (1997). As the maximal orbital inclination was set to $e_{\text{max}}/2$ due to the energy equipartition relation (Greenberg et al., 1991). The standard value for q_m is the classical value (e.g. Dohnanyi, 1969; Fujiwara et al., 1977; Thébault & Augereau, 2007).

opening angle ε (maximum inclination $i = e/2$) and it to be rotationally symmetric in respect to each other angular argument (θ, Ω, ω) . The resulting distribution $n(m, q, e)$ is only dependent on the periastron q , eccentricity e and the mass m . Simplifying the dimensions of our phase space to three, we also limit the ability to simulate some dynamical phenomena, such as secular perturbation. The newest version of ACE is able to simulate planetary perturbations by including the longitude of pericenter $\tilde{\pi}$, but this increases the dimensions of the phase space and increases both the numerical diffusion and the total time needed for a simulation (Sende & Löhne, 2019).

ACE is using an exponential Euler integrator on a logarithmic grid of the parameters q , m and e . For the initial values in a run, only q and e are somewhat constrained

by resolved observations, while a good value for the initial mass has to be found over multiple simulation attempts. The code is capable of handling erosive collisions, like cratering and rebounding collisions, as well as disruptive collisions and handles all the dynamical effects like pressure and drag forces and gravity, following the formula laid out in Krivov et al. (2005). Once the changes in $n(m, q, e)$ are calculated, **ACE** transforms this value into the spatial number density $N(m, r)$, which gives the number of particles in a unit volume in the mass range from $[m, m + dm]$ at the given distance r .

4.2.2. Age of the system

The age of HR 8799 is still a hotly debated topic with the highest estimates being up to 1 Gyr (Moya et al., 2010) and the lowest estimates going down to 30 Myr (Zuckerman et al., 2011; Baines et al., 2012; Bell et al., 2015). Most estimates place the system’s age at 30 Myr up to 100 Myr with the HR 8799’s membership in the Columba moving group being one argument for values closer to 30 Myr (Torres et al., 2008; Zuckerman et al., 2011; Bell et al., 2015). We reevaluate the chance of HR 8799 being a member of the Columba group with the Banyan Σ code (Gagné et al., 2018) using the astrometry from Gaia’s 2nd data release (Gaia Collaboration et al., 2018) and a radial velocity of -12.6 ± 1.4 km/s (Gontcharov, 2006). The resulting membership probability is 48.7%, much lower than previous analyses using pre-Gaia data suggested (Zuckerman et al., 2011; Malo et al., 2013; Read et al., 2018). With the likelihood of HR 8799 being a member of the Colomba moving group reduced, we conclude that the system’s age cannot be better determined than 60_{-30}^{+100} Myr (Marois et al., 2008). In the following we assume the system’s age to be equal to the collisional age of the system.

4.2.3. Excited disc

As a first approach we placed the initial planetesimals on orbits with high eccentricities and semimajor axes, so that their periastra lie in between 140 – 220 AU. This was in an attempt to create a halo which was seen in the Herschel/PACS data but was missing in the corresponding dummy model. Any changes to the semi-major axis or the eccentricity were always done while keeping the periastra and the inner edge of the disc in mind. An example run is shown in red in Fig. 4.2 with its parameters in Tab. 4.2, which also features common problems we encounter with this setup. When comparing this model with the PACS data we see that the halo seen in Matthews et al. (2014a) is now represented in the image and the model is even overrepresenting its flux in the $70 \mu\text{m}$ image. In contrast to this we underrepresent the flux in the inner part of the

Table 4.2.: Parameters of some proposed disc components and our preferred model.

Parameter	Empirical Matthews+14	Empirical Booth+16	Excited disc	Wide Cold disc	Preferred Model
<i>1st Population</i>					
a [AU]	100 – 310	145 – 430	-	150 – 440	140 – 440
e	-	-	-	0.1	0.1
γ	1.0	0.6	-	0.6	1.0
<i>2nd Population</i>					
a [AU]	310 – 2000	-	360 – 440	-	360 – 440
e	-	-	0.5 – 0.6	-	0.3 – 0.5
γ	1.7	-	1.0	-	1.0

Notes: a stands for the semimajor axis, e is the eccentricity, and γ is the slope of the radial distribution of the optical depth with the form $r^{-\gamma}$. When referring to small grains, we specifically mean grains of a few μm up to a few 10s of μm , and large grains from $\sim 100 \mu\text{m}$ up to 1 cm.

disc, even more so in the ALMA data. The high eccentricity orbits cause the dust to be distributed over a larger area, leading to a much shallower optical depth distribution. Although the peak is in the correct position in the ALMA data it requires a lot of extra material to reach the levels observed. All this is contradicted by the SED that tells us to use less material. Another problem with this model are the high eccentricities, which are difficult to justify. Unable to explain the eccentricities and unable to resolve the mass contradiction without fundamentally changing the idea of the approach, we go on to change the ideas of the approach, as we conclude that this model is unable to explain the observations.

4.2.4. Wide cold disc

In the next approach we switch the approach from high eccentricity orbits in a narrow ring to a wide disc with low eccentricities similar to the model presented by Booth et al. (2016). After trying different eccentricities, initial masses and the position of the disc we finally settled for the values only marginally different from the model in Booth et al. (2016). Since the parameters here are not unique either, this small discrepancy between the two models is negligible. One example of this model is shown in blue in Fig. 4.2 and its parameters in Tab. 4.2. The shortcomings of this model were present in all the iterations we tried but in this version they are the least pronounced. Both the 70 and the 100 μm show that the profile is not stretched far enough and the profile literally falls

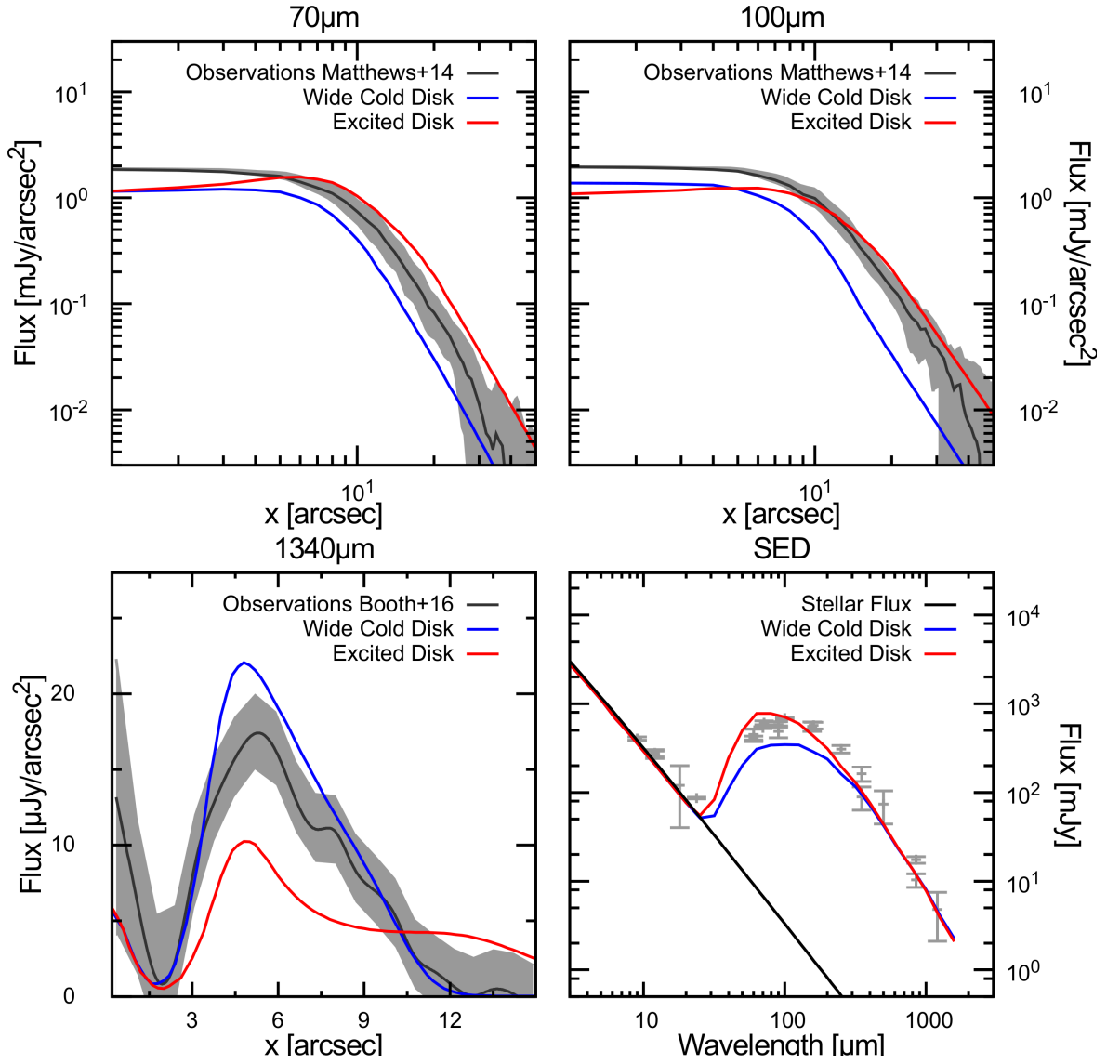


Figure 4.2.: Radial profiles at 70, 100, 1340 μm and the SED for the excited disc and a wide cold model. In black: observations and error bars (in grey). In red: an excited debris disc from 360 - 440 AU with eccentricities of 0.5 – 0.6. In blue: a debris disc with planetesimals from 150 AU to 440 AU with eccentricities up to 0.1.

short. If the halo does stem from radiation pressure, since we now incorporate the dust dynamics and thus also radiation pressure, the halo should be visible in this model, but we do not see it in the PACS data. Contrary to previous studies (Su et al., 2009; Matthews et al., 2014a) this suggests that the halo cannot be sustained by radiation pressure alone. In the ALMA profile the peak is too high, while the peak flux in the SED is too low, while the tail end in both is well reproduced. Again we are given different hints at different wavelengths for how to alleviate the discrepancies. More mass is needed in the PACS data, but less in the ALMA data, but more again for the SED. Looking at the dynamical side of the model we are again at an impasse, as we need to explain how destructive collisions are possible at such large distances. We assumed the planetesimals to have eccentricities of up to 0.1 throughout the disc. In need of a stirring mechanism capable of stirring the disc equally over the entire range of the disc and unable to solve the other problems encountered in this model, we conclude that a wide cold disc also cannot reproduce the observations.

4.2.5. Synthesis model

In the previous attempts a single population was insufficient to reproduce the radial profiles, with each model only recreating certain aspects of the observations. High eccentricities were found to lead to the extended emission and low eccentricities made it possible to reproduce the flux levels. So trying to reap the benefits of both we applied a synthesis model combining both approaches, an excited as well as a wide cold population, resembling in some ways a scattered disc, as was discussed for HR 8799 in Wyatt et al. (2017). We chose the high eccentric orbits in our modelling variations in such a way that the periastra do not reach closer than 130 AU. The masses of each population were varied independently from each other except for the initial radial slope of the optical depth, for which we used the same value for both components.

For the images we set a warm component between 6 – 8 AU with a mass obtained by adjusting the flux of the 24 μm photometry point. The contribution of such a warm component to the overall profiles is negligible except for the innermost part of the ALMA profile. The peak in these profiles can be attributed to the combined flux of the warm component and the star.

In the PACS images in Fig. 4.3 we see that the synthesis model reproduces the extended emission while also accurately predicting the inner regions of the disc. Although the model overpredicts the flux further out in the 70 μm profile, it also manages to recreate the slopes at these outer regions. To show if any population is solely responsible for this excess, we plotted each component separately by generating two images, one with only

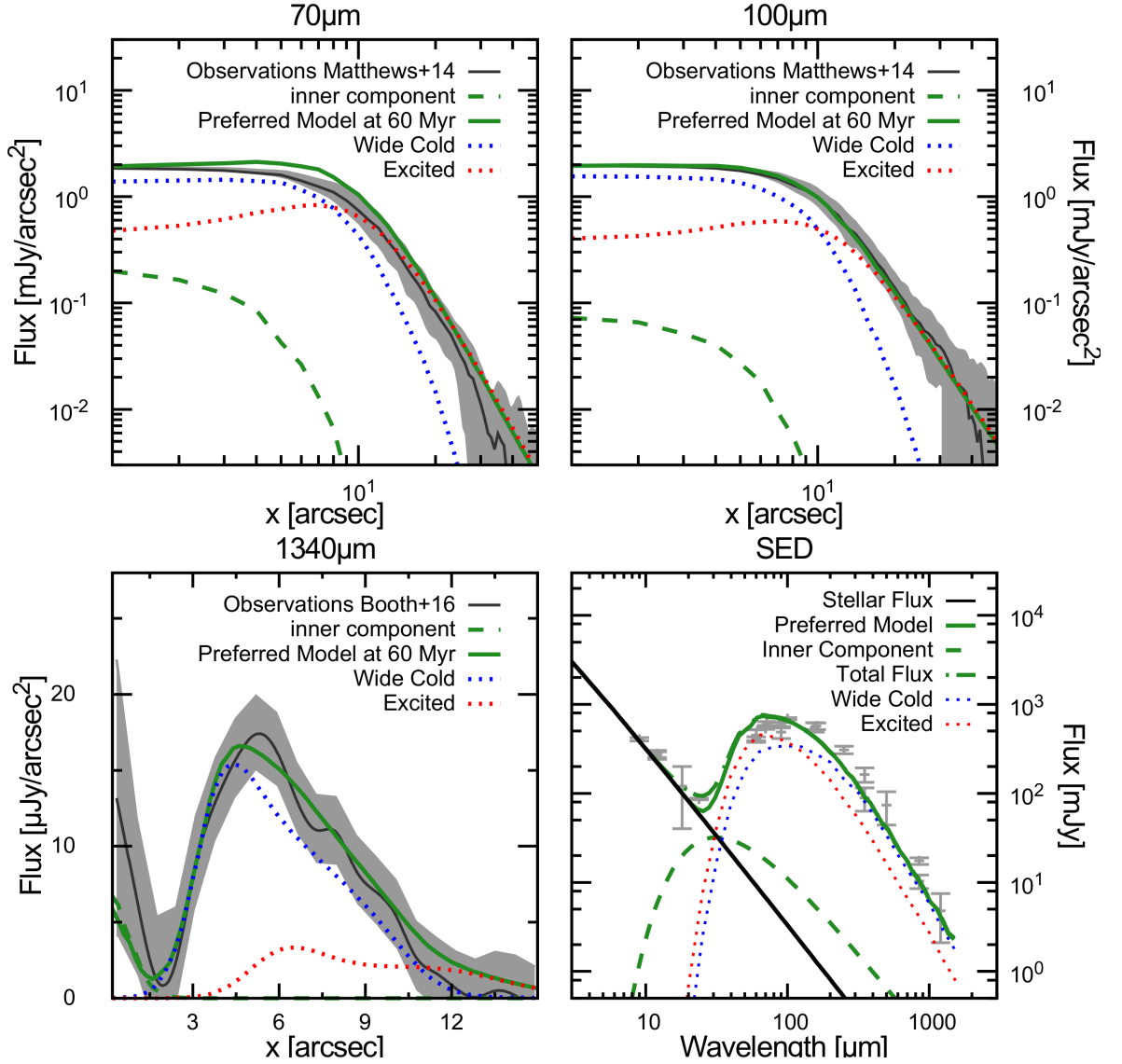


Figure 4.3.: Radial profiles at 70, 100, 1340 μm and the SED for the synthesis model. In black: observations and error bars (in grey). In green: The preferred model, comprising a wide cold disc and an excited one, drawn in a solid line, while the inner component was plotted with a dashed line. In red and blue: The individual contributions of the excited and wide cold population with a dotted line.

objects on orbits of $e < 0.3$ and one only with objects on orbits of $e \geq 0.3$. From these separate plots we see that the excess stems from the overlap of populations. Addressing this is rather difficult as the interplay of the two components is responsible for the entire image and even small changes require a complete restart of the modelling program. We are content with the result, since the error is rather small and we were not able to find a configuration that was able to solve this problem. A reduction of the PACS profile height can be achieved for example by setting the outer edge closer to the star, but that interferes with the profile slope in that region at each wavelength. Perhaps a more nuanced model of a scattered disc might be able to alleviate the problem, but our crude version was not able to. Finally the ALMA profile at $1340 \mu\text{m}$ in Fig. 4.3 fits the observations within the error bars rather well. The SED also overpredicts the flux at shorter wavelengths. In total the synthesis model is able to sufficiently well reproduce both observations and the photometry data, with only a few minor discrepancies.

4.3. Discussion

4.3.1. Comparison to the Kuiper Belt

Both of the empirical models of Matthews et al. (2014a) and Booth et al. (2016) do well in reproducing their respective observations, but fail once applied to the observations of the other. In our modelling attempts we found a single population approach insufficient in reproducing the observation. Adding a dynamically excited population to a extended cold population lead to the model most closely recreating the observations. Such a structure is reminiscent of the Kuiper Belt in our own solar system with a low eccentricity population and a scattered population (Fig. 4.4). The marginal differences between the observations and the model can be attributed to the restrictions in our modelling setup. In reality the transition between even a freshly scattered disc and low eccentricity unscattered population is smooth, but we are bound by our grid of orbital parameters. Just using two populations we already almost double the disc parameters in the code. To achieve a smoother transition between the two populations would require an unwieldy large number of disc parameters which would also need to be tuned in respect to one another. A satisfactory solution would not be achievable in any reasonable amount of time. The only limiting factor is the periastron and the inner edge of the disc (see Fig. 4.4). Even with this constraint we are still left with for example the population masses and the a - e -configurations of each population, all of which need to be considered in respect to one another.

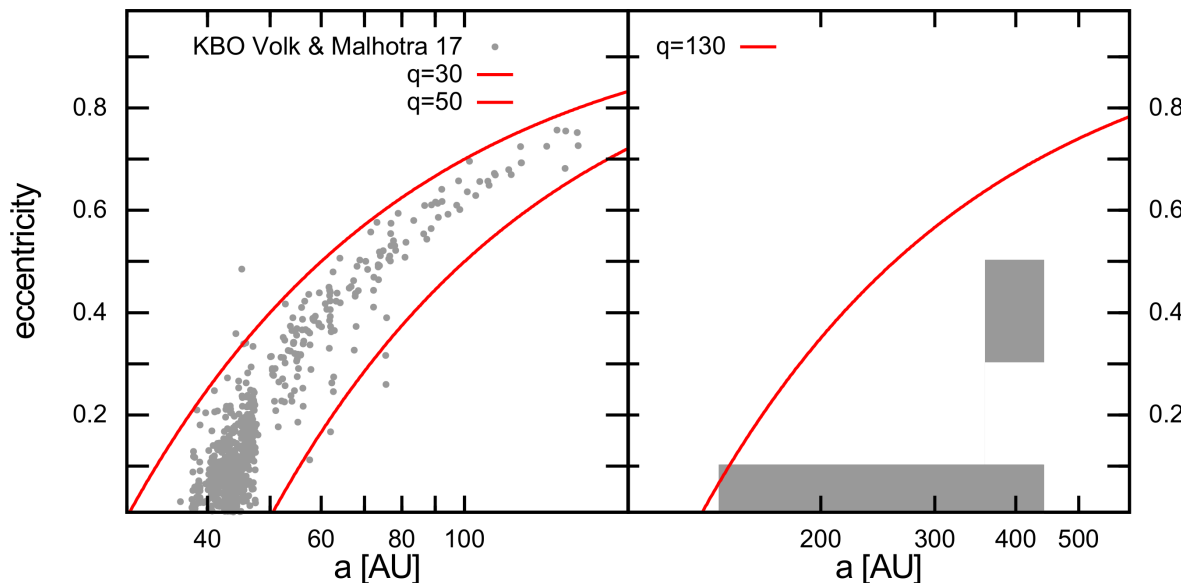


Figure 4.4.: Left: Kuiper Belt population from Volk & Malhotra (2017) in the a - e -plane with rough boundaries. Right: Population of our preferred model with an inner edge of the disc as boundary. This comparison highlights that our model, while similar in approach, is missing the complexity of a continuous distribution.

4.3.2. New SMA data

New SMA observations of HR 8799 at $1340\ \mu\text{m}$ were presented by Wilner et al. (2018), where, in contrast to Booth et al. (2016), the visibilities were fitted. In this model the inner edge of the disc again appears to be closer to 110 AU. The outer edge still extends to 500 AU. This result would be more in line with the previously by Herschel observed discs. We can incorporate this result rather than the inner edge reported by Booth et al. (2016), by moving the cold population closer to the star. Since the halo would still require an additional mechanism other than radiation pressure, we conclude that the position of the inner edge does not change our results in regards to the structure of the disc.

4.3.3. Origin of the scattered disc

Our proposed scattered disc can be the result of many different processes. The Kuiper Belt is believed to have acquired its scattered disc as the result of the migration of the giant planets (Kaib & Sheppard, 2016; Gomes et al., 2018). Migration is also part of the proposed formation scenarios for the giant planets of HR 8799 (Marois et al., 2010; Patience et al., 2011; Dodson-Robinson et al., 2009). With our preferred model we can consider what its proposed initial population masses imply for the planetary

CHAPTER 4. KUIPER BELT ANALOGUES

formation.

Our model suggests an initial mass of $133 M_{\oplus}$ for the extended population and $67 M_{\oplus}$ for the scattered population, with planetesimals sizes reaching up to 100 km. Since the scattered population likely originated from the cold population we can assume a total initial mass for the disc of $200 M_{\oplus}$. Extending this disc further to the innermost planet we find a total mass of solids for the protoplanetary disc of $270 M_{\oplus}$. So our model provides $70 M_{\oplus}$ of mass for the giant planets, which is enough to form their cores. These values, however, do pose a problem as the scattered mass is very high and requires an explanation as to how they were scattered.

Both Booth et al. (2016) and Read et al. (2018) recently suggested a fifth planet to explain the location of the inner edge seen in the ALMA data. N-body simulations done by Read et al. (2018) found that a planet with a mass of $0.1 M_{\text{Jup}}$ ($\sim 30 M_{\oplus}$) and a semi-major axis of 138 AU best explains the inner edge in Booth et al. (2016). Now could such a planet, if real, scatter the disc? Wyatt et al. (2017) studied close encounters between planets and planetesimals. Applying their results to the fifth planet shows that its encounters scatter planetesimals into bound orbits but does not eject them, thus succeeding in creating the scattered. The mass of $\sim 30 M_{\oplus}$ for that planet, however, is cause for concern, as the scattered population is more than double that ($\sim 70 M_{\oplus}$). It is unlikely that a much less massive planet scattered this much more massive population. Read et al. (2018) found a range of planets that could explain the observations similarly well. They ranged from $1 M_{\text{Jup}}$ to $0.04 M_{\text{Jup}}$ in mass corresponding a semimajor axis from 115 AU to 130 AU (with the most massive planets closest to the star) or from 140 AU to 160 AU (with the most massive planets farthest away from the star). Referring to the results of Wyatt et al. (2017), we can exclude any planet with a mass exceeding $0.8 M_{\text{Jup}}$ as their close encounters eject material from the system. Even so a fifth planet scattering material onto bound orbits is still possible.

So long as the fifth planet is not confirmed, we focus the rest of the discussion on the four confirmed planets. Referring once again to the work done by Wyatt et al. (2017), we see that the gas giants by themselves eject material onto unbound orbits in close encounters. This could in theory still be a source for dust in the far out system, but unless there is a method to support this process over a long period, it should only operate for a short time. For it to become a permanent feature in the system, a continuous flux of material would need to enter the orbit of the gas giants, which is an unlikely proposal. So scattering via giant planets is not considered to be responsible for the scattered disc.

Migration on the other hand would not move material onto the orbit of the planet, but the planet onto the orbit of the material. This could alleviate some of the problems

we have encountered so far. Migration is a mechanism that has been in the discussion for the planet formation of HR 8799 for some time, as neither core accretion nor gravitational instability are capable of creating all four gas giants without it (e.g. Currie et al., 2011). Although in the following we focus on outward migration, a similar case can be made for inward migration. To discuss the effects of migration we use a variant of the schematic from Wyatt et al. (2017) as seen in Fig. 4.5. In their work the results of close encounters were considered in a gasless environment, but since large planetesimals are less affected by the gas, we can use the same image to get an approximate understanding. The diagram is separated into three segments showing the results of close encounters of an planetesimals with a planet of a certain mass at a certain distance from the star. The three main results are ejection, accretion or scattering onto a bound orbit. The shaded region shows how these segments change over the lifetime of HR 8799 as planetesimals encounter the planets more often. We added the core formation region for an outward migration to this diagram and added roughly their evolutionary paths. If the planets migrated fully formed, we see that they eject every planetesimals that crosses their orbit during migration. So we consider the fully formed planets to be a rather unlikely source for scatter. Changing the migrating planet’s mass is imperative in order to scatter material onto bound orbits. One way to achieve this is by considering that the planets acquired their envelope during or after their migration, which would reduce the mass that have to be considered for scattering down to the mass of the core. Their migration rate is slower and they could easily create the scattered disc of planetesimals we see in our model.

Such an evolutionary track could be verified by checking the material composition of the planets, which can be inferred from the planet’s atmosphere’s spectra (e.g. Lee et al., 2013; Lavie et al., 2017). These studies found that the compositions are consistent with core accretion scenarios, which would require outward migration, and with gravitational instability scenarios incorporating late time accretion. The latter is not specifically favoured in our model as gravitational instability can form the planets at their current orbits and does not require migration. If enough material is crossing such a planet’s orbit during formation, it can be responsible for the scattered population, although that does seem unlikely. Core accretion on the other hand would need to incorporate some form of migration, which would involve scattering, migration or even core migration scenarios discussed here.

Another method of relocating planets in a system is by planet-planet scattering events, which is also a possibility for the HR 8799 system. The eccentric orbit of a scattered planetary core could be circularised by the debris disc through dynamical friction (Thommes et al., 1999) if the gas envelope is accreted after the scattering

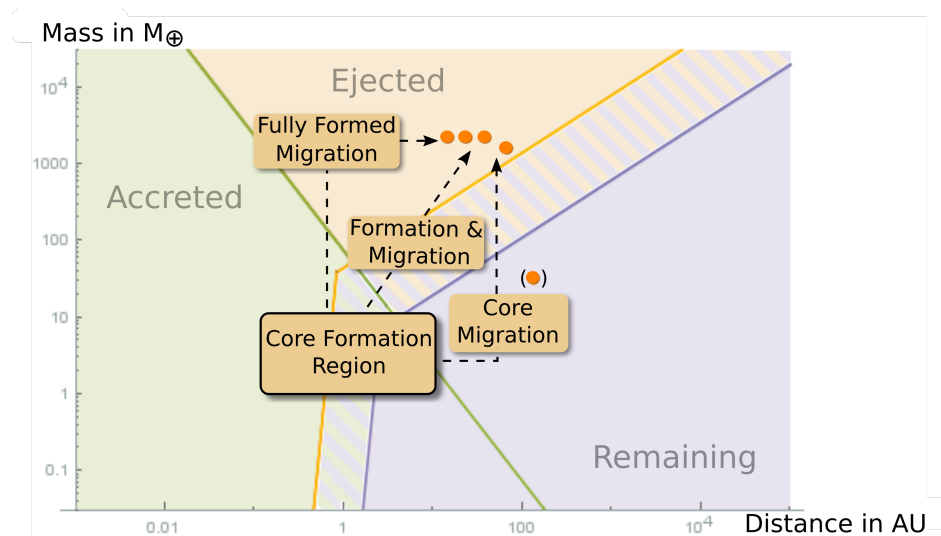


Figure 4.5.: Wyatt et al. (2017) diagram with regions indicating the results of close encounters color coded. Orange: Material encountering planets in this region are ejected. Green: Material is accreted in an encounter. Purple: Material encountering planets have been scattered onto bound orbits. As multiple encounters occur more material can be ejected or accreted, leading to a shrinking region of material remaining after an encounter. The evolution of this is shown by the shaded region. The dashed line and boxes show the evolution over time of an example planet for different formation scenarios.

event and circularisation (Bromley & Kenyon, 2011; Currie et al., 2011). Without a doubt it is easier to circularise the orbit of a planet core rather than a fully grown planet.

4.3.4. Other systems

With a scattered disc proposed for HR 8799 it is natural to ask whether some characteristics of this system can hint at similarly structured discs in other systems. One of the distinct features of the HR 8799 debris disc is its large radial extent as seen in the (sub-)mm images. It's relative width in these images is $\Delta r/r \approx 1$, with $\Delta r/r$ being the width to radius ratio. So a first good indicator for scattered disc-hosting systems are those that appear similarly extended at (sub-)mm wavelengths. In a list of 26 debris disc resolved with ALMA or SMA compiled by Matrà et al. (2018), we found 11 discs showing a relative width of $\Delta r/r > 0.8$. One of them was HR 8799. Having 11 systems in this limited sample of 25 showing similarly extended emission, one might assume this feature to be a rather common one. This may be an overestimation as a second dust belt in many of these systems impedes a correct determination of the belt width.

Another feature present in HR 8799 and needed for the scattered disc scenario are

planets. Krivov & Booth (2018) checked the list from Matrà et al. (2018) to see which required additional stirring mechanisms to explain destructive collisions throughout the disc. They found three such discs: HR 8799, HD 95086 and 49 Cet. Two of these (HD 95086 and HR 8799) have at least one directly imaged planet with the planet in HD 95086's planet having a large gap to the inner edge of its cold component (Rameau et al., 2013). 49 Cet has as of yet no confirmed planets. We propose these two systems, due to the presence of an extended disc and the likelihood of planets, as good candidates for hosting a scattered disc.

5. Conclusion

5.1. Summary

The goal of this work was to analyse extrasolar debris discs and compare them to the two-component debris disc of our solar system. Many other systems show signs of a two component structure, with a cold outer component and a warm inner component. The origin of the latter is still hotly debated, since there are multiple mechanisms in the solar system that contribute to the warm component. Cometary sources and dust transport from further out in the system are as likely to be the source in extrasolar systems as asteroid belt analogues. Unfortunately we cannot easily differentiate between them. To determine if an asteroid belt is plausible we assumed that both components of the two component systems are collisionally supported debris belts (i.e. an asteroid and a Kuiper Belt analogue), that originated from a single extended protoplanetary disc. For the implementation we used the analytical evolution model of Löhne et al. (2008), parameterized with the total mass (or density at 1 AU) of the protoplanetary disc and the slope of the surface density profile. This model was then applied to 225 suspected two component systems with radii and fractional luminosities from the Spitzer/IRS catalogue (Chen et al., 2014). We found that:

- (i) The overwhelming majority of the systems (220 of 225, or 98%) are compatible with the two-belt scenario. Using the standard gas-to-dust ratio of 100:1, we found an average protoplanetary disc mass of $M_{\text{PPD}}/M_{\odot} = (3.3_{-0.3}^{+0.4}) \times 10^{-3}$, or $M_{\text{PPD}}/M_{\star} = (2.0_{-0.2}^{+0.3}) \times 10^{-3}$, and an average slope of the surface density distribution of $p = -0.93 \pm 0.06$. These results are compatible with the results for protoplanetary disc (sub-)mm observations and with density profiles derived from “minimum-mass extrasolar nebulae” studies for extrasolar systems with multiple planets.
- (ii) Compatibility with the two-belt, i.e., asteroid and Kuiper Belt, scenario does not rule out other mechanisms. Dust transport or cometary dust sources, for example, are still viable solutions. We checked if dust transport could support

warm components in our sample with a simple transport model and found that it is indeed viable for a fraction of the discs. A combination of these mechanisms is possible as well.

- (iii) From the remaining five systems one of them turned out to have a dubious two-component status (HIP 11486). The other four systems are two-component systems, but fail to be reproduced by our model. All of these systems are old (≥ 1 Gyr) and show a warm component at $\sim 2\text{--}3$ AU with a fractional luminosity of $(3\text{--}8) \times 10^{-4}$. These turn out to be too bright and too close to the star to be sustained by collisional cascade in an asteroid belt analogue and the transport model also failed to create the flux levels by transport from an outer cold component.
- (iv) For these atypical systems cometary or transient mechanisms have to be invoked. Cometary sources could stem from comets scattered inward from an outer belt or from long-period comets from “mini-Oort clouds”. Alternatively, transient phenomena, like dust from recent major collisions or from planetary system instabilities, can also be responsible. We found that 2% of our systems exhibit such irregularities, which is close to the value found in other studies.

In the second part of this work, we considered models for the outer debris disc of HR 8799 proposed by Matthews et al. (2014a) based on Herschel data and proposed by Booth et al. (2016) based on ALMA (Atacama Large Millimetre Array) 1.34 mm data. We try to answer some questions as to how such a wide debris disc can collisionally evolve and draw comparisons to the Kuiper Belt. For this we applied the ACE code (Analysis of Collisional Evolution) and compared the model results to the observations. We found that previous models do not agree with each other when they are extrapolated beyond their set of observations.

Our modelling shows the following:

- (i) Both a wide planetesimal disc and an excited narrowed disc fail to reproduce the observations. Those models notably included radiation pressure and failed to recreate the halo seen in the observations, indicating that radiation pressure is not able to reproduce the observed halo.
- (ii) Applying a two-population model with a wide cold debris disc and a scattered population of planetesimals leads to the best fits of the observations of HR 8799. This structure is reminiscent of the architecture of the outer solar system with its Kuiper Belt and the scattered population, suggesting a similar origin.

- (iii) Scattered populations probably form through interaction with planets and may be a common feature. HR 8799 features four to five planets, with their evolution scenarios often involving migration or even planet-planet-scattering events. The fifth planet, if real, can be massive enough to be a viable option for creating the scattered disc. The other four giant planets are too massive to scatter material onto bound orbits, thus are unable to have created the scattered disc. The scattered population could be created by the planet cores, if they migrated before or during the accretion of their envelope.

To summarise, we found that asteroid belts are a possibly common feature in extrasolar systems with two components and we could identify multiple abnormal systems. Alternative methods like transport and cometary sources were discussed for all systems, as a combination of these provide the dust of the warm component in our solar system. We found that the cold component in HR 8799 can be well fit with a scattered disc, a similar structure to the one found in the Kuiper Belt. With that we discussed the origin of such a scattered disc with respect how the Kuiper Belt is believed to have formed. Both works are examples for how a comparison to the solar system can inform the discussion of extrasolar systems.

5.2. Parting thoughts

With the continued study of debris discs we find many systems to be vastly different from our own, but drawing parallels and extrapolating from the solar system, we are able to, bit by bit, gain a fundamental understanding of the broader picture. Essential to this approach is not only an understanding of our own system, but also a good basis of data for extrasolar discs. The quality and the amount of debris disc data increases steadily (e.g. Ertel et al., 2020; Esposito et al., 2020) and brings with it further insights and better modelling opportunities (e.g. Lestrade et al., 2020; Plavchan et al., 2020).

Our picture of warm components is not as refined as for their colder counterparts because most observations are unresolved and the uncertain nature of their origin. We know from resolved near-infrared interferometric observations that about 20% of stars at all ages and spectral classes possess exozodiacal dust within 1 AU (see, e.g. Absil et al., 2013; Ertel et al., 2014, 2018, and references therein). Ertel et al. (2020) have shown a strong correlation between the presence of cold dust and hot dust. They were able to identify two distinct populations of exozodiacal dust: “docile” populations, likely to be supported by continuous dust transport/production, and catastrophic populations, requiring recent or periodic events like comets to produce the dust observed.

Compared to warm components we have much more detailed knowledge about the cold components and thus access to much more detailed modelling. Our work was one of the first to suggest a scattered disc in an extrasolar system and support it with modelling. Similar structural analogies have by now been found in extrasolar discs, with observations of β Pic hinting at a two population architecture in the outer cold component similar to the hot and cold classical Kuiper Belt populations (Matrà et al., 2019). Clumps within the same disc of β Pic have been attributed to either recent collisions or to resonant populations created by planets (e.g. Wyatt, 2003; Jackson et al., 2014; Matrà et al., 2019). The latter would again imply a similar evolution to the Kuiper Belt. This shows that the search of Kuiper Belt analogues is ongoing and additional data will uncover more systems with similarities.

There are, of course, also features that differ from the solar system. The most striking difference to consider is the sheer amount of material involved in the extrasolar system debris discs. The masses of the solar system discs are much lower, which could be linked to the Nice Model and the depletion due to the Early Heavy Bombardment (Gomes et al., 2005; Morbidelli et al., 2018; de Sousa et al., 2020). Booth et al. (2009) show that not only can this explain the lack of material in our system, but also show that the bombardment happens rather quickly and is thus hard to be observed in action. Furthermore we are able to observe features in other systems not seen in our own, e.g. very wide cold components that can best be described by two separate dust distributions (Ricci et al., 2015; Bonnefoy et al., 2017; Boccaletti et al., 2019; Marino et al., 2019). The study of such discs is deeply involved in planetary formation and planetary influence. All of these are examples for how the study of Kuiper Belt analogues is deeply connected to the study of planet formation and the influence of planets on the disc evolution.

Overall we see ample opportunity for additional studies and for the application and development of the results of our work.

A. SED-Data for HR 8799

Table A.1.: Photometry of HR 8799

Photometric Band	Magnitude [mag]	Remarks	Ref.
B	6.090 ± 0.300		(1)
B	6.196		(2)
B	6.210 ± 0.010		(3)
B	6.214 ± 0.009		(4)
V	5.960 ± 0.010		(4)
V	5.959		(2)
V	5.960 ± 0.010		(3)
I	5.690 ± 0.300		(1)
J	5.383 ± 0.027		(5)
H	5.280 ± 0.018		(5)
K _S	5.240 ± 0.018		(5)
Wavelength [μm]	Flux [mJy]		
9	404.035 ± 17.808	(a)	(6)
12	278 ± 26	(b)	(7)
12	267 ± 25	(b)	(8)
18	120.533 ± 80.276	(c)	(6)
23.68	86.6 ± 1.7	(d)	(9)
60	445 ± 70	(e)	(8)
60	450 ± 71	(e)	(7)
60	412 ± 21		(10)
71.42	610 ± 31		(9)
70	537 ± 15	(f)	(11)
90	585 ± 41		(10)
90	488.632 ± 74.838	(g)	(12)
100	687 ± 20	(f)	(11)
155.89	555 ± 66		(9)
160	570 ± 50	(f)	(11)
250	309 ± 30	(f)	(11)
350	163 ± 30	(f)	(11)
350	89 ± 26		(13)
500	74 ± 30	(f)	(11)
850	10.3 ± 1.8		(14)
850	17.4 ± 1.5		(15)
1200	4.8 ± 2.7		(16)

Remarks: (a) color corrected 7000K = 1.184 (b) color corrected 5000K = 1.43 (c) color corrected 7000K = 0.990 (d) calibrated with Brott & Hauschildt (2005) model 7400 K (e) color corrected 50K = 0.91; (f) BG source subtracted; (g) color corrected 50K = 0.979

References: (1) The USNO-B1.0 Catalogue (Monet et al., 2003); (2) NOMAD Catalogue (Zacharias et al., 2004), from Tycho-2 Catalogue (Høg et al., 2000); (3) The Guide Star Catalogue Version 2.3.2 (Lasker et al., 2008); (4) The Hipparcos and Tycho Catalogues (Perryman et al., 1997); (5) 2MASS All-Sky Catalogue (Skrutskie et al., 2006); (6) Akari/IRC Mid-Infrared All-Sky Survey Point Source Catalogue (Ishihara et al., 2010); (7) IRAS Faint Source Catalogue, $|b| > 10$, Version 2.0 (Moshir et al., 1990); (8) IRAS Catalogue of Point Sources, Version 2.0 (Helou & Walker, 1988); (9) (Su et al., 2009); (10) (Moór et al., 2006); (11) (Matthews et al., 2014a); (12) Akari/FSI All-Sky Survey Point Source Catalogues (Yamamura et al., 2010); (13) (Patience et al., 2011); (14) (Williams & Andrews, 2006); (15) SONS-Survey (Holland et al., 2017); (16) (Sylvester et al., 1996)

Bibliography

- Absil, O., Defrère, D., Coudé du Foresto, V., et al. (2013), “A near-infrared interferometric survey of debris-disc stars. III. First statistics based on 42 stars observed with CHARA/FLUOR”, *Astron. Astrophys.*, 555:A104
- Arakawa, M. (1999), “Collisional disription of ice by high-velocity impact”, *Icarus*, 142, 34–45
- Artymowicz, P. (1993), “On the Wave Excitation and a Generalized Torque Formula for Lindblad Resonances Excited by External Potential”, *Astrophys. J.*, 419, 155
- Artymowicz, P. (2004), “Dynamics of Gaseous Disks with Planets”, in L. Caroff, L. J. Moon, D. Backman, & E. Praton (Editors), *Debris Disks and the Formation of Planets*, vol. 324 of *Astronomical Society of the Pacific Conference Series*, p. 39
- Augereau, J. & Beust, H. (2006), “The AU Mic debris ring. Density profile and dynamics of the dust”, *Astron. Astrophys.*, 455, 987–999
- Aumann, H. H. (1985), “IRAS observations of matter around nearby stars.”, *PASP*, 97, 885-891
- Aumann, H. H., Beichman, C. A., Gillett, F. C., et al. (1984), “Discovery of a shell around Alpha Lyrae”, *Astrophys. J.*, 278, L23–L27
- Backman, D. E. & Paresce, F. (1993), “Main-sequence stars with circumstellar solid material - The VEGA phenomenon”, in E. H. Levy & J. I. Lunine (Editors), *Protostars and Planets III*, pp. 1253–1304
- Baines, E. K., White, R. J., Huber, D., et al. (2012), “The CHARA Array Angular Diameter of HR 8799 Favors Planetary Masses for its Imaged Companions”, *Astrophys. J.*, 761:57
- Ballering, N. P., Rieke, G. H., Su, K. Y. L., et al. (2013), “A Trend between Cold Debris Disk Temperature and Stellar Type: Implications for the Formation and Evolution of Wide-orbit Planets”, *Astrophys. J.*, 775:55

- Bannister, M. T., Kavelaars, J. J., Petit, J.-M., et al. (2016), “The Outer Solar System Origins Survey. I. Design and First-quarter Discoveries”, *Astron. J.*, 152, #3:70
- Bannister, M. T., Shankman, C., Volk, K., et al. (2017), “OSSOS. V. Diffusion in the Orbit of a High-perihelion Distant Solar System Object”, *Astron. J.*, 153, #6:262
- Baruteau, C., Crida, A., Paardekooper, S. J., et al. (2014), “Planet-Disk Interactions and Early Evolution of Planetary Systems”, in H. Beuther, R. S. Klessen, C. P. Dullemond, & T. Henning (Editors), *Protostars and Planets VI*, p. 667
- Baruteau, C. & Papaloizou, J. C. B. (2013), “Disk-Planets Interactions and the Diversity of Period Ratios in Kepler’s Multi-planetary Systems”, *Astrophys. J.*, 778, #1:7
- Batygin, K. & Brown, M. E. (2016), “Evidence for a Distant Giant Planet in the Solar System”, *Astron. J.*, 151:22
- Bell, C. P. M., Mamajek, E. E., & Naylor, T. (2015), “The Isochronal Age Scale of Young Moving Groups in the Solar Neighbourhood”, *Proceedings of the International Astronomical Union*, 10, #S314, 41–48
- Benz, W. & Asphaug, E. (1999), “Catastrophic Disruptions Revisited”, *Icarus*, 142, 5-20
- Beust, H., Vidal-Madjar, A., Ferlet, R., et al. (1990), “The β Pictoris circumstellar disk. X — Numerical simulations of infalling evaporating bodies”, *Astron. Astrophys.*, 236, 202–216
- Blum, J. (2018), “Dust Evolution in Protoplanetary Discs and the Formation of Planetesimals. What Have We Learned from Laboratory Experiments?”, *Space Sci. Rev.*, 214:52
- Blum, J., Gundlach, B., Krause, M., et al. (2017), “Evidence for the formation of comet 67P/Churyumov-Gerasimenko through gravitational collapse of a bound clump of pebbles”, *MNRAS*, 469, S755-S773
- Blum, J. & Wurm, G. (2008), “The Growth Mechanisms of Macroscopic Bodies in Protoplanetary Disks”, *Ann. Rev. Astron. Astrophys.*, 46, 21–56
- Boccaletti, A., Thébault, P., Pawellek, N., et al. (2019), “Two cold belts in the debris disk around the G-type star NZ Lupi”, *Astron. Astrophys.*, 625:A21

Bibliography

- Boehnke, P. & Harrison, T. M. (2016), “Illusory Late Heavy Bombardments”, *Proceedings of the National Academy of Science*, 113, #39, 10802-10806
- Bohren, C. F. & Huffman, D. R. (1983), *Absorption and Scattering of Light by Small Particles*, Wiley and Sons: New York – Chichester – Brisbane – Toronto – Singapore
- Bonnefoy, M., Milli, J., Ménard, F., et al. (2017), “Belt(s) of debris resolved around the Sco-Cen star HIP 67497”, *Astron. Astrophys.*, 597:L7
- Bonsor, A., Augereau, J.-C., & Thebault, P. (2012), “Scattering of small bodies by planets: a potential origin for exozodiacal dust ?”, *Astron. Astrophys.*, 548:A104
- Bonsor, A. & Wyatt, M. C. (2012), “The scattering of small bodies in planetary systems: constraints on the possible orbits of cometary material”, *MNRAS*, 420, 2990-3002
- Bonsor, A., Wyatt, M. C., Kral, Q., et al. (2018), “Using warm dust to constrain unseen planets”, *MNRAS*, 480, #4, 5560-5579
- Booth, M., Jordán, A., Casassus, S., et al. (2016), “Resolving the planetesimal belt of HR 8799 with ALMA”, *MNRAS*, 460, L10-L14
- Booth, M., Kennedy, G., Sibthorpe, B., et al. (2013), “Resolved debris discs around A stars in the Herschel DEBRIS survey”, *MNRAS*, 428, 1263-1280
- Booth, M., Wyatt, M. C., Morbidelli, A., et al. (2009), “The history of the Solar system’s debris disc: observable properties of the Kuiper belt”, *MNRAS*, 399, 385-398
- Booth, R. A., Meru, F., Lee, M. H., et al. (2018), “Breakthrough revisited: investigating the requirements for growth of dust beyond the bouncing barrier”, *MNRAS*, 475, 167-180
- Boss, A. P. (1997), “Giant planet formation by gravitational instability.”, *Science*, 276, 1836-1839
- Bottke, W. F., Durda, D. D., Nesvorný, D., et al. (2005), “The fossilized size distribution of the main asteroid belt”, *Icarus*, 175, 111-140
- Briggs, R. E. (1962), “Steady-state space distribution of meteoric particles under the operation of the Poynting-Robertson effect”, *Astron. J.*, 67, 710–723
- Bromley, B. C. & Kenyon, S. J. (2011), “Migration of Planets Embedded in a Circumstellar Disk”, *Astrophys. J.*, 735:29

- Brott, I. & Hauschildt, P. H. (2005), “A PHOENIX Model Atmosphere Grid for Gaia”, in C. Turon, K. S. O’Flaherty, & M. A. C. Perryman (Editors), *The Three-Dimensional Universe with Gaia*, vol. 576 of *ESA Special Publication*, p. 565
- Brown, M. E. (2001), “The Inclination Distribution of the Kuiper Belt”, *Astron. J.*, 121, 2804-2814
- Brown, M. E. & Batygin, K. (2019), “Orbital Clustering in the Distant Solar System”, *Astron. J.*, 157, #2:62
- Brown, R. L., Wild, W., & Cunningham, C. (2004), “ALMA - the Atacama large millimeter array”, *Advances in Space Research*, 34, 555-559
- Bruggeman, D. A. G. (1935), “Berechnung verschiedener physikalischer Konstanten von heterogenen Substanzen. I. Dielektrizitätskonstanten und Leitfähigkeiten der Mischkörper aus isotropen Substanzen”, *Annalen der Physik*, 416, #7, 636-664
- Bryden, G., Beichman, C. A., Trilling, D. E., et al. (2006), “Frequency of Debris Disks around Solar-Type Stars: First Results from a Spitzer MIPS Survey”, *Astrophys. J.*, 636, 1098–1113
- Burns, J. A., Lamy, P. L., & Soter, S. (1979), “Radiation forces on small particles in the solar system”, *Icarus*, 40, 1-48
- Carpenter, J. M., Bouwman, J., Mamajek, E. E., et al. (2009), “Formation and Evolution of Planetary Systems: Properties of Debris Dust Around Solar-Type Stars”, *Astrophys. J. Suppl.*, 181, 197-226
- Chatterjee, S., Ford, E. B., Matsumura, S., et al. (2008), “Dynamical Outcomes of Planet-Planet Scattering”, *Astrophys. J.*, 686, 580-602
- Chen, C. H., Mittal, T., Kuchner, M., et al. (2014), “The Spitzer Infrared Spectrograph Debris Disk Catalog. I. Continuum Analysis of Unresolved Targets”, *Astrophys. J. Suppl.*, 211:25
- Chen, C. H., Sargent, B. A., Bohac, C., et al. (2006), “Spitzer IRS Spectroscopy of IRAS-discovered Debris Disks”, *Astrophys. J. Suppl.*, 166, 351-377
- Chiang, E. & Laughlin, G. (2013), “The minimum-mass extrasolar nebula: in situ formation of close-in super-Earths”, *MNRAS*, 431, 3444-3455
- Clement, M. S., Raymond, S. N., & Kaib, N. A. (2019), “Excitation and Depletion of the Asteroid Belt in the Early Instability Scenario”, *Astron. J.*, 157, #1:38

Bibliography

- Cohen, M., Wheaton, W. A., & Megeath, S. T. (2003), “Spectral Irradiance Calibration in the Infrared. XIV. The Absolute Calibration of 2MASS”, *Astron. J.*, 126, 1090-1096
- Crida, A. (2009), “Minimum Mass Solar Nebulae and Planetary Migration”, *Astrophys. J.*, 698, 606-614
- Currie, T., Burrows, A., Itoh, Y., et al. (2011), “A Combined Subaru/VLT/MMT 1-5 μm Study of Planets Orbiting HR 8799: Implications for Atmospheric Properties, Masses, and Formation”, *Astrophys. J.*, 729:128
- Czechowski, A. & Mann, I. (2010), “Formation and Acceleration of Nano Dust in the Inner Heliosphere”, *Astrophys. J.*, 714:89
- de Sousa, R. R., Morbidelli, A., Raymond, S. N., et al. (2020), “Dynamical evidence for an early giant planet instability”, *Icarus*, 339:113605
- Defrère, D., Hinz, P. M., Skemer, A. J., et al. (2015), “First-light LBT Nulling Interferometric Observations: Warm Exozodiacal Dust Resolved within a Few AU of η Crv”, *Astrophys. J.*, 799:42
- Deienno, R., Gomes, R. S., Walsh, K. J., et al. (2016), “Is the Grand Tack model compatible with the orbital distribution of main belt asteroids?”, *Icarus*, 272, 114-124
- Dermott, S. F., Jayaraman, S., Xu, Y. L., et al. (1994), “A circumsolar ring of asteroidal dust in resonant lock with the Earth”, *Nature*, 369, 719–723
- Dikarev, V., Grün, E., Baggaley, J., et al. (2004), “Modeling the Sporadic Meteoroid Background Cloud”, *Earth, Moon and Planets*, 95, 109-122
- Dodson-Robinson, S. E., Veras, D., Ford, E. B., et al. (2009), “The Formation Mechanism of Gas Giants on Wide Orbits”, *Astrophys. J.*, 707, 79-88
- Dohnanyi, J. S. (1969), “Collisional model of asteroids and their debris”, *J. Geophys. Res.*, 74, 2531–2554
- Draine, B. T. (2003), “Interstellar Dust Grains”, *Ann. Rev. Astron. Astrophys.*, 41, 241-289
- Duncan, M., Quinn, T., & Tremaine, S. (1987), “The formation and extent of the solar system comet cloud”, *Astron. J.*, 94, 1330–1338

- Durda, D. D. & Dermott, S. F. (1997), “The collision evolution of the asteroid belt and its contribution to the zodiacal cloud”, *Icarus*, 130, 140–164
- Eiroa, C., Marshall, J. P., Mora, A., et al. (2013), “DUSt around NEarby Stars. The survey observational results”, *Astron. Astrophys.*, 555:A11
- Ertel, S., Absil, O., Defrère, D., et al. (2014), “A near-infrared interferometric survey of debris-disk stars. IV. An unbiased sample of 92 southern stars observed in H band with VLTI/PIONIER”, *Astron. Astrophys.*, 570:A128
- Ertel, S., Defrère, D., Hinz, P., et al. (2018), “The HOSTS Survey—Exozodiacal Dust Measurements for 30 Stars”, *Astron. J.*, 155, #5:194
- Ertel, S., Defrère, D., Hinz, P., et al. (2020), “The HOSTS Survey for Exozodiacal Dust: Observational Results from the Complete Survey”, *Astron. J.*, 159, #4:177
- Espósito, T. M., Kalas, P., Fitzgerald, M. P., et al. (2020), “Debris Disk Results from the Gemini Planet Imager Exoplanet Survey’s Polarimetric Imaging Campaign”, *Astron. J.*, 160, #1:24
- Fabrycky, D. C. & Murray-Clay, R. A. (2010), “Stability of the Directly Imaged Multiplanet System HR 8799: Resonance and Masses”, *Astrophys. J.*, 710, 1408-1421
- Faramaz, V., Ertel, S., Booth, M., et al. (2016), “Inner mean-motion resonances with eccentric planets: A possible origin for exozodiacal dust clouds”, *ArXiv e-prints*, [arXiv:1611.02196]
- Ferlet, R., Vidal-Madjar, A., & Hobbs, L. M. (1987), “The Beta Pictoris circumstellar disk. V – Time variations of the CA II-K line”, *Astron. Astrophys.*, 185, 267–270
- Fernandez, J. A. & Ip, W. H. (1984), “Some dynamical aspects of the accretion of Uranus and Neptune: The exchange of orbital angular momentum with planetesimals”, *Icarus*, 58, #1, 109-120
- Ferreira, S. E. S., Potgieter, M. S., & Moeketsi, D. M. (2003), “Modulation effects of a changing solar wind speed on low-energy electrons”, *Advances in Space Research*, 32, #4, 675-680
- Fraser, W. C., Brown, M. E., Morbidelli, A., et al. (2014), “The Absolute Magnitude Distribution of Kuiper Belt Objects”, *Astrophys. J.*, 782, #2:100
- Fujiwara, A., Kamimoto, G., & Tsukamoto, A. (1977), “Destruction of basaltic bodies by high-velocity impact”, *Icarus*, 31, 277–288

Bibliography

- Gagné, J., Mamajek, E. E., Malo, L., et al. (2018), “BANYAN. XI. The BANYAN Σ Multivariate Bayesian Algorithm to Identify Members of Young Associations with 150 pc”, *Astrophys. J.*, 856:23
- Gaia Collaboration, Brown, A. G. A., Vallenari, A., et al. (2018), “Gaia Data Release 2. Summary of the contents and survey properties”, *Astron. Astrophys.*, 616:A1
- Gaidos, E. (2017), “A minimum mass nebula for M dwarfs”, *MNRAS*, 470, #1, L1-L5
- Garaud, P., Meru, F., Galvagni, M., et al. (2013), “From Dust to Planetesimals: An Improved Model for Collisional Growth in Protoplanetary Disks”, *Astrophys. J.*, 764:146
- Geiler, F. & Krivov, A. V. (2017), “Does warm debris dust stem from asteroid belts?”, *MNRAS*, 468, 959-970
- Geiler, F., Krivov, A. V., Booth, M., et al. (2019), “The scattered disc of HR 8799”, *MNRAS*, 483, #1, 332-341
- Gladman, B., Holman, M., Grav, T., et al. (2002), “Evidence for an Extended Scattered Disk”, *Icarus*, 157, #2, 269-279
- Goldreich, P. & Tremaine, S. (1979), “The excitation of density waves at the Lindblad and corotation resonances by an external potential.”, *Astrophys. J.*, 233, 857-871
- Goldreich, P. & Tremaine, S. (1980), “Disk-satellite interactions.”, *Astrophys. J.*, 241, 425-441
- Golimowski, D. A., Ardila, D. R., Krist, J. E., et al. (2006), “Hubble Space Telescope ACS Multiband Coronagraphic Imaging of the Debris Disk around β Pictoris”, *Astron. J.*, 131, 3109–3130
- Gomes, R., Levison, H. F., Tsiganis, K., et al. (2005), “Origin of the cataclysmic Late Heavy Bombardment period of the terrestrial planets”, *Nature*, 435, 466-469
- Gomes, R., Nesvorný, D., Morbidelli, A., et al. (2018), “Checking the compatibility of the cold Kuiper belt with a planetary instability migration model”, *Icarus*, 306, 319-327
- Gomes, R. S., Morbidelli, A., & Levison, H. F. (2004), “Planetary migration in a planetesimal disk: why did Neptune stop at 30 AU?”, *Icarus*, 170, 492-507
- Gontcharov, G. A. (2006), “Pulkovo Compilation of Radial Velocities for 35 495 Hipparcos stars in a common system”, *Astronomy Letters*, 32, 759-771

- Goździewski, K. & Migaszewski, C. (2009), “Is the HR8799 extrasolar system destined for planetary scattering?”, *MNRAS*, 397, L16-L20
- Goździewski, K. & Migaszewski, C. (2014), “Multiple mean motion resonances in the HR 8799 planetary system”, *MNRAS*, 440, 3140-3171
- Goździewski, K. & Migaszewski, C. (2018), “The Orbital Architecture and Debris Disks of the HR 8799 Planetary System”, *Astrophys. J. Suppl.*, 238, #1:6
- Gray, R. O., Corbally, C. J., Garrison, R. F., et al. (2003), “Contributions to the Nearby Stars (NStars) Project: Spectroscopy of Stars Earlier than M0 within 40 Parsecs: The Northern Sample. I.”, *Astron. J.*, 126, 2048-2059
- Greaves, J. S., Kennedy, G. M., Thureau, N., et al. (2014), “Alignment in star-debris disc systems seen by Herschel”, *MNRAS*, 438, L31-L35
- Greaves, J. S. & Wyatt, M. C. (2010), “Debris discs and comet populations around Sun-like stars: the Solar System in context”, *MNRAS*, 404, 1944-1951
- Greenberg, R., Bottke, W. F., Carusi, A., et al. (1991), “Planetary accretion rates: Analytical derivation”, *Icarus*, 94, 98–111
- Grigorieva, A., Thébault, P., Artymowicz, P., et al. (2007), “Survival of icy grains in debris discs. The role of photosputtering”, *Astron. Astrophys.*, 475, 755–764
- Grün, E., Zook, H. A., Fechtig, H., et al. (1985), “Collisional balance of the meteoritic complex”, *Icarus*, 62, 244–272
- Gulbis, A. A. S., Elliot, J. L., Adams, E. R., et al. (2010), “Unbiased Inclination Distributions for Objects in the Kuiper Belt”, *Astron. J.*, 140, #2, 350-369
- Gustafson, B. A. S. (1994), “Physics of zodiacal dust”, *Ann. Rev. Earth Planet. Sci.*, 22, 553–595
- Hansen, B. M. S. (2009), “Formation of the Terrestrial Planets from a Narrow Annulus”, *Astrophys. J.*, 703, #1, 1131-1140
- Hayashi, C. (1981), “Structure of the Solar Nebula, Growth and Decay of Magnetic Fields and Effects of Magnetic and Turbulent Viscosities on the Nebula”, *Prog. Theor. Phys. Suppl.*, 70, 35-53
- Heisler, J. & Tremaine, S. (1986), “The influence of the galactic tidal field on the Oort comet cloud”, *Icarus*, 65, 13-26

Bibliography

- Helou, G. & Walker, D. W. (Editors) (1988), *Infrared astronomical satellite (IRAS) catalogs and atlases. Volume 7: The small scale structure catalog*, vol. 7
- Heng, K. & Tremaine, S. (2010), “Long-lived planetesimal discs”, *MNRAS*, 401, 867-889
- Hernández, J., Briceño, C., Calvet, N., et al. (2006), “Spitzer Observations of the Orion OB1 Association: Second-Generation Dust Disks at 5-10 Myr”, *Astrophys. J.*, 652, 472-481
- Hildebrand, R. H. (1983), “The Determination of Cloud Masses and Dust Characteristics from Submillimetre Thermal Emission”, *Quart. J. Roy. Astron. Soc.*, 24, 267
- Hillenbrand, L. A., Carpenter, J. M., Kim, J. S., et al. (2008), “The Complete Census of 70-um-Bright Debris Disks within the FEPS (Formation and Evolution of Planetary Systems) Spitzer Legacy Survey of Sun-like Stars”, *Astrophys. J.*, 677, 630-656
- Høg, E., Fabricius, C., Makarov, V. V., et al. (2000), “The Tycho-2 catalogue of the 2.5 million brightest stars”, *Astron. Astrophys.*, 355, L27-L30
- Holland, W. S., Matthews, B. C., Kennedy, G. M., et al. (2017), “SONS: The JCMT legacy survey of debris discs in the submillimetre”, *MNRAS*, 470, #3, 3606-3663
- Hughes, A. M., Wilner, D. J., Andrews, S. M., et al. (2011), “Resolved Submillimeter Observations of the HR 8799 and HD 107146 Debris Disks”, *Astrophys. J.*, 740:38
- Ida, S. & Lin, D. N. C. (2004), “Toward a Deterministic Model of Planetary Formation. I. A Desert in the Mass and Semimajor Axis Distributions of Extrasolar Planets”, *Astrophys. J.*, 604, #1, 388-413
- Ishihara, D., Onaka, T., Kataza, H., et al. (2010), “The AKARI/IRC mid-infrared all-sky survey”, *Astron. Astrophys.*, 514:A1
- Ishihara, D., Takeuchi, N., Kobayashi, H., et al. (2016), “Faint warm debris disks around nearby bright stars explored by AKARI and IRSF”, *ArXiv e-prints*, [arXiv:1608.04480]
- Izidoro, A., Raymond, S. N., Morbidelli, A. r., et al. (2015), “Terrestrial planet formation constrained by Mars and the structure of the asteroid belt”, *MNRAS*, 453, #4, 3619-3634
- Jackson, A. P. & Wyatt, M. C. (2012), “Debris from terrestrial planet formation: the Moon-forming collision”, *MNRAS*, 425, 657-679

- Jackson, A. P., Wyatt, M. C., Bonsor, A., et al. (2014), “Debris froms giant impacts between planetary embryos at large orbital radii”, *MNRAS*, 440, 3757-3777
- Jewitt, D., Luu, J., & Trujillo, C. (1998), “Large Kuiper Belt Objects: The Mauna Kea 8K CCD Survey”, *Astron. J.*, 115, #5, 2125-2135
- Johansen, A., Youdin, A. N., & Lithwick, Y. (2012), “Adding particle collisions to the formation of asteroids and Kuiper belt objects via streaming instabilities”, *Astron. Astrophys.*, 537:A125
- Jones, M. H., Bewsher, D., & Brown, D. S. (2013), “Imaging of a Circumsolar Dust Ring Near the Orbit of Venus”, *Science*, 342, 960-963
- Joswiak, D. J., Brownlee, D. E., Pepin, R. O., et al. (2007), “Densities and Mineralogy of Cometary and Asteroidal Interplanetary Dust Particles Collected in the Stratosphere”, *Dust in Planetary Systems*, 643, 141-144
- Jura, M., Chen, C. H., Furlan, E., et al. (2004), “Mid-Infrared Spectra of Dust Debris around Main-Sequence Stars”, *Astrophys. J. Suppl.*, 154, 453-457
- Kaib, N. A. & Sheppard, S. S. (2016), “Tracking Neptune’s Migration History through High-perihelion Resonant Trans-Neptunian Objects”, *Astron. J.*, 152:133
- Kataoka, A., Okuzumi, S., Tanaka, H., et al. (2014), “Opacity of fluffy dust aggregates”, *Astron. Astrophys.*, 568:A42
- Kataoka, A., Tanaka, H., Okuzumi, S., et al. (2013), “Fluffy dust forms icy planetesimals by static compression”, *Astron. Astrophys.*, 557:L4
- Kavelaars, J. J., Jones, R. L., Gladman, B. J., et al. (2009), “The Canada-France Ecliptic Plane Survey—L3 Data Release: The Orbital Structure of the Kuiper Belt”, *Astron. J.*, 137, #6, 4917-4935
- Kelsall, T., Weiland, J. L., Franz, B. A., et al. (1998), “The COBE Diffuse Infrared Background Experiment Search for the Cosmic Infrared Background. II. Model of the Interplanetary Dust Cloud”, *Astrophys. J.*, 508, 44–73
- Kennedy, G. M. (2018), “Exocomet orbit fitting: accelerating coma absorption during transits of β Pictoris”, *MNRAS*, 479, #2, 1997-2006
- Kennedy, G. M. & Piette, A. (2015), “Warm exo-Zodi from cool exo-Kuiper belts: the significance of P-R drag and the inference of intervening planets”, *MNRAS*, 449, 2304-2311

Bibliography

- Kennedy, G. M. & Wyatt, M. C. (2010), “Are debris disks self-stirred?”, *MNRAS*, 405, 1253-1270
- Kennedy, G. M. & Wyatt, M. C. (2014), “Do two-temperature debris discs have multiple belts?”, *MNRAS*, 444, 3164-3182
- Kennedy, G. M., Wyatt, M. C., Kalas, P., et al. (2014), “Discovery of the Fomalhaut C debris disc”, *MNRAS*, 438, L96-L100
- Kenyon, S. J. & Bromley, B. C. (2002), “Collisional cascades in planetesimal disks. I. Stellar flybys”, *Astron. J.*, 123, 1757–1775
- Kenyon, S. J. & Bromley, B. C. (2004), “Collisional cascades in planetesimal disks. II. Embedded planets”, *Astron. J.*, 127, 513–530
- Kenyon, S. J. & Bromley, B. C. (2008), “Variations on Debris Disks: Icy Planet Formation at 30-150 AU for 1-3 M_{\odot} Main-Sequence Stars”, *Astrophys. J. Suppl.*, 179, 451-483
- Kenyon, S. J. & Bromley, B. C. (2009), “Rapid Formation of Icy Super-Earths and the Cores of Gas Giant Planets”, *Astrophys. J.*, 690, L140-L143
- Kenyon, S. J. & Bromley, B. C. (2010), “Variations on Debris Disks. II. Icy Planet Formation as a Function of the Bulk Properties and Initial Sizes of Planetesimals”, *Astrophys. J. Suppl.*, 188, 242-279
- Kimura, H., Kunitomo, M., Suzuki, T. K., et al. (2018), “Hot Grain Dynamics by Electric Charging and Magnetic Trapping in Debris Disks”, *arXiv e-prints*, arXiv:1808.03389
- Kirchschlager, F., Wolf, S., Brunngräber, R., et al. (2018), “Modelling of mid-infrared interferometric signature of hot exozodiacal dust emission”, *MNRAS*, 473, 2633-2638
- Kirchschlager, F., Wolf, S., Krivov, A. V., et al. (2017), “Constraints on the structure of hot exozodiacal dust belts”, *MNRAS*, 467, 1614-1626
- Klahr, H. H. & Bodenheimer, P. (2003), “Turbulence in Accretion Disks: Vorticity Generation and Angular Momentum Transport via the Global Baroclinic Instability”, *Astrophys. J.*, 582, 869-892
- Kral, Q., Krivov, A. V., Defrère, D., et al. (2017), “Exozodiacal clouds: hot and warm dust around main sequence stars”, *The Astronomical Review*, 13, #2, 69-111

- Krivov, A. V. & Booth, M. (2018), “Self-stirring of debris discs by planetesimals formed by pebble concentration”, *MNRAS*, 479, 3300-3307
- Krivov, A. V., Eiroa, C., Löhne, T., et al. (2013), “Herschel’s ”Cold Debris Disks”: Background Galaxies or Quiescent Rims of Planetary Systems?”, *Astrophys. J.*, 772:32
- Krivov, A. V., Ide, A., Löhne, T., et al. (2018), “Debris disc constraints on planetesimal formation”, *MNRAS*, 474, 2564-2575
- Krivov, A. V., Löhne, T., & Sremčević, M. (2006), “Dust distributions in debris disks: effects of gravity, radiation pressure and collisions”, *Astron. Astrophys.*, 455, 509-519
- Krivov, A. V., Mann, I., & Krivova, N. A. (2000), “Size distributions of dust in circumstellar debris discs”, *Astron. Astrophys.*, 362, 1127-1137
- Krivov, A. V., Queck, M., Löhne, T., et al. (2007), “On the nature of clumps in debris disks”, *Astron. Astrophys.*, 462, #1, 199-210
- Krivov, A. V., Sremčević, M., & Spahn, F. (2005), “Evolution of a Keplerian disk of colliding and fragmenting particles: a kinetic model with application to the Edgeworth Kuiper belt”, *Icarus*, 174, 105-134
- Kuchner, M. J. (2004), “A Minimum-Mass Extrasolar Nebula”, *Astrophys. J.*, 612, 1147-1151
- Lagrange, A.-M., Bonnefoy, M., Chauvin, G., et al. (2010), “A Giant Planet Imaged in the Disk of the Young Star β Pictoris”, *Science*, 329, 57-
- Lagrange, A.-M., Ferlet, R., & Vidal-Madjar, A. (1987), “The β Pictoris circumstellar disk. IV— Redshifted UV lines.”, *Astron. Astrophys.*, 173, 289–292
- Lasker, B. M., Lattanzi, M. G., McLean, B. J., et al. (2008), “The Second-Generation Guide Star Catalog: Description and Properties”, *Astron. J.*, 136, 735-766
- Lavie, B., Mendonça, J. M., Mordasini, C., et al. (2017), “HELIOS-RETRIEVAL: An Open-source, Nested Sampling Atmospheric Retrieval Code; Application to the HR 8799 Exoplanets and Inferred Constraints for Planet Formation”, *Astron. J.*, 154:91
- Lawler, S. M., Pike, R. E., Kaib, N., et al. (2019), “OSSOS. XIII. Fossilized Resonant Dropouts Tentatively Confirm Neptune’s Migration Was Grainy and Slow”, *Astron. J.*, 157, #6:253

Bibliography

- Lee, E. J. & Chiang, E. (2016), “A Primer on Unifying Debris Disk Morphologies”, *ArXiv e-prints*, [arXiv:1605.06118]
- Lee, J.-M., Heng, K., & Irwin, P. G. J. (2013), “Atmospheric Retrieval Analysis of the Directly Imaged Exoplanet HR 8799b”, *Astrophys. J.*, 778, #2:97
- Leinert, C., Röser, S., & Buitrago, J. (1983), “How to maintain the spatial distribution of interplanetary dust”, *Astron. Astrophys.*, 118, 345–357
- Lestrade, J. F., Augereau, J. C., Booth, M., et al. (2020), “Debris disks around stars in the NIKA2 era”, in *European Physical Journal Web of Conferences*, vol. 228 of *European Physical Journal Web of Conferences*, p. 00015
- Lestrade, J.-F., Matthews, B. C., Sibthorpe, B., et al. (2012), “A DEBRIS disk around the planet hosting M-star GJ 581 spatially resolved with Herschel”, *Astron. Astrophys.*, 548:A86
- Levison, H. F., Kretke, K. A., Walsh, K. J., et al. (2015), “Growing the terrestrial planets from the gradual accumulation of sub-meter sized objects”, *Proceedings of the National Academy of Science*, 112, #4, 14180-14185
- Levison, H. F., Morbidelli, A., Vanlaerhoven, C., et al. (2008), “Origin of the structure of the Kuiper belt during a dynamical instability in the orbits of Uranus and Neptune”, *Icarus*, 196, 258-273
- Li, A. & Greenberg, J. M. (1998), “A comet dust model for the beta Pictoris disk”, *Astron. Astrophys.*, 331, 291-313
- Lin, D. N. C., Bodenheimer, P., & Richardson, D. C. (1996), “Orbital migration of the planetary companion of 51 Pegasi to its present location”, *Nature*, 380, #6575, 606-607
- Lin, D. N. C. & Papaloizou, J. (1986a), “On the Tidal Interaction between Protoplanets and the Primordial Solar Nebula. II. Self-Consistent Nonlinear Interaction”, *Astrophys. J.*, 307, 395
- Lin, D. N. C. & Papaloizou, J. (1986b), “On the Tidal Interaction between Protoplanets and the Protoplanetary Disk. III. Orbital Migration of Protoplanets”, *Astrophys. J.*, 309, 846
- Lissauer, J. J. (1987), “Timescales for planetary accretion and the structure of the protoplanetary disk”, *Icarus*, 69, 249–265

- Löhne, T., Augereau, J.-C., Ertel, S., et al. (2012a), “Modelling the huge, Herschel-resolved debris ring around HD 207129”, *Astron. Astrophys.*, 537:A110
- Löhne, T., Eiroa, C., Augereau, J.-C., et al. (2012b), “Debris disks as seen by Herschel/DUNES”, *Astron. Nachr.*, 333, 441–446
- Löhne, T., Krivov, A. V., Kirchschrager, F., et al. (2017), “Collisions and drag in debris discs with eccentric parent belts”, *Astron. Astrophys.*, 605:A7
- Löhne, T., Krivov, A. V., & Rodmann, J. (2008), “Long-Term Collisional Evolution of Debris Disks”, *Astrophys. J.*, 673, 1123-1137
- Love, S. G. & Brownlee, D. E. (1993), “A Direct Measurement of the Terrestrial Mass Accretion Rate of Cosmic Dust”, *Science*, 262, 550-553
- Lubow, S. H. & Ida, S. (2010), *Planet Migration*, pp. 347–371
- Luppe, P., Krivov, A. V., Booth, M., et al. (2020), “Observability of dusty debris discs around M-stars”, *MNRAS*, 499, #3, 3932-3942
- MacQueen, R. M. (1968), “Infrared observations of the outer solar corona”, *Astrophys. J.*, 154, 1059–1076
- Malhotra, R. (1993), “The origin of Pluto’s peculiar orbit”, *Nature*, 365, 819-821
- Malo, L., Doyon, R., Lafrenière, D., et al. (2013), “Bayesian Analysis to Identify New Star Candidates in Nearby Young Stellar Kinematic Groups”, *Astrophys. J.*, 762:88
- Marboeuf, U., Bonsor, A., & Augereau, J. C. (2016), “Extrasolar comets: The origin of dust in exozodiacal disks?”, *Planet. Space Sci.*, 133, 47-62
- Marino, S., Carpenter, J., Wyatt, M. C., et al. (2018), “A gap in the planetesimal disc around HD 107146 and asymmetric warm dust emission revealed by ALMA”, *MNRAS*, p. 1705
- Marino, S., Wyatt, M. C., Panić, O., et al. (2017), “ALMA observations of the η Corvi debris disc: inward scattering of CO-rich exocomets by a chain of 3-30 M_{Earth} planets?”, *MNRAS*, 465, 2595-2615
- Marino, S., Yelverton, B., Booth, M., et al. (2019), “A gap in HD 92945’s broad planetesimal disc revealed by ALMA”, *MNRAS*, 484, #1, 1257-1269
- Marois, C., Macintosh, B., Barman, T., et al. (2008), “Direct Imaging of Multiple Planets Orbiting the Star HR 8799”, *Science*, 322, 1348-

Bibliography

- Marois, C., Zuckerman, B., Konopacky, Q. M., et al. (2010), “Images of a fourth planet orbiting HR 8799”, *Nature*, 468, 1080-1083
- Masset, F. S. & Papaloizou, J. C. B. (2003), “Runaway Migration and the Formation of Hot Jupiters”, *Astrophys. J.*, 588, #1, 494-508
- Matrà, L., Marino, S., Kennedy, G. M., et al. (2018), “An Empirical Planetesimal Belt Radius-Stellar Luminosity Relation”, *Astrophys. J.*, 859:72
- Matrà, L., Wyatt, M. C., Wilner, D. J., et al. (2019), “Kuiper Belt-like Hot and Cold Populations of Planetesimal Inclinations in the β Pictoris Belt Revealed by ALMA”, *Astron. J.*, 157, #4:135
- Matthews, B., Kennedy, G., Sibthorpe, B., et al. (2014a), “Resolved Imaging of the HR 8799 Debris Disk with Herschel”, *Astrophys. J.*, 780:97
- Matthews, B. C., Krivov, A. V., Wyatt, M. C., et al. (2014b), “Observations, modeling, and theory of debris disks”, in H. Beuther, R. Klessen, C. Dullemond, & T. Henning (Editors), *Protostars and Planets VI*, pp. 521–544, U. Arizona Press, Tucson
- McNamara, H., Jones, J., Kauffman, B., et al. (2004), “Meteoroid Engineering Model (MEM): A Meteoroid Model For The Inner Solar System”, *Earth, Moon and Planets*, 95, 123-139
- Meech, K. J., Yang, B., Kleyna, J., et al. (2016), “Inner solar system material discovered in the Oort cloud”, *Science Advances*, 2:e1600038
- Meng, H. Y. A., Rieke, G. H., Su, K. Y. L., et al. (2012), “Variability of the Infrared Excess of Extreme Debris Disks”, *Astrophys. J. Lett.*, 751:L17
- Mennesson, B., Millan-Gabet, R., Serabyn, E., et al. (2014), “Constraining the Exozodiacal Luminosity Function of Main-sequence Stars: Complete Results from the Keck Nuller Mid-infrared Surveys”, *Astrophys. J.*, 797:119
- Moerchen, M. M., Telesco, C. M., Packham, C., et al. (2007), “Mid-Infrared Resolution of a 3 AU Radius Debris Disk around ζ Leporis”, *Astrophys. J.*, 655, L109–L112
- Monet, D. G., Levine, S. E., Canzian, B., et al. (2003), “The USNO-B Catalog”, *Astron. J.*, 125, 984-993
- Montesinos, B., Eiroa, C., Krivov, A. V., et al. (2016), “Incidence of debris discs around FGK stars in the solar neighbourhood”, *Astron. Astrophys.*, 593, A51

- Moór, A., Ábrahám, P., Derekas, A., et al. (2006), “Nearby Debris Disk Systems with High Fractional Luminosity Reconsidered”, *Astrophys. J.*, 644, 525–542
- Moór, A., Apai, D., Pascucci, I., et al. (2009), “The Discovery of New Warm Debris Disks Around F-type Stars”, *Astrophys. J. Lett.*, 700, L25-L29
- Moór, A., Kóspál, Á., Ábrahám, P., et al. (2016), “New Debris Disks in Nearby Young Moving Groups”, *Astrophys. J.*, 826:123
- Moore, A., Hasan, I., & Quillen, A. C. (2013), “Limits on orbit-crossing planetesimals in the resonant multiple planet system, KOI-730”, *MNRAS*, 432, 1196-1202
- Morales, F. Y., Rieke, G. H., Werner, M. W., et al. (2011), “Common Warm Dust Temperatures Around Main-sequence Stars”, *Astrophys. J. Lett.*, 730:L29
- Morbidelli, A., Levison, H. F., & Gomes, R. (2008), *The Dynamical Structure of the Kuiper Belt and Its Primordial Origin*, p. 275
- Morbidelli, A., Levison, H. F., Tsiganis, K., et al. (2005), “Chaotic capture of Jupiter’s Trojan asteroids in the early Solar System”, *Nature*, 435, #7041, 462-465
- Morbidelli, A., Nesvorný, D., Laurenz, V., et al. (2018), “The timeline of the lunar bombardment: Revisited”, *Icarus*, 305, 262-276
- Morey, É. & Lestrade, J.-F. (2014), “On the steady state collisional evolution of debris disks around M dwarfs”, *Astron. Astrophys.*, 565:A58
- Moro-Martín, A., Malhotra, R., Bryden, G., et al. (2010), “Locating Planetesimal Belts in the Multiple-planet Systems HD 128311, HD 202206, HD 82943, and HR 8799”, *Astrophys. J.*, 717, 1123-1139
- Moshir, M., Kopan, G., Conrow, T., et al. (1990), *IRAS Faint Source Catalogue, version 2.0*.
- Moya, A., Amado, P. J., Barrado, D., et al. (2010), “Age determination of the HR8799 planetary system using asteroseismology”, *MNRAS*, 405, L81-L85
- Mukai, T. & Yamamoto, T. (1982), “Solar wind pressure on interplanetary dust”, *Astron. Astrophys.*, 107, #1, 97–100
- Murray, N., Hansen, B., Holman, M., et al. (1998), “Migrating Planets”, *Science*, 279, 69

Bibliography

- Mustill, A. J. & Wyatt, M. C. (2009), “Debris disc stirring by secular perturbations from giant planets”, *MNRAS*, 399, 1403-1414
- Nesvold, E. R., Naoz, S., Vican, L., et al. (2016), “Circumstellar Debris Disks: Diagnosing the Unseen Perturber”, *Astrophys. J.*, 826, #1:19
- Nesvorný, D., Jenniskens, P., Levison, H. F., et al. (2010), “Cometary Origin of the Zodiacal Cloud and Carbonaceous Micrometeorites. Implications for Hot Debris Disks”, *Astrophys. J.*, 713, 816-836
- Nesvorný, D. & Vokrouhlický, D. (2016), “Neptune’s Orbital Migration Was Grainy, Not Smooth”, *Astrophys. J.*, 825, #2:94
- Nesvorný, D., Vokrouhlický, D., Bottke, W. F., et al. (2018), “Evidence for very early migration of the Solar System planets from the Patroclus-Menoetius binary Jupiter Trojan”, *Nature Astronomy*, 2, 878-882
- O’Brien, D. P. & Greenberg, R. (2003), “Steady-state size distributions for collisional populations: analytical solution with size-dependent strength”, *Icarus*, 164, 334–345
- Okuzumi, S., Tanaka, H., Kobayashi, H., et al. (2012), “Rapid Coagulation of Porous Dust Aggregates outside the Snow Line: A Pathway to Successful Icy Planetesimal Formation”, *Astrophys. J.*, 752:106
- Oort, J. H. (1950), “The structure of the cloud of comets surrounding the Solar System and a hypothesis concerning its origin”, *Bull. Astron. Inst. Netherlands*, 11, 91-110
- Paolicchi, P., Verlicchi, A., & Cellino, A. (1996), “An improved semi-empirical model of catastrophic impact processes. I. Theory and laboratory experiments”, *Icarus*, 121, 126–157
- Parker, E. N. (1958), “The perturbation of interplanetary dust grains by the solar wind”, *Astrophys. J.*, 128, 664–676
- Patience, J., Bulger, J., King, R. R., et al. (2011), “Spatially resolved submillimeter imaging of the HR 8799 debris disk”, *Astron. Astrophys.*, 531, L17+
- Pawellek, N. & Krivov, A. V. (2015), “The Dust Grain Size–Stellar Luminosity Trend in Debris Discs”, *MNRAS*, 454, 3207–3221
- Pawellek, N., Krivov, A. V., Marshall, J. P., et al. (2014), “Disk Radii and Grain Sizes in Herschel-resolved Debris Disks”, *Astrophys. J.*, 792:65

- Pearce, T. D., Krivov, A. V., & Booth, M. (2020), “Gas trapping of hot dust around main-sequence stars”, *MNRAS*, 498, #2, 2798-2813
- Perryman, M. A. C., Lindegren, L., Kovalevsky, J., et al. (1997), “The HIPPARCOS Catalogue”, *Astron. Astrophys.*, 323, L49–L52
- Peterson, A. W. (1967), “Experimental detection of thermal radiation from interplanetary dust”, *Astrophys. J.*, 148, L37–L39
- Petit, J. M., Chambers, J., Franklin, F., et al. (2002), *Primordial Excitation and Depletion of the Main Belt*, pp. 711–723
- Plavchan, P., Barclay, T., Gagné, J., et al. (2020), “A planet within the debris disk around the pre-main-sequence star AU Microscopii”, *Nature*, 582, #7813, 497-500
- Plavchan, P., Jura, M., & Lipsky, S. J. (2005), “Where Are the M Dwarf Disks Older Than 10 Million Years?”, *Astrophys. J.*, 631, 1161-1169
- Poglitsch, A., Waelkens, C., Geis, N., et al. (2010), “The Photodetector Array Camera and Spectrometer (PACS) on the Herschel Space Observatory”, *Astron. Astrophys.*, 518:L2
- Pollack, J. B., Hubickyj, O., Bodenheimer, P., et al. (1996), “Formation of the Giant Planets by Concurrent Accretion of Solids and Gas”, *Icarus*, 124, 62-85
- Rameau, J., Chauvin, G., Lagrange, A.-M., et al. (2013), “Discovery of a Probable 4-5 Jupiter-mass Exoplanet to HD 95086 by Direct Imaging”, *Astrophys. J. Lett.*, 772:L15
- Raymond, S. N. & Armitage, P. J. (2013), “Mini-Oort clouds: compact isotropic planetesimal clouds from planet-planet scattering”, *MNRAS*, 429, L99-L103
- Raymond, S. N., Armitage, P. J., & Gorelick, N. (2009), “Planet-Planet Scattering in Planetesimal Disks”, *Astrophys. J. Lett.*, 699, L88-L92
- Raymond, S. N. & Cossou, C. (2014), “No universal minimum-mass extrasolar nebula: evidence against in situ accretion of systems of hot super-Earths”, *MNRAS*, 440, L11-L15
- Raymond, S. N. & Izidoro, A. (2017), “The empty primordial asteroid belt”, *Science Advances*, 3, #9, e1701138

Bibliography

- Read, M. J., Wyatt, M. C., Marino, S., et al. (2018), “Shaping HR8799’s outer dust belt with an unseen planet”, *MNRAS*
- Reidemeister, M., Krivov, A. V., Schmidt, T. O. B., et al. (2009), “A possible architecture of the planetary system HR 8799”, *Astron. Astrophys.*, 503, 247-258
- Reidemeister, M., Krivov, A. V., Stark, C. C., et al. (2011), “The cold origin of the warm dust around ϵ Eridani”, *Astron. Astrophys.*, 527, A57
- Rhee, J. H., Song, I., Zuckerman, B., et al. (2007), “Characterization of Dusty Debris Disks: The IRAS and Hipparcos Catalogs”, *Astrophys. J.*, 660, 1556-1571
- Ricci, L., Carpenter, J. M., Fu, B., et al. (2015), “ALMA Observations of the Debris Disk around the Young Solar Analog HD 107146”, *Astrophys. J.*, 798:124
- Rieke, G. H., Gáspár, A., & Ballering, N. P. (2016), “Magnetic Grain Trapping and the Hot Excesses around Early-type Stars”, *Astrophys. J.*, 816:50
- Roberge, A., Chen, C. H., Millan-Gabet, R., et al. (2012), “The Exozodiacal Dust Problem for Direct Observations of Exo-Earths”, *PASP*, 124, 799-808
- Sadakane, K. & Nishida, M. (1986), “Twelve additional ‘Vega-like’ stars”, *PASP*, 98, 685-689
- Safronov, V. S. (1969), *Evolution of the Protoplanetary Cloud and Formation of the Earth and Planets*, Nauka, Moscow (in Russian). [English translation: NASA TTF-677, 1972.]
- Schräpler, R., Blum, J., Krijt, S., et al. (2018), “The Physics of Protoplanetary Dust Agglomerates. X. High-velocity Collisions between Small and Large Dust Agglomerates as a Growth Barrier”, *Astrophys. J.*, 853:74
- Schüppler, C., Krivov, A. V., Löhne, T., et al. (2016), “Origin and evolution of two-component debris discs and an application to the ϵ^1 Eridani system”, *MNRAS*, 461, 2146-2154
- Schüppler, C., Löhne, T., Krivov, A. V., et al. (2014), “Collisional modelling of the debris disc around HIP 17439”, *Astron. Astrophys.*, 567:A127
- Schüppler, C., Löhne, T., Krivov, A. V., et al. (2015), “Collisional modelling of the AU Microscopii debris disc”, *Astron. Astrophys.*, 581:A97

- Sende, J. A. & Löhne, T. (2019), “Twisted debris: how differential secular perturbations shape debris disks”, *Astron. Astrophys.*, 631:A141
- Sezestre, É., Augereau, J. C., & Thébault, P. (2019), “Hot exozodiacal dust: an exo-cometary origin?”, *Astron. Astrophys.*, 626:A2
- Shankman, C., Kavelaars, J. J., Bannister, M. T., et al. (2017), “OSSOS. VI. Striking Biases in the Detection of Large Semimajor Axis Trans-Neptunian Objects”, *Astron. J.*, 154, #2:50
- Shannon, A., Jackson, A. P., & Wyatt, M. C. (2019), “Oort cloud asteroids: collisional evolution, the Nice Model, and the Grand Tack”, *MNRAS*, 485, #4, 5511-5518
- Sibthorpe., B., Kennedy, G. M., Wyatt, M. C., et al. (2018), “Analysis of the Herschel DEBRIS Sun-like star sample: Analyses and implications”, *MNRAS*
- Skrutskie, M. F., Cutri, R. M., Stiening, R., et al. (2006), “The Two Micron All Sky Survey (2MASS)”, *Astron. J.*, 131, 1163-1183
- Smith, B. A. & Terrile, R. I. (1984), “A circumstellar disk around β Pictoris”, *Science*, 226, 1421-1424
- Smoluchowski, M. V. (1916), “Drei Vorträge über Diffusion, Brownsche Bewegung und Koagulation von Kolloidteilchen”, *Zeitschrift für Physik*, 17, 557-585
- Song, I., Zuckerman, B., Weinberger, A. J., et al. (2005), “Extreme collisions between planetesimals as the origin of warm dust around a Sun-like star”, *Nature*, 436, 363-365
- Staubach, P., Grün, E., & Jehn, R. (1997), “The meteoroid environment near Earth”, *Adv. Space Res.*, 19, #2, 301-308
- Stewart, S. T. & Leinhardt, Z. M. (2009), “Velocity-Dependent Catastrophic Disruption Criteria for Planetesimals”, *Astrophys. J. Lett.*, 691, L133-L137
- Su, K. Y. L., Rieke, G. H., Malhotra, R., et al. (2013), “Asteroid Belts in Debris Disk Twins: Vega and Fomalhaut”, *Astrophys. J.*, 763:118
- Su, K. Y. L., Rieke, G. H., Stansberry, J. A., et al. (2006), “Debris Disk Evolution around A Stars”, *Astrophys. J.*, 653, 675-689
- Su, K. Y. L., Rieke, G. H., Stapelfeldt, K. R., et al. (2009), “The Debris Disk Around HR 8799”, *Astrophys. J.*, 705, 314-327

Bibliography

- Sylvester, R. J., Skinner, C. J., Barlow, M. J., et al. (1996), “Optical, infrared and millimetre-wave properties of Vega-like systems”, *MNRAS*, 279, 915–939
- Tanaka, H., Takeuchi, T., & Ward, W. R. (2002), “Three-Dimensional Interaction between a Planet and an Isothermal Gaseous Disk. I. Corotation and Lindblad Torques and Planet Migration”, *Astrophys. J.*, 565, #2, 1257-1274
- Tegler, S. C. & Romanishin, W. (2000), “Extremely red Kuiper-belt objects in near-circular orbits beyond 40 AU”, *Nature*, 407, #6807, 979-981
- Thébault, P. & Augereau, J.-C. (2007), “Collisional processes and size distribution in spatially extended debris discs”, *Astron. Astrophys.*, 472, 169-185
- Thommes, E. W., Duncan, M. J., & Levison, H. F. (1999), “The formation of Uranus and Neptune in the Jupiter-Saturn region of the Solar System”, *Nature*, 402, 635-638
- Thureau, N. D., Greaves, J. S., Matthews, B. C., et al. (2014), “An unbiased study of debris discs around A-type stars with Herschel”, *MNRAS*, 445, 2558-2573
- Torres, C. A. O., Quast, G. R., Melo, C. H. F., et al. (2008), *Young Nearby Loose Associations*, p. 757
- Torres, S., Cai, M. X., Brown, A. G. A., et al. (2019), “Galactic tide and local stellar perturbations on the Oort cloud: creation of interstellar comets”, *Astron. Astrophys.*, 629:A139
- Trujillo, C. A. & Sheppard, S. S. (2014), “A Sedna-like body with a perihelion of 80 astronomical units”, *Nature*, 507, #7493, 471-474
- Ueda, T., Kobayashi, H., Takeuchi, T., et al. (2017), “Size Dependence of Dust Distribution around the Earth Orbit”, *Astron. J.*, 153:232
- Vitense, C., Krivov, A. V., Kobayashi, H., et al. (2012), “An improved model of the Edgeworth-Kuiper debris disk”, *Astron. Astrophys.*, 540:A30
- Vokrouhlický, D., Nesvorný, D., & Dones, L. (2019), “Origin and Evolution of Long-period Comets”, *Astron. J.*, 157, #5:181
- Volk, K. & Malhotra, R. (2011), “Inclination Mixing in the Classical Kuiper Belt”, *Astrophys. J.*, 736, #1:11
- Volk, K. & Malhotra, R. (2017), “The Curiously Warped Mean Plane of the Kuiper Belt”, *Astron. J.*, 154:62

- Walsh, K. J., Morbidelli, A., Raymond, S. N., et al. (2011), “A low mass for Mars from Jupiter’s early gas-driven migration”, *Nature*, 475, 206-209
- Ward, W. R. (1997), “Protoplanet Migration by Nebula Tides”, *Icarus*, 126, #2, 261-281
- Ward, W. R. & Hourigan, K. (1989), “Orbital Migration of Protoplanets: The Inertial Limit”, *Astrophys. J.*, 347, 490
- Weidenschilling, S. J. (1977), “The distribution of mass in the planetary system and solar nebula”, *Astrophys. Space Sci.*, 51, 153-158
- Weidenschilling, S. J. & Cuzzi, J. N. (1993), “Formation of planetesimals in the solar nebula”, in E. H. Levy & J. I. Lunine (Editor), *Protostars and Planets III*, pp. 1031–1060
- Weidenschilling, S. J. (1977), “Aerodynamics of solid bodies in the solar nebula”, *MNRAS*, 180, 57–70
- Weidling, R., Güttler, C., Blum, J., et al. (2009), “The Physics of Protoplanetesimal Dust Agglomerates. III. Compaction in Multiple Collisions”, *Astrophys. J.*, 696, #2, 2036-2043
- Weissman, P. R. & Levison, H. F. (1997), “Origin and Evolution of the Unusual Object 1996 PW: Asteroids from the Oort Cloud?”, *Astrophys. J.*, 488, #2, L133-L136
- Williams, J. P. & Andrews, S. M. (2006), “The Dust Properties of Eight Debris Disk Candidates as Determined by Submillimeter Photometry”, *Astrophys. J.*, 653, 1480-1485
- Williams, J. P. & Cieza, L. A. (2011), “Protoplanetary Disks and Their Evolution”, *Ann. Rev. Astron. Astrophys.*, 49, 67-117
- Wilner, D. J., MacGregor, M. A., Andrews, S. M., et al. (2018), “Resolved Millimeter Observations of the HR 8799 Debris Disk”, *Astrophys. J.*, 855:56
- Windmark, F., Birnstiel, T., Güttler, C., et al. (2012a), “Planetesimal formation by sweep-up: How the bouncing barrier can be beneficial to growth”, *Astron. Astrophys.*, 540:A73
- Windmark, F., Birnstiel, T., Ormel, C. W., et al. (2012b), “Breaking through: the effects of a velocity distribution on barriers to dust growth (Corrigendum)”, *Astron. Astrophys.*, 548:C1

Bibliography

- Wolff, S., Dawson, R. I., & Murray-Clay, R. A. (2012), “Neptune on Tiptoes: Dynamical Histories that Preserve the Cold Classical Kuiper Belt”, *Astrophys. J.*, 746, #2:171
- Wood, B. E., Müller, H.-R., Zank, G. P., et al. (2002), “Measured Mass-Loss Rates of Solar-like Stars as a Function of Age and Activity”, *Astrophys. J.*, 574, 412-425
- Wyatt, M. C. (2003), “Resonant Trapping of Planetesimals by Planet Migration: Debris Disk Clumps and Vega’s Similarity to the Solar System”, *Astrophys. J.*, 598, 1321–1340
- Wyatt, M. C. (2005), “The insignificance of P-R drag in detectable extrasolar planetesimal belts”, *Astron. Astrophys.*, 433, 1007–1012
- Wyatt, M. C. (2006), “Dust in Resonant Extrasolar Kuiper Belts: Grain Size and Wavelength Dependence of Disk Structure”, *Astrophys. J.*, 639, 1153-1165
- Wyatt, M. C., Bonsor, A., Jackson, A. P., et al. (2017), “How to design a planetary system for different scattering outcomes: giant impact sweet spot, maximizing exocomets, scattered discs”, *MNRAS*, 464, 3385-3407
- Wyatt, M. C., Booth, M., Payne, M. J., et al. (2010), “Collisional evolution of eccentric planetesimal swarms”, *MNRAS*, 402, 657-672
- Wyatt, M. C. & Dent, W. R. F. (2002), “Collisional processes in extrasolar planetesimal discs — dust clumps”, *MNRAS*, 334, 589–607
- Wyatt, M. C., Dermott, S. F., Telesco, C. M., et al. (1999), “How Observations of Circumstellar Disk Asymmetries Can Reveal Hidden Planets: Pericenter Glow and Its Application to the HR4796 Disk”, *Astrophys. J.*, 527, 918–944
- Wyatt, M. C., Greaves, J. S., Dent, W. R. F., et al. (2005), “Submillimeter Images of a Dusty Kuiper Belt around η Corvi”, *Astrophys. J.*, 620, 492–500
- Wyatt, M. C., Smith, R., Greaves, J. S., et al. (2007a), “Transience of hot dust around sun-like stars”, *Astrophys. J.*, 658, 569-583
- Wyatt, M. C., Smith, R., Su, K. Y. L., et al. (2007b), “Steady State Evolution of Debris Disks around A Stars”, *Astrophys. J.*, 663, 365-382
- Wyatt, M. C., van Lieshout, R., Kennedy, G. M., et al. (2018), “Modelling the KIC8462852 light curves: compatibility of the dips and secular dimming with an exocomet interpretation”, *MNRAS*, 473, #4, 5286-5307

- Yamamura, I., Makiuti, S., Ikeda, N., et al. (2010), “VizieR Online Data Catalog: AKARI/FIS All-Sky Survey Point Source Catalogues (ISAS/JAXA, 2010)”, *VizieR Online Data Catalog*, 2298
- Youdin, A. N. & Goodman, J. (2005), “Streaming Instabilities in Protoplanetary Disks”, *Astrophys. J.*, 620, 459-469
- Zacharias, N., Monet, D. G., Levine, S. E., et al. (2004), “The Naval Observatory Merged Astrometric Dataset (NOMAD)”, *BAAS*, 36, 1418-+
- Zellner, N. E. B. (2017), “Cataclysm No More: New Views on the Timing and Delivery of Lunar Impactors”, *Origins of Life and Evolution of the Biosphere*, 47, #3, 261-280
- Zsom, A., Ormel, C. W., Güttler, C., et al. (2010), “The outcome of protoplanetary dust growth: pebbles, boulders, or planetesimals? II. Introducing the bouncing barrier”, *Astron. Astrophys.*, 513:A57
- Zuckerman, B., Rhee, J. H., Song, I., et al. (2011), “The Tucana/Horologium, Columba, AB Doradus, and Argus Associations: New Members and Dusty Debris Disks”, *Astrophys. J.*, 732:61
- Zuckerman, B. & Song, I. (2004), “Dusty Debris Disks as Signposts of Planets: Implications for Spitzer Space Telescope”, *Astrophys. J.*, 603, 738-743

List of Figures

1.1.	Left: A spectral energy distribution (SED) of the infrared excess of Vega taken from Aumann et al. (1984). The black body spectra used in the model are a 85 K model (thick line) and a 350 K model (dashed line). The latter is only based on the $17\ \mu\text{m}$ upper limit data and therefore arbitrary. Right: First resolved image of β Pic (Smith & Terrile, 1984). The disc can clearly be seen extending from the star to the top left and bottom right of the image.	8
2.1.	Sketch of an orbit with some of the elements needed to describe it. In addition to the reference lines and planes the following parameters are shown: Ω being the longitude of the ascending node, ω being the argument of the pericenter, i being the inclination and the true anomaly being θ	16
2.2.	Different β -values and their corresponding orbits assuming initially circular orbits and only gravity and radiation pressure as acting forces from Krivov et al. (2006).	18
2.3.	Sketch of debris disc spectral energy distributions (SED) at different temperatures and their expected distance and wavelength regime (Kirchschlager et al., 2017).	26

List of Figures

3.1. $R_f = f_w/f_c$ plotted over $R_T = T_w/T_c$ for the sample. The line is calculated with the method described in Kennedy & Wyatt (2014) and in the text. Assumptions made: a star with $L = 9 L_\odot$ (the log-averaged value for the sample), a cold component at $r_c = 100$ AU with $f_c \approx 10^{-4}$, and warm components with various r_w and f_w . For each artificial system, we simulated measurements at 13 wavelengths from a few μm to sub-mm, each with a 5% error. The reduced χ^2 -values are gathered from the results of attempting to fit a single component to the fiducial measurements. Systems with $\chi^2 < 5$ imply a single component model to be plausible; $\chi^2 \geq 5$ solidifies the need for a second component. The two component solution for systems with $\chi^2 < 5$ and systems with $f_c < 4 \times 10^{-6}$ is deemed to be too uncertain. The affected systems are shown in green. 31

3.2. Radius–fractional luminosity plane with the two component systems in our sample, cold (circles) and warm (triangles) components from a system are connected with a straight line. Black symbols denote systems that passed all additional tests we put them through ($\chi^2 \geq 5$ and $f_c > 4 \times 10^{-6}$), while green shows systems that failed in one or more cases ($\chi^2 < 5$ or $f_c < 4 \times 10^{-6}$). To keep the diagram readable, we chose to depict roughly a fifth of the entire sample. 32

3.3. Formation of a two-component debris disc. 34

3.4. Left: Histogramm of radial profile slopes p , right: Histogramm of scaling factors x_{scal} . Black: all systems with good fits, red: bad fits. 38

3.5. Scatter plot of the scaling factor x_{scal} against the exponent p . Black symbols stand for the good fits and the red circles for the poor fits. The systems with poor fits are listed in Table 3.2. 39

3.6. Left: Total disc mass to stellar mass ratio M_{PPD}/M_\star and exponent p . The outlier in the top right is the ~ 5 Myr old system HD 36444 that may not be a debris disc, but rather a protoplanetary or transitional disc (Hernández et al., 2006). Poorly fit systems are listed in Table 3.2. Right: Distribution of the initial masses of the protoplanetary discs in units of stellar mass. For the gas to solids ratio in the protoplanetary disc 100 : 1 was chosen. 40

3.7. Similar plot to Fig. 3.1, but only showing systems with good fits. Curves show the transported dust levels calculated by the Kennedy & Piette (2015) model for our assumed cold components. For all six cases the central star has a mass $1.8 M_{\odot}$ and each component has a relative width of $dr/r = 0.1$. Linestyles indicate the position of the outer component (solid: 100 AU, dashed: 30 AU), whereas the colours indicate the fractional luminosity of the outer component (magenta: 10^{-6} , orange: 10^{-5} , blue: 10^{-4}). Symbol shapes reference the disc radius (circles: $r_c > 50$ AU, triangles: $r_c < 50$ AU), while symbol colours again refer to their fractional luminosity (magenta: $\sim 10^{-6}$, orange: $\sim 10^{-5}$, blue: $\sim 10^{-4}$). Therefore a disc is compatible with the transport scenario if its triangle/circle symbol is below the solid/dashed line of the same colour. 42

3.8. Similar plot to Fig. 3.1 and Fig. 3.2, but only showing systems with good fits in grey and the five failed systems numbered as they are in Tab. 3.2 in red. 45

4.1. Radial profiles at 70, 100, 1340 μm and the SED for the previously proposed system architectures. In black: observations and error bars (in grey). Red: a debris disc from 100 - 310 AU and a halo of small grains out to 2000 AU (Matthews et al., 2014a). Blue: a debris disc with planetesimals from 145 AU to 430 AU with eccentricities up to 0.1 (Booth et al., 2016). 50

4.2. Radial profiles at 70, 100, 1340 μm and the SED for the excited disc and a wide cold model. In black: observations and error bars (in grey). In red: an excited debris disc from 360 - 440 AU with eccentricities of 0.5 - -0.6. In blue: a debris disc with planetesimals from 150 AU to 440 AU with eccentricities up to 0.1. 55

4.3. Radial profiles at 70, 100, 1340 μm and the SED for the synthesis model. In black: observations and error bars (in grey). In green: The preferred model, comprising a wide cold disc and an excited one, drawn in a solid line, while the inner component was plotted with a dashed line. In red and blue: The individual contributions of the excited and wide cold population with a dotted line. 57

List of Figures

4.4. Left: Kuiper Belt population from Volk & Malhotra (2017) in the a-e-plane with rough boundaries. Right: Population of our preferred model with an inner edge of the disc as boundary. This comparison highlights that our model, while similar in approach, is missing the complexity of a continuous distribution. 59

4.5. Wyatt et al. (2017) diagram with regions indicating the results of close encounters color coded. Orange: Material encountering planets in this region are ejected. Green: Material is accreted in an encounter. Purple: Material encountering planets have been scattered onto bound orbits. As multiple encounters occur more material can be ejected or accreted, leading to a shrinking region of material remaining after an encounter. The evolution of this is shown by the shaded region. The dashed line and boxes show the evolution over time of an example planet for different formation scenarios. 62

List of Tables

3.1. Changes to Eq. (3.13) depending on the evolutionary stage.	37
3.2. Systems with poor fits.	43
4.1. List of ACE parameters	52
4.2. Parameters of some proposed disc components and our preferred model.	54
A.1. Photometry of HR 8799	69

Acknowledgements

"Non est ad astra mollis e terris via"

"There is no easy way from the earth to the stars"

SENECA THE YOUNGER

I'd like to thank Prof. Dr. Alexander V. Krivov for his help on my publications and in general. I know that I am sometimes not easy to work with, but you helped me and remained patient throughout this time. In every discussion you made sure to address points that I was sure to miss, but kept the dialogue casual. I could not have asked for a better teacher throughout my studies.

I'd also like to thank Torsten Löhne and Mark Booth from the institute. Their input in discussing the publications and the work done for them was invaluable. Also the almost daily discussion about whatever came to mind during lunch breaks was a welcome distraction from work, although they seem like a distant memory now (they kind of are, over a year at his point). Another colleague I'd like to extend this thanks to is Jan Sende, whose friendship held throughout my time at the university. Your willingness to explain some arcane programming or to discuss a problem kept my mind open to new solutions.

Furthermore I'd like to thank my family and all the other friends and colleagues who supported me on my way through this thesis, I definitely needed it. It has been a long, arduous journey and I am not entirely serious when I say: hopefully you all can stop asking now about when it is finished.

Ehrenwörtliche Erklärung

Ich erkläre hiermit ehrenwörtlich, dass ich die vorliegende Arbeit selbstständig, ohne unzulässige Hilfe Dritter und ohne Benutzung anderer als der angegebenen Hilfsmittel und Literatur angefertigt habe. Die aus anderen Quellen direkt oder indirekt übernommenen Daten und Konzepte sind unter Angabe der Quelle gekennzeichnet.

Weitere Personen waren an der inhaltlich-materiellen Erstellung der vorliegenden Arbeit nicht beteiligt. Insbesondere habe ich hierfür nicht die entgeltliche Hilfe von Vermittlungs- bzw. Beratungsdiensten (Promotionsberater oder andere Personen) in Anspruch genommen. Niemand hat von mir unmittelbar oder mittelbar geldwertige Leistungen für Arbeiten erhalten, die im Zusammenhang mit dem Inhalt der vorgelegten Dissertation stehen.

Die Arbeit wurde bisher weder im In- noch Ausland in gleicher oder ähnlicher Form einer anderen Prüfungsbehörde vorgelegt.

Die geltende Promotionsordnung der Physikalisch-Astronomischen Fakultät ist mir bekannt.

Ich versichere ehrenwörtlich, dass ich nach bestem Wissen die reine Wahrheit gesagt und nichts verschwiegen habe.

Jena, 12. April 2021

Fabian Geiler